TU Delft

Delft University of Technology

Document Version
Final published version

Licence
Unspecified

Citation (APA)
Ali, A. Z. (2026). *UV-Visible Light Driven Bismuth Vanadate (BiVO4) based Photoanodes for the Removal of Organic Micropollutants in Water*. [Dissertation (TU Delft), Delft University of Technology]. https://doi.org/10.4233/uuid:7196faa7-9797-46e5-b043-64c1b4a7d9e0

Important note
To cite this publication, please use the final published version (if applicable).
Please check the document version above.

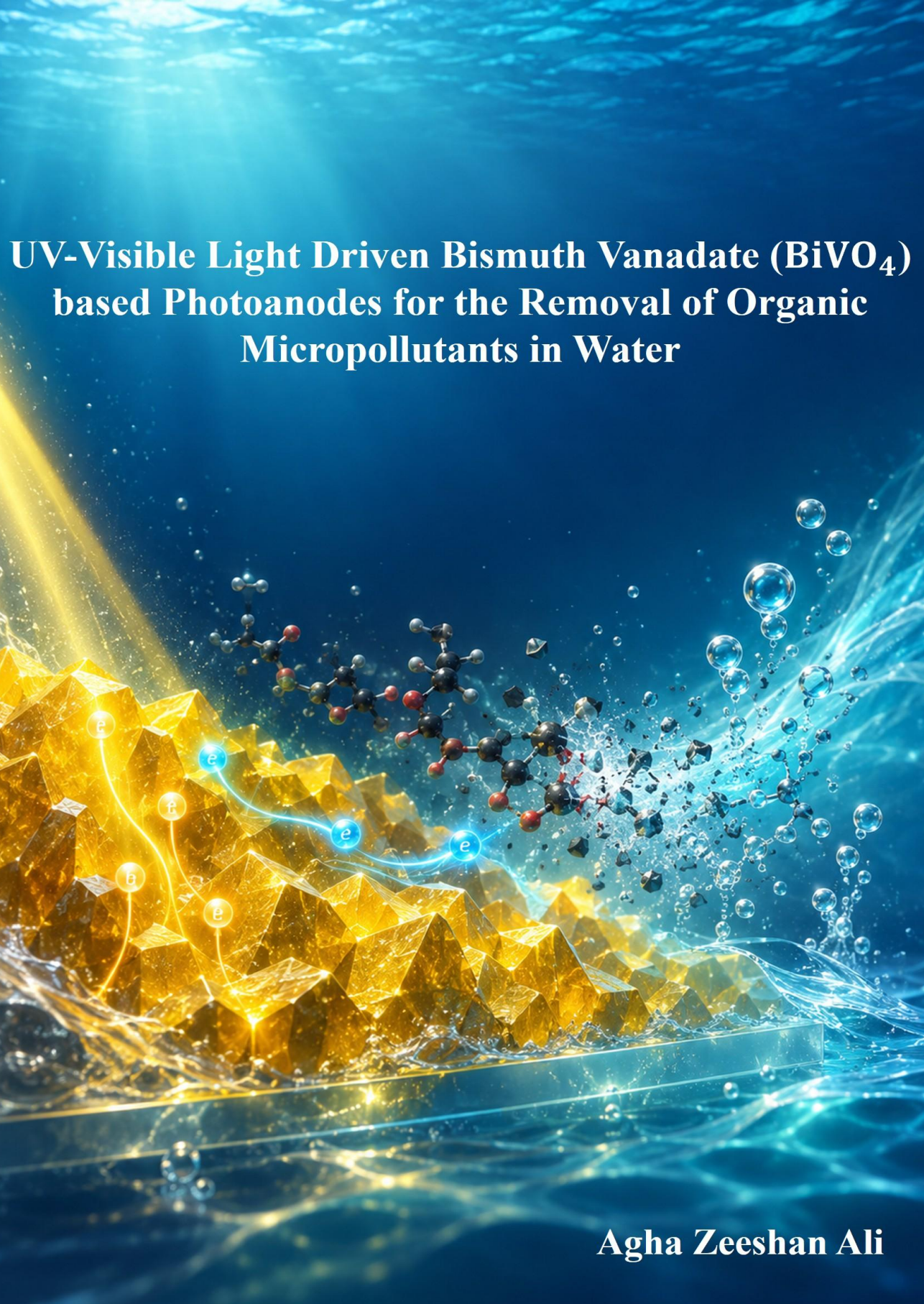
Copyright
In case the licence states “Dutch Copyright Act (Article 25fa)”, this publication was made available Green Open Access via the TU Delft Institutional Repository pursuant to Dutch Copyright Act (Article 25fa, the Taverne amendment). This provision does not affect copyright ownership.
Unless copyright is transferred by contract or statute, it remains with the copyright holder.

Sharing and reuse
Other than for strictly personal use, it is not permitted to download, forward or distribute the text or part of it, without the consent of the author(s) and/or copyright holder(s), unless the work is under an open content license such as Creative Commons.

Takedown policy
Please contact us and provide details if you believe this document breaches copyrights.
We will remove access to the work immediately and investigate your claim.

This work is downloaded from Delft University of Technology.

UV-Visible Light Driven Bismuth Vanadate ($BiVO_4$) based Photoanodes for the Removal of Organic Micropollutants in Water



Agha Zeeshan Ali

UV-Visible Light Driven Bismuth Vanadate ($BiVO_4$) based Photoanodes for the Removal of Organic Micropollutants in Water

Dissertation

for the purpose of obtaining the degree of doctor
at Delft University of Technology
by the authority of the Rector Magnificus,
Prof.dr.ir. H. Bijl,
chair of the Board of Doctorates
to be defended publicly on
Tuesday, 20 October 2026 at 10:00

by

Agha Zeeshan ALI

This dissertation has been approved by the promotors.

Composition of the doctoral committee:

Rector Magnificus,	chairperson
Prof.dr.ir. L.C. Rietveld	Delft University of Technology, promotor
Prof.dr.ir. J.P. van der Hoek	Delft University of Technology, promotor
Dr.ir. H.L.F.M. Spanjers	Delft University of Technology, promotor

Independent members:

Prof.dr.ir. J.R. van Ommen	Delft University of Technology, Netherlands
Dr.ir. C.H.M. Hofman	KWR Water Research Institute, Netherlands
Prof.dr.ir. R. Dewil	Katholieke Universiteit Leuven, Belgium
Prof.dr.-ing. Y. Zhang	Nanjing Tech University, China

Reserve member:

Prof.dr.ir. J.B. van Lier	Delft University of Technology

Keywords: Photoelectrocatalysis, water treatment, organic micropollutants, photocatalysis, advanced oxidation processes, photoanodes, heterojunction anodes

Printed by: Ridderprint

Cover by: Agha Zeeshan Ali

Copyright: 2026 by Agha Zeeshan Ali

An electronic version of this dissertation is available at: http://repository.tudelft.nl

Samenvatting

De toenemende verontreiniging van oppervlaktewater en grondwater met organische microverontreinigingen (organic micropollutants, OMP's) vormt een ernstig risico voor het milieu en de volksgezondheid. Deze OMP's zijn afkomstig uit onder andere huishoudelijke en industriële afvalwaterstromen en omvatten farmaceutische stoffen, pesticiden, stoffen uit persoonlijke verzorgingsproducten en industriële chemicaliën. Hoewel deze stoffen doorgaans voorkomen in concentraties variërend van ng L^{-1} tot enkele µg L^{-1}, zijn veel ervan persistent en biologisch actief en kunnen zij bijdragen aan antibioticaresistentie, hormoonverstorende effecten en in sommige gevallen zelfs carcinogene effecten. De huidige afvalwaterzuiveringstechnologieën zijn onvoldoende in staat om veel van de in afvalwater aanwezige OMP's volledig te verwijderen. Daarom zijn aanvullende zuiveringsstappen noodzakelijk.

Binnen de geavanceerde zuiveringstechnologieën hebben foto-elektrokatalytische geavanceerde oxidatieprocessen (photoelectrocatalytic advanced oxidation processes, PEC-AOP's) toenemende belangstelling gekregen vanwege hun vermogen om reactieve zuurstofspecies (reactive oxygen species, ROS) te genereren, zoals hydroxylradicalen (•OH) en superoxideradicalen ($•O_2^-$). Deze reactieve species kunnen OMP's afbreken tot minder schadelijke verbindingen of deze zelfs volledig mineraliseren. Bismutvanadaat ($BiVO_4$) is naar voren gekomen als een fotokatalysator die actief is onder zichtbaar licht en daardoor veelbelovend is voor toepassing in PEC-AOP's. Dit is onder andere te danken aan de relatief kleine bandgap van ongeveer 2,4 eV en de goede fotostabiliteit. De praktische toepassing ervan wordt echter beperkt door snelle recombinatie van ladingsdragers en door beperkingen bij opschaling naar toepassingen met realistisch afvalwater. De meeste bestaande studies richten zich op één enkele verontreiniging bij relatief hoge concentraties van 1–10 mg L^{-1} in gedemineraliseerd of ultrapuur water. Er is daarentegen relatief weinig aandacht besteed aan realistischer omstandigheden waarin mengsels van verschillende OMP's bij concentraties lager dan 1 mg L^{-1} aanwezig zijn. Daarnaast zijn slechts weinig studies gericht op opschaling met behulp van simulaties op proces- of reactorniveau. Belangrijke kennislacunes betreffen daarom zowel de gelijktijdige verwijdering van meerdere OMP's bij concentraties lager dan 1 mg L^{-1} als de vertaling van inzichten uit laboratoriumexperimenten naar conceptuele reactormodellen waarin realistische operationele variabelen worden meegenomen.

Dit proefschrift presenteert een uitgebreide studie naar $BiVO_4$-gebaseerde fotoanoden voor de foto-elektrokatalytische verwijdering van OMP's, met als doel zowel afzonderlijke als meerdere OMP's effectief te verwijderen uit gedemineraliseerd water bij concentraties lager dan 1 mg L^{-1}. Om deze doelstelling te bereiken, werd eerst zuiver $BiVO_4$ onderzocht als referentie-fotoanode die actief is onder zichtbaar licht. Vervolgens werden twee heterojunctiestrategieën onderzocht om de intrinsieke beperking van $BiVO_4$ als gevolg van recombinatie van ladingsdragers te verminderen. Een $BiVO_4$/BiOI-heterojunctie werd

geselecteerd om de ladingsscheiding te verbeteren en de absorptie van zichtbaar licht te vergroten. Daarnaast werd TiO_2-GO gekoppeld aan $BiVO_4$ om de ladingsscheiding en de eigenschappen van het grensvlak verder te verbeteren. Grafeenoxide (GO) werd aan de TiO_2-laag toegevoegd vanwege het vermogen om de ladingsscheiding te bevorderen en vanwege het hoge specifieke oppervlak, waardoor de adsorptie en interactie van OMP-moleculen met het fotoanode-oppervlak kunnen worden verbeterd. Daarnaast werd de opschaling van de reactor onderzocht met behulp van computational fluid dynamics (CFD).

Zuivere $BiVO_4$-fotoanoden werden vervaardigd op met fluor gedoteerde tinoxide-substraten (FTO) met behulp van een eenvoudige dipcoatingmethode, gevolgd door thermische behandeling gedurende 2 uur bij 460 °C. De fotoanoden werden structureel en opto-elektronisch gekarakteriseerd en vervolgens getest voor de gelijktijdige verwijdering van drie milieurelevante OMP's: acetaminofen, benzotriazool en propranolol, elk met een concentratie van 45 $\mu g\ L^{-1}$ in gedemineraliseerd water. Bij een aangelegde potentiaal van 1 V ten opzichte van Ag/AgCl en onder gesimuleerde zonnestraling werden binnen 2 uur verwijderingsrendementen van 99% bereikt voor zowel acetaminofen als propranolol en van 70% voor benzotriazool. De afbraak volgde eerste-ordekinetiek, met snelheidsconstanten van respectievelijk $2{,}84 \times 10^{-2}$, $2{,}44 \times 10^{-2}$ en $9{,}35 \times 10^{-3}\ min^{-1}$ voor acetaminofen, propranolol en benzotriazool. Hieruit bleek dat benzotriazool aanzienlijk langzamer werd afgebroken. Quenching-experimenten toonden aan dat •OH het dominante reactieve species was.

Daarnaast werden bismutvanadaat/bismutoxyjodide ($BiVO_4$/BiOI)-heterojunctiefotoanoden vervaardigd via elektrodepositie, waarbij zowel de depositietijd als de aangelegde depositiepotentiaal werden geoptimaliseerd. Na structurele en opto-elektronische karakterisering werden de fotoanoden getest voor de verwijdering van acetaminofen met een concentratie van 40 $\mu g\ L^{-1}$ in gedemineraliseerd water. In een drie-elektroden-PEC-cel bereikte de $BiVO_4$/BiOI-fotoanode, bij een aangelegde potentiaal van 1 V ten opzichte van Ag/AgCl en onder gesimuleerde zonnestraling, binnen 2 uur een verwijderingsrendement van 87% voor acetaminofen. Ter vergelijking werd met de zuivere $BiVO_4$-fotoanode een verwijderingsrendement van 66% bereikt. De eerste-orde-snelheidsconstante nam toe van $9{,}32 \times 10^{-3}\ min^{-1}$ voor $BiVO_4$ tot $1{,}46 \times 10^{-2}\ min^{-1}$ voor $BiVO_4$/BiOI, wat overeenkomt met een toename van 57%. Deze verbetering werd toegeschreven aan een efficiëntere ladingsscheiding en een verminderde recombinatie van ladingsdragers als gevolg van de vorming van de heterojunctie.

Vervolgens werd een bismutvanadaat/titaandioxide-grafeenoxide ($BiVO_4$/TiO_2-GO)-heterojunctiefotoanode onderzocht als tweede strategie om de PEC-prestaties van $BiVO_4$ te verbeteren. TiO_2 werd gekoppeld aan $BiVO_4$ om een heterojunctie te vormen en daarmee de ladingsscheiding te verbeteren. GO werd in de TiO_2-laag opgenomen om de ladingsscheiding verder te bevorderen en het specifieke oppervlak voor interactie met OMP-moleculen te vergroten. De $BiVO_4$/TiO_2-GO-fotoanoden werden vervaardigd met behulp van ultrasone

sproeipyrolyse, een schaalbare depositietechniek waarmee uniforme coatings kunnen worden verkregen. Structurele en optische karakterisering bevestigden de succesvolle vorming van de heterojunctie tussen $BiVO_4$ en TiO_2-GO. De vervaardigde fotoanoden werden getest voor de gelijktijdige verwijdering van vier OMP's: benzotriazool, carbamazepine, cafeïne en diclofenac, elk met een concentratie van 40 µg L^{-1} in gedemineraliseerd water. In een drie-elektroden-PEC-reactor, bedreven bij een aangelegde potentiaal van 1 V ten opzichte van Ag/AgCl en onder gesimuleerde zonnestraling, bereikte de $BiVO_4/TiO_2$-GO-heterojunctiefotoanode binnen 3 uur verwijderingsrendementen van 100% voor diclofenac, 54% voor carbamazepine, 36% voor benzotriazool en 33% voor cafeïne. In vergelijking met de zuivere $BiVO_4$-fotoanode vertoonde de heterojunctie ongeveer 50% hogere verwijderingsrendementen voor benzotriazool, carbamazepine en cafeïne. De bijbehorende eerste-orde-snelheidsconstanten bedroegen $3{,}90 \times 10^{-2}$ min^{-1} voor diclofenac, $4{,}30 \times 10^{-3}$ min^{-1} voor carbamazepine, $2{,}60 \times 10^{-3}$ min^{-1} voor benzotriazool en $2{,}40 \times 10^{-3}$ min^{-1} voor cafeïne. De aanzienlijk snellere afbraak van diclofenac kon worden verklaard door de gecombineerde verwijdering via zowel fotolyse als PEC-oxidatie, evenals door verschillen in stofspecifieke reactiviteit ten opzichte van de gevormde reactieve species.

Om de opschaalbaarheid en de operationele prestaties van het systeem te beoordelen, werden CFD-simulaties uitgevoerd voor een conceptuele, op $BiVO_4/TiO_2$-GO gebaseerde PEC-reactor voor de gelijktijdige verwijdering van dezelfde vier OMP's als beschreven in de voorgaande paragraaf. In het model werden experimenteel bepaalde afbraaksnelheden, stromingsdynamica, reactorgeometrie en lichtverdeling geïntegreerd. De simulatieresultaten lieten zien dat zowel de reactorgeometrie als het stromingsregime een aanzienlijke invloed hebben op de fotonenverdeling en het massatransport. Geoptimaliseerde kanaalconfiguraties resulteerden in een voorspelde verbetering van de OMP-verwijdering met 20–30%. Operationele parameters zoals het debiet, de lichtintensiteit en de afstand tussen de elektroden werden geïdentificeerd als kritische ontwerpvariabelen. Het model voorspelde hogere verwijderingsrendementen onder turbulente stromingscondities als gevolg van werveldiffusie en verbeterde convectieve menging. Onder geoptimaliseerde turbulente omstandigheden en bij een lichtintensiteit van 400 W m^{-2} voorspelde het reactormodel een verwijderingsrendement van 80% voor alle vier de OMP's binnen 25 minuten.

Concluderend werd in dit proefschrift aangetoond dat $BiVO_4$-gebaseerde fotoanoden in staat zijn om meerdere OMP's bij zeer lage concentraties effectief te verwijderen uit gedemineraliseerd water onder UV-zichtbare bestraling. De combinatie van experimentele inzichten en CFD-gebaseerde opschaling identificeert belangrijke routes om de kloof tussen prestaties op laboratoriumschaal en het ontwerp van praktisch toepasbare PEC-reactoren te overbruggen. De resultaten van dit onderzoek dragen daarmee bij aan de verdere ontwikkeling van PEC-AOP-technologie voor toekomstige integratie als tertiaire zuiveringsstap in afvalwaterzuiveringssystemen gericht op de verwijdering van organische microverontreinigingen.

Summary

The increasing contamination of surface water and groundwater with organic micropollutants (OMPs) poses serious environmental and public health risks. These OMPs, originating from municipal and industrial wastewater streams, include pharmaceuticals, pesticides, personal care products and industrial chemicals. Although typically present in concentrations ranging from ng L^{-1} to few µg L^{-1}, they are persistent, bioactive and can lead to antibiotic resistance, endocrine disruption and even carcinogenic effects. Current wastewater treatment technologies are ineffective towards the complete removal of most OMPs present in the wastewater. Therefore, additional treatment steps are essential.

Among advanced treatment methods, photoelectrocatalytic based advanced oxidation processes (PEC-AOPs) have attracted increasing interest due to their ability to generate reactive oxygen species (ROS), such as hydroxyl radicals (•OH) and superoxide radicals ($•O_2^-$). These ROS can degrade OMPs into less harmful products or mineralizing them entirely. Bismuth vanadate ($BiVO_4$) has emerged as a visible-light-responsive photocatalyst for PEC-AOPs due to its narrow band gap (~2.4 eV) and photostability. However, its practical application is limited by fast charge recombination and limited scalability in real wastewater. Most studies are limited to a single pollutant at high concentrations (1–10 mg L^{-1}) in demineralized or ultra-pure water, with limited attention to real-world scenarios involving mixtures of OMPs at concentrations below 1 mg L^{-1}. Moreover, few studies address scalability using process level simulations. Knowledge gaps thus include understanding the simultaneous removal of multiple OMPs at concentrations below 1 mg L^{-1} and integrating lab-scale reaction insights into conceptual reactor models using realistic operational variables.

This dissertation presents a comprehensive study on $BiVO_4$ based photoanodes for the photoelectrocatalytic removal of OMPs, with the objective of effectively removing single and multiple OMPs from demineralized water at concentrations below 1 mg L^{-1}. To achieve this objective, pristine $BiVO_4$ was first investigated as a baseline visible-light-responsive photoanode. Subsequently, two heterojunction strategies were investigated to overcome the intrinsic charge-carrier recombination limitation of $BiVO_4$. $BiVO_4$/BiOI was selected to enhance charge separation and extend visible-light absorption, whereas TiO_2-GO was coupled with $BiVO_4$ to further improve charge separation and interfacial properties. In the TiO_2-GO layer, graphene oxide (GO) was incorporated because of its ability to promote charge separation and provide a high specific surface area for adsorption of OMP molecules. In addition, the study explored reactor scale-up using computational fluid dynamics (CFD). Pristine $BiVO_4$ photoanodes using a simple dip-coating method on fluorine-doped tin oxide (FTO) substrates have been fabricated, followed by thermal annealing at 460°C for 2 h. These photoanodes were structurally and opto-electronically characterized and subsequently tested for the simultaneous removal of three environmentally relevant OMPs - acetaminophen, benzotriazole and propranolol - each at 45 µg L^{-1} in demineralized water. When operated at an

applied voltage of 1 V (vs Ag/AgCl) under simulated solar irradiation, the photoanode achieved removal efficiency of 99% for both acetaminophen and propranolol and 70% for benzotriazole within 2 h. The degradation followed first-order kinetics, with rate coefficients of 2.84×10^{-2}, 2.44×10^{-2}, and 9.35×10^{-3} min^{-1} for acetaminophen, propranolol, and benzotriazole, respectively, demonstrating substantially slower degradation of benzotriazole. Quenching experiments indicated that •OH was the dominant reactive species.

In addition, bismuth vanadate/bismuth oxyiodide ($BiVO_4$/BiOI) heterojunction photoanodes have been fabricated using an electrodeposition method, with optimization of deposition time and voltage. Following structural and optoelectronic characterization, the photoanodes were tested for the removal of acetaminophen (40 µg L^{-1}) in demineralized water. In a three-electrode PEC cell, the $BiVO_4$/BiOI photoanode, operated at an applied voltage of 1 V (vs Ag/AgCl) under simulated solar irradiation, achieved a removal efficiency of 87% for acetaminophen within 2 h, compared to 66% achieved by the pristine $BiVO_4$ photoanode. The first-order rate coefficient increased from 9.32×10^{-3} min^{-1} for $BiVO_4$ to 1.46×10^{-2} min^{-1} for $BiVO_4$/BiOI, corresponding to a 57% increase. The improvement was associated with enhanced charge separation and reduced charge-carrier recombination resulting from heterojunction formation.

Subsequently, pristine bismuth vanadate/titanium dioxide-graphene oxide ($BiVO_4$/TiO_2-GO) heterojunction photoanodes have been fabricated using ultrasonic spray pyrolysis, a scalable and uniform deposition technique. Structural and optical characterization confirmed the successful formation of the heterojunction between $BiVO_4$ and TiO_2-GO. The fabricated photoanodes were tested for the simultaneous removal of four OMPs; benzotriazole, carbamazepine, caffeine and diclofenac, each at 40 µg L^{-1} in demineralized water. In a three-electrode PEC reactor operated at an applied voltage of 1 V (vs Ag/AgCl) under simulated solar irradiation, the $BiVO_4$/TiO_2-GO heterojunction photoanode achieved removal efficiencies of 100% for diclofenac, 54% for carbamazepine, 36% for benzotriazole and 33% for caffeine within 3 h. Compared to the pristine $BiVO_4$ photoanode, the heterojunction showed approximately 50% higher removal efficiencies for benzotriazole, carbamazepine and caffeine. The corresponding first-order rate coefficients were 3.90×10^{-2} min^{-1} for diclofenac, 4.30×10^{-3} min^{-1} for carbamazepine, 2.60×10^{-3} min^{-1} for benzotriazole, and 2.40×10^{-3} min^{-1} for caffeine. The substantially faster degradation of diclofenac reflected its combined removal through photolysis and PEC oxidation and differences in compound-specific reactivity toward the generated reactive species. To assess the scalability and operational performance of the system, CFD simulations were conducted to model a conceptual $BiVO_4$/TiO_2-GO based PEC reactor for the simultaneous removal of the same four OMPs as mentioned in previous paragraph. The model incorporated experimentally derived degradation kinetics, flow dynamics, reactor geometry, and light distribution. Simulation results demonstrated that reactor geometry and flow regime considerably affect photon distribution and mass transfer, with optimized channel configurations, improving predicted OMP removal by 20–30%.

Operational variables such as flow rate, light intensity, and electrode spacing were identified as critical design parameters. The model predicted enhanced removal efficiencies under turbulent flow conditions due to eddy diffusion and convective mixing. Under optimized turbulent conditions and a light intensity of 400 W m^{-2}, the reactor achieved 80% removal of all four OMPs within 25 min.

In conclusion, in this dissertation it was demonstrated that $BiVO_4$ based photoanodes are capable of effectively removing multiple OMPs at trace concentrations in demineralized water under UV-visible light. The combination of experimental insights and CFD-based upscaling highlights critical pathways to bridge lab-scale performance with practical PEC reactor design. These findings contribute to advancing PEC-AOP technology for future integration into tertiary wastewater treatment systems aimed at OMP abatement.

Table of Contents

Chapter 1 Introduction..... 10

Chapter 2 $BiVO_4$ based photoanodes for the photoelectrocatalytic removal of trace organic pollutants from water: A mini review on recent developments..... 19

Chapter 3 Photoelectrocatalytic based simultaneous removal of multiple organic micro-pollutants by using a visible light driven $BiVO_4$ photoanode..... 27

Chapter 4 Photo-electrocatalytic based removal of acetaminophen: Application of visible light driven heterojunction based $BiVO_4$/BiOI photoanode 53

Chapter 5 Simultaneous removal of multiple organic micropollutants via UV-visible light driven $BiVO_4/TiO_2$-GO photoanode: Experimental and CFD study..... 73

Chapter 6 Conclusions and outlook..... 99

Chapter 1
Introduction

1. Occurrence and harmful effects of organic micropollutants

Organic micropollutants (OMPs) encompass a broad range of organic compounds, including pharmaceuticals, pesticides, personal care products and industrial chemicals. These contaminants are typically present in water bodies at very low concentrations, ranging from nanograms per litre (ng L^{-1}) to micrograms per litre (µg L^{-1}) [1]. Anti-inflammatory compounds such as acetaminophen and diclofenac are among the most frequently detected OMPs in wastewater effluents and surface waters [2]. Current, conventional wastewater treatment technologies are ineffective towards the complete removal of most OMPs present in the wastewater [3]. Hence, a wide range of OMPs are being released into surface water through effluent discharge from wastewater treatment plants (WTTPs). European groundwater bodies are also being contaminated with OMPs due to the interaction between groundwater and surface water resources such as rivers and wetlands, contaminated with OMPs [4]. Fig. 1.1 illustrates the common sources and pathways through which OMPs are being released into the environment.

Despite their low concentration in surface waters, OMPs pose a threat to both the aquatic environment and human health, if not effectively removed during drinking water treatment. Even a low concentration (50-2300 ng L^{-1}) of the biocide triclosan (antiseptic agent) is found to be toxic to green algae, which can disturb the balance of entire aquatic ecosystems [4]. Human ingestion of OMPs (e.g., through inadequately treated drinking water) can lead to serious health effects such as endocrine disruption, cancer and developmental disorders [5]. Pharmaceuticals like estrone and 17-β estradiol, having estrogenic properties, can cause breast

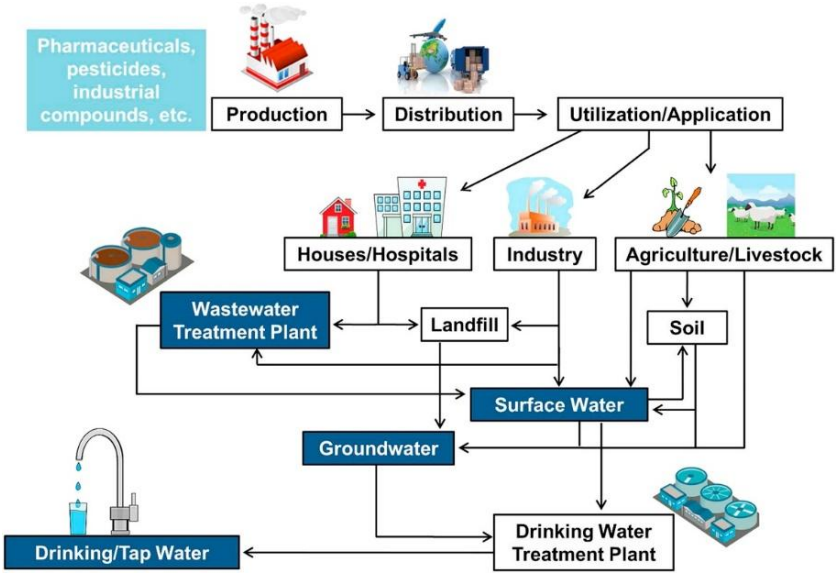


Fig. 1.1: *Sources and routes of organic micropollutants release in the environment [101].*

cancer and fertility problems in women [6]. Acetaminophen, frequently detected in surface waters, may cause liver toxicity and other chronic health effects with prolonged exposure.[7]. Most of the OMPs in the recent European watch list of substances for union wide monitoring are pharmaceuticals, such as antibiotics, antidepressants and azole compounds [8].

In surface water and groundwater, OMPs are rarely found as individual contaminants; rather, they typically occur as a mixture of several OMPs [9]. The physicochemical interaction between OMPs impacts the overall toxicity of surface water and groundwater [10]. Several studies have shown that mixtures of OMPs can be more toxic than the sum of (the toxicity of) individual compounds, even when each is present at a concentration below its no-observed effect level [11]. A mixture containing pharmaceuticals and pesticides can cause toxic effects in zebra fish embryos, aquatic invertebrates and algae [12]. Therefore, the toxicity of mixtures of OMPs, present in environmental samples, should be evaluated and treatment technologies should simultaneously remove multiple OMPs.

2. Technologies to remove OMPs in water

2.1 Current technologies to remove OMPs in water

Conventional wastewater treatment technologies are effective towards the removal of carbon, nitrogen, and phosphorous from wastewater, with a high removal efficiency [13]. However, conventional wastewater treatment technologies are not effective towards the complete removal of OMPs. Several treatment technologies have already been applied in some WWTPs to remove OMPs, including adsorption, ozonation, membrane filtration, and advanced oxidation processes (AOPs). These technologies are typically implemented as a quaternary treatment step, but their application remains limited and site-specific [14]. While the proposed Urban Wastewater Treatment Directive by the European Parliament does not prescribe specific technologies, it encourages the implementation of effective treatment for OMP removal. According to the directive, all EU member states must ensure that by 2045, WWTPs are equipped with suitable technologies to effectively remove OMPs from wastewater. (“Procedure File: 2022/0345(COD) | Legislative Observatory | European Parliament”).

Adsorption is one of the methods for removing OMPs from wastewater, and technologies based on this principle can also allow for adsorbent reuse, provided the material can be effectively regenerated. The main advantages of adsorption methods for OMP removal are their operational simplicity and the fact that no harmful chemicals are required. Activated carbon materials are widely used as adsorbents due to their high specific surface area and porous structure, which provide numerous active sites for the adsorption of OMP molecules [16]. The adsorption mechanisms involve both physical and chemical adsorption, intraparticle diffusion, and interactions between OMPs and the functional groups present on the adsorbent surface [17]. Activated carbon can effectively remove a wide range of OMPs, including pharmaceuticals, pesticides, and synthetic dyes [18]. However, its regeneration is energy-

intensive and costly. Thermal regeneration is the most common method, but it can cause partial degradation of the carbon structure, leading to reduced adsorption capacity over time [19]. Moreover, both the production and thermal regeneration of activated carbon are associated with a high CO_2 footprint, presenting a significant environmental challenge. [20]. As one of the alternative adsorbents, carbon nanotubes also have a high specific surface area to adsorb OMPs through van der Waals forces, hydrogen bonding and electrostatic interaction. However, their tendency to agglomerate in water makes recycling difficult, and a post-treatment filtration step is often required to completely remove carbon nanotubes from the treated effluent [21]. Additionally, the high production cost of carbon nanotubes and their potential toxicity to aquatic organisms limit their suitability for large-scale applications.

Ozonation, one of oxidation processes used for OMPs removal, involves the use of ozone, being one of the strongest oxidants and disinfectants in water treatment, through the dosage of ozone gas. Ozone can oxidize OMP molecules either directly or indirectly by generating hydroxyl radicals (•OH) in water. •OH are highly reactive and possess a higher oxidation potential (2.8 V) than ozone (2.07 V) itself [22]. •OH can oxidize OMPs through various pathways, including hydrogen abstraction, which produces organic radicals [21]. The removal efficiency after a given time period of ozonation for a specific OMP depends on the reaction rate coefficients of both ozone and •OH with the OMP molecules. Removal efficiency of ozonation is higher for OMPs containing electron rich moieties, which include phenols, anilines and amines [23]. In most of the cases, ozonation does not completely oxidise the OMP molecules in water but only converts them into smaller transformation products. Incomplete oxidation or mineralization of OMPs during ozonation can result from the selective and compound-specific reactivity of molecular ozone and from limited exposure to hydroxyl radicals (•OH). Although •OH reacts rapidly and non-selectively with most OMPs, typically with second-order rate constants of 10^8-10^{10} M^{-1} s^{-1}, its steady-state concentration and lifetime in water are very low because of rapid reactions with both target compounds and scavenging constituents in the water matrix, such as natural organic matter and carbonate/bicarbonate species. Consequently, competition for •OH and insufficient oxidant exposure may limit complete mineralization and lead to the formation and persistence of transformation products [24][25]. Adsorption can then be added as a post treatment step after ozonation to adsorb the unoxidized OMPs and (most) oxidation by-products [24].

Membrane separation is an alternative treatment method, more commonly used in drinking water treatment. Membrane filtration is a pressure-driven process that removes pollutants by passing feed water through a membrane, which retains contaminants larger than the membrane's pore size. Microfiltration and ultrafiltration are commonly used in water treatment to remove suspended solids, colloids, bacteria, and some viruses. [26]. The pore sizes of microfiltration and ultrafiltration membranes are not suitable for effectively removing OMPs. However, nanofiltration and reverse osmosis have been employed in pilot-scale studies for the removal of OMPs from WWTP effluents [27,28]. Size exclusion, electrostatic repulsion, and

solute-membrane interactions are the primary mechanisms involved in the removal of OMPs in nanofiltration and reverse osmosis processes. Nanofiltration and reverse osmosis are efficient in the removal of large ionic OMPs but these membranes show lower removal for small hydrophilic OMPs [26,29]. Most of the nanofiltration and reverse osmosis membranes are negatively charged, which creates a electrostatic repulsion for negatively charged organic molecules [30]. Therefore, nanofiltration and reverse osmosis membranes are more selective for the removal of negatively charged OMPs, especially when the molecules are too small to be removed by size exclusion alone. High operational costs, membrane fouling, and the accumulation of OMP concentrates over time are generally considered as major drawbacks of using nanofiltration and reverse osmosis for large-scale applications [31].

Advanced oxidation processes (AOPs), such as the Fenton reaction, UV/H_2O_2, electrochemical oxidation (eAOP), photocatalytic oxidation, photoelectrocatalytic (PEC) oxidation, and sulfate radical-based AOPs, can fully oxidize OMPs in aqueous solutions, particularly under optimized conditions where sufficient reactive oxygen species (e.g., •OH and superoxide radicals ($•O_2^-$)) are generated to achieve complete mineralization. [32]. In Fenton reactions, the production of hydroxyl radicals (•OH) from hydrogen peroxide (H_2O_2) is catalysed by iron species such as Fe^{2+}, Fe_2O_3, and Fe_3O_4 [33]. In the UV/H_2O_2 process, H_2O_2 undergoes photolysis upon exposure to ultraviolet (UV) light, leading to the generation of •OH, then unselectively oxidizing OMPs present in the water [34]. In eAOPs, electrochemical cells, consisting of an anode and a cathode are used and •OH are electrochemically produced at the surface of the anode by a water oxidation reaction. Boron doped diamond has widely been studied as an anode material for the removal of OMPs in either synthetic wastewater or real WTTP effluent [35]. Semiconducting photocatalysts are used in photocatalytic oxidation for the production of •OH and $^{\bullet}O_2^-$ to oxidize the OMPs within the vicinity of photocatalysts [36]. Photocatalysts that absorb UV and visible light, such as titanium dioxide (TiO_2) and zinc oxide (ZnO), have widely been reported in literature for the removal of dyes, pharmaceuticals, and other OMPs from water. [37]. Photocatalytic materials generate electron (e^-) – hole (h^+) pairs when irradiated with photons whose energy equals or exceeds the catalyst's band gap. Photogenerated holes at the catalyst surface oxidize adsorbed water or hydroxide ions to produce highly reactive •OH, while the electrons reduce dissolved oxygen to form superoxide radicals ($•O_2^-$). However, the short lifetimes of these charge carriers often lead to fast recombination, significantly reducing the efficacy of photocatalytic AOPs [38].

2.2 Photoelectrocatalytic based advanced oxidation process

PEC based AOP combines the principles of photocatalytic AOP and eAOP. Similar to photocatalytic AOP, PEC systems use semiconducting photocatalysts as photoanodes in a photoelectrochemical cell to generate reactive oxygen species such as •OH and $^{\bullet}O_2^-$ [39]. A positive voltage is applied to the photoanode to reduce the rate of recombination of photogenerated holes and electrons in the photocatalyst. Fig. 1.2 illustrates the PEC process

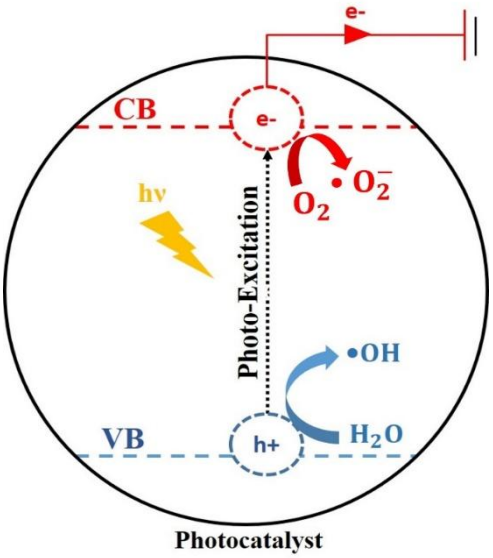


Fig. 1.2: *Illustration of the PEC process for the in-situ generation of hydroxyl (•OH) and superoxide radicals ($•O_2^-$).*

VB = valence band of the photocatalyst

CB = conduction band of the photocatalyst

for the production of •OH and $•O_2^-$ in water. Reducing the rate of recombination in the photocatalysts enhances the removal efficiency of the photoanode for OMPs in water [39]. Several metal oxide photocatalysts such as TiO_2[40], tungsten trioxide [41], ZnO [42] and zirconium dioxide [43] have been used in previous studies for the removal of pharmaceuticals (1-10 mg L^{-1}) and dyes (1-10 mg L^{-1}) in water. Most of these photocatalysts have the intrinsic drawback that they can only absorb photons in the UV range of the solar spectrum due to their large band gap energy (3.0 - 3.5 eV). The UV range of solar spectrum is less than 10%, meaning that majority of the solar energy is not utilized if UV driven photocatalysts are used.

Bismuth vanadate ($BiVO_4$) is a visible light driven metal oxide photocatalyst with a small band gap energy (~2.4 eV) [44]. Over the past decade, monoclinic scheelite-phase $BiVO_4$ has been used as a photoanode material for PEC based removal of OMPs (1–10 mg L^{-1}) from water [45]. To reduce the rate of recombination of photogenerated charge carriers, $BiVO_4$ is often combined with other photocatalysts to form a heterojunction [45]. Most of the previous studies used $BiVO_4$ as a photoanode for the PEC based removal of only one OMP in water with a pollutant concentration between 1 and 10 mg L^{-1}, although OMPs typically occur as mixtures in surface water and groundwater, while their concentrations in these environments generally range from ng L^{-1} to µg L^{-1}[1].

2.3 Knowledge gaps

Based on the literature review presented in Chapter 2, it can be concluded that PEC based AOP utilizing $BiVO_4$ based photoanodes can remove OMPs from water. However, several knowledge gaps must be addressed to enable the successful implementation of this technology in practice:

- Although $BiVO_4$-based photoanodes have been investigated for PEC degradation of organic pollutants, most previous studies have employed pollutant concentrations in the mg L^{-1} range. At environmentally relevant concentrations in the µg L^{-1} range, the lower flux of pollutant molecules toward the photoanode surface may increase the importance

of mass-transfer limitations relative to surface reaction kinetics. Consequently, there is limited understanding of the degradation kinetics and controlling processes of OMPs at environmentally relevant concentrations.

- OMPs occur as mixtures in aquatic environments, whereas PEC studies using $BiVO_4$ photoanodes have predominantly investigated individual pollutants. During simultaneous treatment, individual OMPs can exhibit markedly different degradation kinetics because of differences in molecular structure, reactivity toward photogenerated reactive species, and transport to the photoanode-electrolyte interface. However, there is limited understanding of the compound-specific degradation behaviour and dominant reactive species during the simultaneous PEC treatment of OMP mixtures at environmentally relevant concentrations.
- Heterojunction formation is an established strategy for improving charge separation and reducing electron–hole recombination in $BiVO_4$ photoanodes. However, it remains unclear how these improvements translate into enhanced PEC degradation kinetics at environmentally relevant OMP concentrations and whether heterojunction photoanodes can maintain their performance during the simultaneous degradation of multiple OMPs. Furthermore, the relationship between heterojunction-induced charge separation, reactive-species generation, and OMP degradation remains poorly understood.
- Translation of laboratory-scale PEC performance to larger continuous-flow reactors is limited by insufficient understanding of how reactor hydrodynamics and geometry influence the transport of OMPs from the bulk liquid to the photoanode surface. Non-uniform flow distribution and insufficient mixing can create mass-transfer limitations and spatially non-uniform degradation, making laboratory-derived reaction kinetics insufficient on their own to predict reactor-scale performance. Therefore, the effects of flow regime, velocity distribution, reactor geometry, and photoanode configuration on OMP mass transfer and PEC reactor performance require further investigation.

3. Research objective and research questions

The main objective of this dissertation is to develop, characterize, and evaluate $BiVO_4$ based heterojunction photoanodes for the photoelectrocatalytic removal of mixtures of organic micropollutants (OMPs) at environmentally relevant concentrations (<50 μg L^{-1}). In addition, the study aims to assess the scalability and reactor performance of the developed system through computational fluid dynamics simulations. To achieve the main research objective, the following research questions (RQ) were formulated.

RQ 1. What are the key limitations in the scientific understanding and technological application of $BiVO_4$-based photoanodes for the photoelectrocatalytic removal of organic micropollutants from water, particularly at environmentally relevant concentrations?

RQ 2. What factors govern the different photoelectrocatalytic degradation kinetics of multiple OMPs during their simultaneous removal by a $BiVO_4$ photoanode at environmentally relevant concentrations?

RQ 3. How does the formation of a $BiVO_4$/BiOI heterojunction influence charge separation and reactive-species generation, and how do these changes affect the degradation kinetics of acetaminophen at environmentally relevant concentration?

RQ 4. How does the formation of a $BiVO_4$/TiO_2-GO heterojunction affect the simultaneous photoelectrocatalytic degradation kinetics of multiple OMPs at environmentally relevant concentrations compared with pristine $BiVO_4$?

RQ 5. How do reactor hydrodynamics and geometry affect the mass transfer of OMPs to the photoanode surface, and how can these parameters be optimized to overcome mass-transfer limitations during scale-up of a PEC reactor?

4. Thesis outline

Chapter 2 presents a comprehensive review of pharmaceutical and industrial pollutants removed using $BiVO_4$-based photoanodes. It discusses strategies to reduce charge carrier recombination in pristine $BiVO_4$ to enhance OMP removal efficiency and evaluates the potential for scaling up $BiVO_4$-based photoanodes for large-scale applications.

Chapter 3 presents the application of $BiVO_4$ photoanodes for the PEC-based simultaneous removal of acetaminophen, benzotriazole, and propranolol, each at an initial concentration of 45 μg L^{-1} in demineralized water. A suitable reaction kinetics model was used to calculate the rate coefficients for each compound. The role of reactive species in OMP degradation was studied through quenching experiments, and the reusability of the fabricated photoanodes was also evaluated.

Chapter 4 discusses the application of a $BiVO_4$/BiOI heterojunction photoanode for the PEC-based removal of acetaminophen (40 μg L^{-1}) in demineralized water. $BiVO_4$, BiOI, and $BiVO_4$/BiOI photoanodes were fabricated using an electrodeposition method. Optical, opto-electronic, and material characterization techniques confirmed the successful deposition of photocatalytic layers and the formation of the heterojunction. The influence of fabrication parameters (deposition time and applied voltage) on removal efficiency was examined to identify optimal conditions. The performance of the heterojunction was also compared to that of pristine $BiVO_4$ photoanodes. A reaction kinetics model was used to calculate the rate coefficient for acetaminophen degradation, and the role of reactive species was assessed through quenching experiments. Additionally, the reusability of the heterojunction photoanode was evaluated**.**

Chapter 5 explores the application of a $BiVO_4$/TiO_2-GO heterojunction photoanode for the PEC-based simultaneous removal of four OMPs; benzotriazole, carbamazepine, caffeine, and

diclofenac in demineralized water. The photoanodes were fabricated using ultrasonic spray pyrolysis, and their UV–visible light absorption properties were confirmed via UV–Vis absorbance spectroscopy. A first-order reaction kinetics model was applied to determine the rate coefficients for all four OMPs.

In addition, this chapter presents the use of CFD simulations to assess the simultaneous removal of benzotriazole, carbamazepine, caffeine, and diclofenac in a conceptually designed PEC water treatment reactor. The model, incorporating lab-derived reaction rate coefficients, was used to evaluate removal efficiency. The effects of reactor geometry and flow dynamics on system performance were also investigated.

Chapter 6 outlines the key conclusions and outlook for future research. It also highlights the scientific contribution of this dissertation as well as the practical implications of the findings.

Chapter 2

$BiVO_4$-based photoanodes for the photoelectrocatalytic removal of trace organic pollutants from water: A mini review on recent developments

This chapter is based on the following publication:

Agha Zeeshan Ali, Sanjeeb Mohapatra, Jan Peter van der Hoek, Henri Spanjers, BiVO4-based photoanodes for the photoelectrocatalytic removal of trace organic pollutants from water: A mini review on recent developments, Current Opinion in Environmental Science & Health, Volume 45, 2025, 100615, https://doi.org/10.1016/j.coesh.2025.100615

Abstract:
This mini review explores the potential of visible light driven $BiVO_4$ based photoanodes for removing trace organic pollutants from water. It highlights the advantages of using $BiVO_4$ based photoanodes over conventional UV driven photoanodes in water treatment. The mechanism of reactive species generation through water oxidation is discussed. The review also highlights the role of sulfate and sulfite radicals in enhancing pollutant degradation. Furthermore, it evaluates how heterojunction formation improves the removal efficiency of $BiVO_4$ based photoanodes by reducing charge carrier recombination. Limited research on $BiVO_4$ based photoanodes for the simultaneous removal of multiple organic pollutants at low concentrations (<1 mg L^{-1}) from real wastewater is identified as a key knowledge gap. Addressing this gap could advance the application of $BiVO_4$ based photoanodes in photoelectrocatalytic based advanced oxidation processes.

Keywords: Photoelectrocatalysis, $BiVO_4$ photoanodes, advanced oxidation processes, visible light driven catalysis, organic pollutant degradation, wastewater treatment.

1. Introduction

Organic pollutants such as synthetic dyes, pharmaceuticals and pesticides contaminate water resources and pose serious risks to human health and aquatic ecosystem [46] [47,48]. The concentrations of these organic pollutants vary by source and location, ranging from a few ng L^{-1} to several μg L^{-1} [49,50]. Conventional wastewater treatment technologies often fail to remove organic pollutants completely. As a result, these pollutants are released into the aquatic environment [51]. Advanced oxidation processes (AOPs) are gaining importance for the removal of organic pollutants [52]. AOPs generate hydroxyl radicals (•OH) and superoxide radicals ($^{\bullet}O_2^-$) in water as the main reactive oxygen species (ROS), which degrade organic pollutants [53,54]. Among AOPs, photoelectrocatalytic (PEC) based AOP has gained attention due to its enhanced charge separation under applied voltage, which improves the ROS generation and removal efficiency for organic pollutants [55,56] [57] [58].

Bismuth vanadate ($BiVO_4$) is a small band gap (~2.4 eV) semiconducting photocatalyst, widely used in PEC AOPs for removing organic pollutants from aqueous solutions [45]. Fig. 2.1 illustrates a typical PEC cell for the removal of organic pollutants using a $BiVO_4$ photoanode. Electrons and holes are generated in the $BiVO_4$ photoanode upon its interaction with the incoming photons. The photogenerated holes oxidize the water molecules to produce •OH, whereas the photogenerated electrons reduce the oxygen to produce $^{\bullet}O_2^-$ [36]. An external voltage is applied to the photoanode to minimize electron-hole recombination, thereby enhancing charge separation [59]. Unlike conventional photocatalysts such as titanium oxide (TiO_2) [60], zinc oxide (ZnO) [61] and tungsten oxide (WO_3) [62], which primarily absorb UV light ($\lambda < 400$ nm), $BiVO_4$ can absorb both UV and visible light ($\lambda \leq 520$ nm), improving solar energy utilization [45]. $BiVO_4$ has demonstrated superior photocatalytic efficiency for water oxidation compared to TiO_2, ZnO, and WO_3 [63]. This is attributed to its favourable conduction

and valence band positions, which allow effective generation of reactive oxygen species (ROS) such as hydroxyl (•OH) and superoxide ($•O_2^-$) radicals. Additionally, $BiVO_4$ has a relatively positive valence band potential (~2.5 V vs. SHE), making it effective for oxidative degradation of organic pollutants [63]. Compared to ZnO, which undergoes photo-corrosion in aqueous solutions [64], $BiVO_4$ is more stable under visible light [65]. Additionally, it can be used effectively under neutral to slightly acidic conditions (pH 5-6), making it suitable for real wastewater treatment applications [66]. This mini review provides an analysis of recent advancements in the application of $BiVO_4$ based photoanodes for the removal of organic pollutants, with a particular emphasis on pharmaceuticals. It highlights the role of heterojunction in enhancing $BiVO_4$ removal efficiency by improving charge separation. Additionally, this review identifies critical knowledge gaps, particularly the limited research on $BiVO_4$ based photoanodes for the simultaneous removal of multiple organic pollutants at low concentrations (<1 mg L^{-1}) in real wastewater. Finally, it offers recommendations to guide future research and advance the application of $BiVO_4$ in PEC based water treatment.

2. Structural and optical properties of $BiVO_4$

$BiVO_4$ is a non-toxic, cost-effective n-type semiconductor with good chemical stability [45]. Its absorbance depends on its crystal structure, existing in three polymorphs: pucherite (orthorhombic), dreyerite (tetragonal zircon), and clinobisvanite (monoclinic scheelite or tetragonal scheelite) [67]. The monoclinic scheelite structure is favoured for photoelectrocatalysis due to its lower band gap energy (about 2.4 eV) [68] and reduced recombination rate of photogenerated carriers compared to the other crystal structures [69]. These properties are linked to the unique local bonding environment in monoclinic scheelite $BiVO_4$, making it more effective for PEC applications [70,71].

3. Photoelectrocatalytic removal of organic pollutants using $BiVO_4$ photoanodes

Monoclinic scheelite $BiVO_4$ photoanodes have been effectively utilized in laboratory scale research for the PEC removal of phenols, dyes and pharmaceuticals. Fluorine doped tin oxide (FTO) is mostly used as a substrate for the deposition of $BiVO_4$ [45]. Bennani et al. (2016) investigated the application of spray coated FTO/$BiVO_4$ photoanodes for the PEC based removal of phenol (20 mg L^{-1}) in demineralized water [72]. The fabricated photoanodes achieved a removal efficiency of 70% with an applied potential of 1.0 V (vs Ag/AgCl) after 4 hr reaction time. Under identical conditions, this efficiency was 14% higher than that observed with TiO_2 photoanodes. The higher removal efficiency of $BiVO_4$ is attributed to the visible light absorption and improved charge separation compared to TiO_2. Bacha et al. (2019) utilized $BiVO_4$ photoanodes to remove methyl orange (10 mg L^{-1}) in demineralized water under visible light, generated with a 300 W xenon lamp [73]. The fabricated photoanode removed only 11% of the methyl orange at an applied voltage of 2.0 V (vs Ag/AgCl) after 2 hr. However, after adding 16 mM of Na_2SO_3 in the electrolyte, 97% of methyl orange was removed after 2 hr with the same photoanode at 2.0V (vs Ag/AgCl). This increase was likely due to the generation

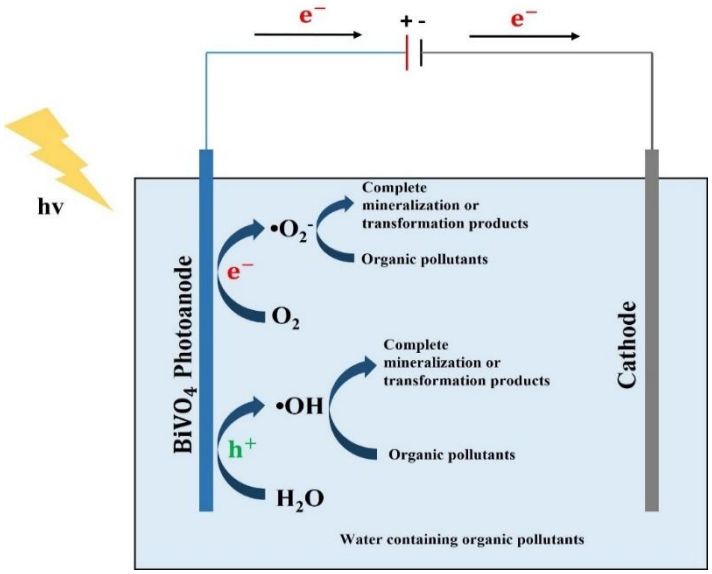


Fig. 2.1: *Schematic of the photoelectrocatalytic removal of organic pollutants from water using a BiVO4 photoanode. Solar photons (hv) interact with the photoanode, generating electron (e-)-hole (h+) pairs. These charge carriers facilitate the formation of hydroxyl and superoxide radicals, which oxidize the organic pollutants.*

of sulphite radicals ($SO_3^{\bullet-}$) through the interaction of sulphite anions (SO_3^{2-}) with the •OH radicals at the $BiVO_4$ surface. Similarly, in another study, the removal efficiency of $BiVO_4$ photoanode for bisphenol A (10 mg L^{-1}) was enhanced by the addition of peroxymonosulfhate (PMS) in the electrolyte [74]. PMS acted as an electron acceptor for the photogenerated electrons in $BiVO_4$, facilitating the generation of •OH radicals and enabling complete removal of bisphenol A at an applied voltage of 0.25 V (vs SCE) within 2 hr. Wang et al. (2020) investigated the use of $BiVO_4$ photoanode and polydopamine modified carbon felt (PDA/CF) cathode for the removal of ofloxacin (8 mg L^{-1}) [75]. They found that addition of 2 mM PMS in the electrolyte accelerates the removal reaction rate by generating sulphate radicals ($SO_4^{\bullet-}$), leading to complete ofloxacin removal within 2 hr at 1.5 V (vs Ag/AgCl). Based on the results of electron spin resonance, •OH radicals and $SO_4^{\bullet-}$ radicals were identified as the main oxidizing species responsible for the removal of ofloxacin. Cheng et al. (2019) demonstrated effective tetracycline (TC) removal using a $BiVO_4$ photoanode paired with a dual hemin/Cu-carbon cloth cathode [76]. The photogenerated holes in $BiVO_4$ produced •OH radicals and also directly oxidized the molecules of TC while the photogenerated electrons were transferred to the cathode for the production of H_2O_2. This combination of $BiVO_4$ photoanode and dual hemin/Cu-carbon cloth cathode removed 93.6% of TC after 2 hr reaction time with an applied voltage of 0.8 V (vs Ag/AgCl) to the photoanode.

$BiVO_4$ based heterojunction photoanodes

To improve charge separation, $BiVO_4$ is often combined with other photocatalysts to form a heterojunction. $BiVO_4$ based heterojunction photoanodes show higher removal efficiency for organic pollutants compared to pristine $BiVO_4$ photoanodes. Cao et al. (2018) investigated a $BiVO_4/Ag_3PO_4$ heterojunction photoanode for the PEC based removal of norfloxacin (5 mg L^{-1}), achieving complete removal within 90 min at 0.5 V (vs SCE), compared to 61.4% removal by pristine $BiVO_4$ photoanode [77]. The enhanced performance is attributed to the enhanced charge separation in the heterojunction photoanode, which increases •OH radicals production, significantly improving the removal kinetics. Table 2.1 summarizes recent studies that utilized $BiVO_4$ heterojunction photoanodes for the removal of organic pollutants.

Table 2.1: *Summary of recent studies using $BiVO_4$ heterojunction photoanodes for the removal of organic pollutants.*

Heterojunction photoanode	Configuration of PEC cell	Light intensity	Pollutant	Removal efficiency	Rate coefficient (k)	Ref
$BiVO_4/MnO_2$	Cathode: Pt sheet Applied potential: 1.5 V (vs Ag/AgCl)	100 W Xenon lamp with $\lambda \geq 420$ nm	Ciprofloxacin (C_0 = 10 mg L^{-1})	76%,2 hr	1.05×10^{-2} min^{-1}	[78]
$BiVO_4/Ag_2S$	Cathode: Pt sheet Applied potential: 1.2 V (vs Ag/AgCl)	100 W Xenon lamp with $\lambda \geq 420$ nm	Ciprofloxacin (C_0 = 10 mg L^{-1}) Sulfamethoxazole (C_0 = 10 mg L^{-1})	80%, 2 hr 86%, 2 hr	1.37×10^{-2} min^{-1} 1.47×10^{-2} min^{-1}	[79]
$BiVO_4/WO_3$	Cathode: Pt plate Applied potential: 1.0 V (vs SCE)	300 W Xenon lamp with $\lambda \geq 420$ nm and intensity of 1 mW cm^{-2}	Norfloxacin (C_0 = 10 mg L^{-1})	67%, 3 hr	2.68×10^{-3} min^{-1}	[80]
$BiVO_4/g\text{-}C_3N_4$	Cathode: Pt wire Applied potential: 1.23 V (vs Ag/AgCl)	300 W Xenon lamp with light intensity of 100 mW cm^{-2}	Methyl orange (C_0 = 5 mg L^{-1})	90%, 75 min	4.56×10^{-2} min^{-1}	[65]
$BiVO_4/WO_3$	Cathode: Pt foil Applied potential: 1.5 V (vs Ag/AgCl)	Solar simulator with light intensity of 100 mW cm^{-2}	Ibuprofen (C_0 = 100 mg L^{-1})	82%, 150 min	Not available	[81]
TiO_2/RuO_2-$BiVO_4$	Cathode: Pt foil Applied potential: 2.0 V (vs SCE)	300 W Xenon lamp with $\lambda \geq 420$ nm	Acetaminophen (C_0 = 332 mg L^{-1})	100%, 3 hr	3.38×10^{-2} min^{-1}	[82]

$BiVO_4$/NiS	Cathode: Pt wire Applied potential: 1.8 V (vs Ag/AgCl)	100 W Xenon lamp	Rhodamine B (C_0 = 10 mg L^{-1}) Sulfamethoxazole (C_0 = 10 mg L^{-1})	73%, 2 hr 57%, 2 hr	0.108 min^{-1} 7.4×10^{-3} min^{-1}	[83]
TiO_2/$BiVO_4$-Bi_2S_3	Cathode: Pt sheet Applied potential: 1.8 V (vs Ag/AgCl)	Xenon lamp with light intensity of 100 mW cm^{-2}	Rhodamine B (C_0 = 10 mg L^{-1})	64.3%, 150 min	6.13×10^{-3} min^{-1}	[84]
$CoFe_2O_4$-$BiVO_4$	Cathode: Pt mesh Applied potential: 0.6 V (vs Ag/AgCl)	300 W Xenon lamp with $\lambda \geq 420$ nm	Tetracycline (C_0 = 20 mg L^{-1})	89%, 1 hr	3.7×10^{-2} min^{-1}	[85]
$BiVO_4$/TiO_2	Cathode: Pt wire Applied potential: 4 V (vs Ag/AgCl)	300 W Xenon lamp with $\lambda \geq 420$ nm with light intensity of 200 mW cm^{-2}	Rhodamine B (C_0 = 10 mg L^{-1})	93.9%, 5 hr	Not available	[86]
$BiVO_4$/ZnO	Cathode: Pt foil Applied potential: 0.8 V (vs SCE)	300 W Xenon lamp with $\lambda \geq 420$ nm	Tetracycline (C_0 = 20 mg L^{-1})	66.1%, 2 hr	1.94×10^{-3} min^{-1}	[87]
$BiVO_4$/MoS_2	Cathode: Pt wire Applied potential: 1.5 V (vs Ag/AgCl)	300 W Xenon lamp with $\lambda \geq 435$ nm	Bisphenol A (C_0 = 10 mg L^{-1})	100%, 75 min	5.12×10^{-2} min^{-1}	[88]
$BiVO_4$/Ag	Cathode: Pt foil Applied potential: 1.5 V (vs Ag/AgCl)	300 W Xenon lamp with $\lambda > 420$ nm	β-naphthol (C_0 = 10 mg L^{-1})	80%, 8 hr	3.33×10^{-3} min^{-1}	[89]
$BiVO_4$/ZnO	Cathode: Pt wire Applied potential: 1.6 V (vs Ag/AgCl)	300 W Xenon lamp with $\lambda \geq 420$ nm	Tetracycline (C_0 = 20 mg L^{-1})	95.4%, 1 hr	4.55×10^{-2} min^{-1}	[90]
$BiVO_4$/α-Fe_2O_3	Cathode: Pt foil Applied potential: 2 V (vs Ag/AgCl)	350 W Xenon lamp	Bisphenol A (C_0 = 20 mg L^{-1})	86.8%, 2 hr	Not available	[91]
$BiVO_4$/g-C_3N_4	Cathode: Pt wire Applied potential: 1 V (vs SCE)	Xenon lamp with $\lambda \geq 420$ nm	Diclofenac sodium (C_0 = 10 mg L^{-1})	30.1%, 2 hr	3.23×10^{-3} min^{-1}	[92]
$BiVO_4$/CuO	Cathode: Pt foil Applied potential: 4.0 V (vs Ag/AgCl)	44 W LED with $\lambda \geq 420$ nm	4-nitrophenol (C_0 = 30 mg L^{-1})	50.2%, 8 hr	1.86×10^{-2} min^{-1}	[93]
$BiVO_4$/ZnO (with exfoliated	Reference electrode: Ag/AgCl	100 W Xenon lamp	Rhodamine B (C_0 = 10 mg L^{-1})	91%, 4 hr	9.21×10^{-3} min^{-1}	[94]

graphite as substrate)	Cathode: Pt sheet Applied current density: 10 mA cm^{-2}	with $\lambda \geq 420$ nm				
$BiVO_4/Cu_2O$	Cathode: Pt foil Applied potential: 0.6 V (vs Ag/AgCl)	300 W Xenon Lamp	Ciprofloxacin (C_0 = 30 mg L^{-1})	60%, 150 min	6.5 × 10^{-3} min^{-1}	[95]
$WO_3/BiVO_4$	Cathode: Pt wire Applied potential: 1.2 V (vs Ag/AgCl)	320 W Xenon lamp	Sodium 2-napthalenesulfonate (S2NS) (C_0 = 50 mg L^{-1}) Benzyl alkyl dimethylammonium (BAC-C12) (C_0 = 50 mg L^{-1})	100%, 150 min 100%, 150 min	Not available	[96]
$BiVO_4/MoS_2$-Co_3O_4	Cathode: Platinum plate Applied potential: 3.5 V	Xenon lamp with light intensity of 100 mW cm^{-2}	Bisphenol A (C_0 = 10 mg L^{-1})	80%, 5 hr	5.8 × 10^{-3} min^{-1}	[97]

4. Conclusions and outlook

$BiVO_4$ based photoanodes have demonstrated comparable and even superior removal efficiency for a number of organic pollutants compared to UV driven photoanodes such as TiO_2 (Table 2.1). In PEC based systems, •OH radicals are the primary reactive species responsible for oxidizing organic pollutants. Several studies have also reported enhanced removal efficiency with the addition of PMS, attributed to the oxidation of organic pollutants by $SO_4^{\bullet -}$ generated through the visible light activation of PMS in the bulk solution. Similarly, heterojunction photoanodes have shown higher removal efficiencies than pristine $BiVO_4$ photoanodes due to improved charge separation. The studies reviewed predominantly targeted synthetic dyes and pharmaceutical compounds, using concentrations in demineralized water ranging from 5 to 50 mg L^{-1}.

There remains ample research potential in the field of PEC-driven removal of organic pollutants using $BiVO_4$ photoanodes. Further studies are particularly needed to explore the effectiveness of $BiVO_4$ based photoanodes for the removal of organic pollutants at concentrations below 1 mg L^{-1}, as most organic pollutants detected in surface water or groundwater range from low ng L^{-1} levels to higher µg L^{-1} levels [98], which can impact the removal kinetics. Additionally, investigating the simultaneous removal of multiple organic pollutants in aqueous solutions is essential, given that pollutants of emerging concern typically occur in aquatic environments as mixtures rather than as isolated compounds [9,99]. Research should also focus on applying $BiVO_4$ based photoanodes to remove organic pollutants from real wastewater or effluent from industrial processes and wastewater treatment plants, as this would provide valuable insights into the removal mechanism and the effect of the overall water composition on the removal efficiency. Moreover, employing process simulation tools such as

CFD modelling for $BiVO_4$ based PEC removal in full-scale reactors could be beneficial. Simulation results can be used for a techno-economic analysis, helping to evaluate the feasibility of reactor designs of scaled up PEC reactors employing $BiVO_4$ based photoanodes. In conclusion, $BiVO_4$ based photoanodes have demonstrated considerable potential in water treatment applications. Given the advancements achieved to date, it is expected that $BiVO_4$ based photoanodes will be increasingly used for full-scale water treatment applications in the future.

Acknowledgement

This work was funded by the European Union. Views and opinions expressed are however those of the author(s) only and do not necessarily reflect those of the European Union or the European Commission. Neither the European Union nor the granting authority can be held responsible for them.

Chapter 3

Photoelectrocatalytic based simultaneous removal of multiple organic micro-pollutants by using a visible light driven $BiVO_4$ photoanode.

This chapter is based on the following publication:

Agha Zeeshan Ali, Sadhna Jagannathan, Yasmina-Doekhi Bennani, Jan Peter van der Hoek, Henri Spanjers, Photoelectrocatalytic based simultaneous removal of multiple organic micro-pollutants by using a visible light driven $BiVO_4$ photoanode, Journal of Water Process Engineering, Volume 56, 2023, 104471, https://doi.org/10.1016/j.jwpe.2023.104471.

Abstract

In this research, photoelectrocatalytic (PEC) based advanced oxidation process (AOP) was studied for the removal of multiple OMPs through an oxidative mechanism. This study investigated the application of a $BiVO_4$ photoanode in simultaneous removal of three selected OMPs: acetaminophen (ACT), benzotriazole (BTA) and propranolol (PRO). This study was carried out in demineralized water with a starting concentration of each organic micro-pollutant (OMP) at 45 μg L^{-1}. In order to fabricate $BiVO_4$ photoanodes, a facile and effective dip-coating method was used to deposit $BiVO_4$ photocatalytic layers on fluorine doped tin oxide (FTO) substrate. UV-vis diffusive reflectance spectroscopy, x-ray diffraction (XRD), x-ray photoelectron spectroscopy (XPS) and scanning electron microscopy (SEM) confirmed the successful fabrication of porous $BiVO_4$ photoanode having an absorbance edge at around 526 nm. The fabricated photoanode showed incident photon to current conversion efficiency (IPCE) of 9.23% (λ_{max} = 445 nm) under 1 Sun standard illumination. Application of the fabricated photoanodes for the simultaneous removal of ACT, PRO and BTA at an applied voltage of 1 V (vs Ag/AgCl) under solar simulated light resulted in 99% removal of both ACT and PRO, and 70% removal of BTA. The first order rate coefficients and half-life times of ACT and PRO were about three times higher than those of BTA.

Keywords: organic micro-pollutants, advanced oxidation process, photoelectrocatalysis, dip-coating, $BiVO_4$ photoanode.

1. Introduction

Organic micro-pollutants (OMPs) encompass a range of chemical substances released into water bodies due to human and industrials activities [100]. Depending on the geographic location and the source, the concentration of OMPs found in the surface water or in treated wastewater can vary, however, it is normally between 300 ng L^{-1} and 2 μg L^{-1} [101]. The major categories of OMPs are pharmaceuticals including the endocrine disruptors, skin/body care products and household cleaning products [102]. The toxic effects of consuming OMPs on humans and marine life are still under investigation and for some OMPs such effects have not been studied yet [103]. Different governmental and international environmental regulatory authorities have issued directives that aim to maintain and improve the integrity of water resources and to protect them from OMPs contamination [104]. Industrial and municipal wastewater effluents significantly contribute to the release of OMPs in surface water [101] because the conventional wastewater treatment processes are not completely removing the OMPs [105]. Efforts to remove OMPs from the WWTP effluents or to convert them into less harmful transformation products are increasing to prevent their release to the surface water [106].

Advanced oxidation processes (AOPs) are an effective way to remove OMPs from aqueous solution including municipal or industrial treated wastewater effluents [107].

Photoelectrocatalytic (PEC) based AOP is a type of AOP in which solar irradiation is used to activate photocatalyts to produce reactive species. Semiconducting photocatalytic materials are used as the anode in PEC based AOP to produce in-situ hydroxyl (•OH) and superoxide ($^{\bullet}O_2^-$) radicals which are the main oxidants [108]. The anode in a PEC cell, the photoanode, is in direct contact with the water containing the OMPs and the removal reaction usually occurs at the photoanode-electrolyte interface. The photoanode produces electron-hole pairs upon its interaction with the incoming solar irradiations. Water is oxidized by the photo-generated holes to produce •OH while the dissolved oxygen is reduced by the electrons to generate $^{\bullet}O_2^-$ [109]. According to the literature, •OH play significant role in the un-selective oxidation of organic pollutants in aqueous solution [45]. Organic pollutants are un-selectively oxidized until their complete mineralization or converted into transformation products by the photo-induced oxidants (•OH and $^{\bullet}O_2^-$) [109]. In aqueous solutions, the application of metallic oxide photocatalysts including iron oxide (Fe_2O_3) [110], titanium dioxide (TiO_2) [111], tungsten trioxide (WO_3) [112], zinc oxide (ZnO) [61] and zirconium dioxide (ZrO_2) [113] have been widely studied in literature for the removal of industrial dyes and pharmaceuticals (1-10 mg L^{-1}) by PEC based AOP. These photocatalysts, however, have one major disadvantage that they can only be utilized under the ultraviolet (UV) light (200-400 nm) of the solar spectrum because they have relatively large band gap energy of around 3.0 to 3.5 eV. To overcome the drawback of UV driven photocatalysts, bismuth vanadate ($BiVO_4$), a narrow band gap (approx. 2.4 eV) photocatalyst has emerged as an alternative to UV driven photocatalysts and can be utilized under the visible light of solar spectrum [74]. Apart from $BiVO_4$ applications in water splitting for hydrogen generation, $BiVO_4$ photoanodes are also being utilized for water treatment applications which include the removal of dyes such as methylene blue [114], rhodamine B [115], methyl orange [116] and pharmaceuticals such as tetracycline hydrochloride [117], ciprofloxacin [79] and ibuprofen [118] within a concentration range of 1 to 10 mg L^{-1} from aqueous solution. Removal efficiency of pristine $BiVO_4$ photoanodes is often reduced due to various factors, such as the microstructure of deposited $BiVO_4$ particles and the recombination of photo-generated holes and electrons. These factors contribute to poor charge transport within the photoanode [94]. Several strategies have been explored in the literature to increase the removal efficiencies of $BiVO_4$ photoanodes such as developing a heterojunction of $BiVO_4$ with other suitable photocatalyst [79], doping of $BiVO_4$ [118] and application of a suitable external bias (voltage) [119] to reduce the rate of recombination in the $BiVO_4$ photoanode and ultimately increase the removal efficiency. To the best of our knowledge there is limited research on the application of $BiVO_4$ photoanode for the OMPs removal in the concentration level between 0 and 150 µg L^{-1}. Moreover, there is a lack of literature available on the utilization of $BiVO_4$ photoanodes for the simultaneous removal of multiple OMPs in aqueous solutions.

Benzotriazole (BTA) is an emerging OMP and is frequently detected in surface water resources [120]. Due to its chemical and physical properties it is mostly included as a corrosion inhibiting chemical in e.g. anti-icing fluids and dishwashing detergents [121,122]. BTA is a polar

compound and is highly soluble (1-5 g L^{-1}) in water [123], and it is only partially removed from wastewater during the biological treatment because of its low biodegradability and low adsorption to organic matter [124]. As a result, BTA is released into the environment through WWTP effluents. Within the European Union it is mostly detected at a concentration level of below 50 µg L^{-1} in the aquatic environment [125]. UV/H_2O_2 oxidation [125], catalytic ozonation [126] and photocatalytic based AOP [127] have been applied in few studies on the removal of BTA (1-10 mg L^{-1}) from synthetic and real WWTP effluent. However, there is limited understanding of the removal kinetics of BTA within the concentration range between 0 and 50 µg L^{-1} which is more closer to the concentration level of BTA that could be present in the aquatic environment. Furthermore, there is no literature available on the removal of BTA by PEC based AOP using either UV or visible light driven photoanodes. Propranolol (PRO) is a β-blocker drug that is mainly used for treating hypertension, heart diseases and migraines [128]. Currently PRO is an OMP of concern because of its excessive usage and persistence to conventional wastewater treatment technologies leading to the contamination of WWTP effluent and ultimately surface water with PRO [129]. Polymeric adsorption [130], catalytic H_2O_2 [131], photocatalytic (nano-particles) [132] and electrochemical AOP [133] based removal of PRO (1-20 mg L^{-1}) have been reported in literature. Similarly, acetaminophen (ACT) is also one of the most commonly detected OMPs in surface water, wastewater and drinking water [7]. ACT is mostly purchased without any prescription and is frequently used for pain and fever alleviation [134]. In many European countries WWTPs release a concentration of ACT between 0 and 20 µg L^{-1} in their effluents due to an incomplete removal of ACT [135]. Electrochemical [136] and PEC based AOP [137] have been reported in the literature to remove ACT from real and simulated WWTP effluents. However, there is limited literature on the simultaneous removal of ACT in multiple OMP solutions by PEC based AOP. Investigating the simultaneous removal of multiple OMPs by using a photoanode will give information on the selectivity of the photoanode and the removal kinetics of each OMP present in the aqueous solution. The exposure of all three OMPs (ACT, BTA, PRO) even at lower concentrations of below 200 µg L^{-1} can cause adverse effects on the reproductive system of aquatic organisms [138] and also intake of these OMPs by humans through drinking water can cause inflammation, tissue damage and serious problems in digestion by changing the gut micro-organism population [139]. We believe that like other pharmaceuticals, ACT and PRO at a concentration below 150 µg L^{-1} can act additively as a mixture of pharmaceuticals and can cause lethal or sub-lethal toxic effects to aquatic organisms, therefore, their complete removal from surface water should be of significant importance. Moreover, frequent release of these OMPs, even at lower concentrations of below 150 µg L^{-1}, can ultimately result in the accumulation of a mixture of these compounds in surface water resources.

In this research we studied the role of a $BiVO_4$ photoanode in the simultaneous removal of ACT, BTA and PRO each having a starting concentration of 45 µg L^{-1} in demineralized water. ACT, BTA and PRO were selected for this study because of their environmental significance and persistent presence as an OMP in the water resources. Furthermore, BTA and PRO are

included in the list of micro-pollutants present in the wastewater provided by the Dutch foundation for Applied Water Research and the Dutch Ministry of Infrastructure and Water Management. First, visible light absorbing photoanodes were fabricated by depositing $BiVO_4$ photocatalytic layer through dip coating method. The structural, morphological, optical and opto-electronic properties of the fabricated photoanodes were analysed and interpreted to validate the successful deposition of $BiVO_4$ photocatalytic layer. Then the photoanodes were employed in a three-electrode PEC cell for the simultaneous removal of three OMPs. Energy consumption analysis was also carried out to find the total energy required to remove ACT, BTA and PRO. The removal kinetics of each OMP was assessed by applying a suitable reaction kinetics model. Quenching experiments were performed by using different types of quenching agents to assess the role of oxidants in the removal of selected OMPs by PEC based AOP.

2. Materials and Methods

2.1 Materials

All the chemical reagents used in this study were purchased from Sigma Aldrich which include nitric acid (HNO_3) (70%, CAS 7697-37-2), bismuth nitrate pentahydrate ($Bi(NO_3)_3.5H_2O$) (98%, CAS 10035-06-0), vanadyl acetyl acetonate ($VO(acac)_2$) (97%, CAS 3153-26-2), sodium sulfate (Na_2SO_4) (99.0%, CAS 7757-82-6), acetaminophen ($C_8H_9NO_2$) (≥99.0%, CAS 103-90-2), propranolol hydrochloride ($C_{16}H_{21}NO_2.HCl$) (CAS 318-98-9) and benzotriazole ($C_6H_5N_3$) (99%, CAS 95-14-7).

2.2 Preparation of $BiVO_4$ photoanode

A facile dip-coating method was used to deposit a $BiVO_4$ photocatalytic layer on commercially purchased fluorine doped tin oxide (FTO) glass slides (4 x 4 cm; surface resistivity 7 Ω sq^{-1}). Firstly, FTO glass slides were ultrasonically cleaned separately in acetone and ethanol for about 5-6 min. The dip coating solution was prepared by adding 0.049 M bismuth nitrate pentahydrate ($Bi(NO_3)_3.5H_2O$) in 50 mL of ultra-pure water whose pH was adjusted to 2.0 - 2.2 by using 1 M nitric acid (HNO_3). After adding the $Bi(NO_3)_3.5H_2O$, the solution was thoroughly mixed and then placed in an ultrasonic bath to make it a homogeneous solution. After about 30 min when the solution was clear, 0.049 M vanadyl acetylacetonate was added to the solution, which was again placed into the ultrasonic bath for homogenous mixing. After about 30 min of ultrasonication, the blue coloured solution was taken out, and at this stage the coating solution was ready to deposit $BiVO_4$ on FTO slides. In order to deposit the $BiVO_4$ layer, the FTO glass slide with its FTO side facing upward was dipped into the coating solution for 5 minutes. After 5 minutes, the FTO glass slide was removed with the help of a pincer and was placed on a hot plate at 100°C for 10 min to evaporate the solvent present in the deposited layer. The same procedure of dipping and drying was used to prepare five photoanodes with 1 layer, 2 layers, 3 layers, 4 layers and 5 layers of $BiVO_4$. In the final step, all photoanodes were annealed in an electric furnace at 460°C for 2 h at a ramping rate of 3°C min^{-1}. After the

annealing step, the bright yellowish coloured photoanodes were stored in a dry place under normal conditions. Photoanodes with different number of $BiVO_4$ layers were prepared to analyse the effect of layer thickness on the removal efficiency of the photoanodes. $BiVO_4$ photoanode with three layers showed fastest removal of ACT in demineralized water as shown in Fig. S.3.1 of supplementary information. Therefore, the three-layer photoanode was selected for further characterization and the application for the removal of selected OMPs by PEC based AOP.

2.3 Structural and morphological characterization

Surface morphology and micro/nano-structure analysis of fabricated photoanodes was carried out by using field emission scanning electron microscopy (SEM), X-ray diffraction (XRD) and X-ray photoelectron spectroscopy (XPS). The detailed description of the characterization techniques is given in our previous research publication [140]. Surface profilometry technique was used to measure the layer thickness of each photoanode by using a Veeco Detak 8 surface profilometer. The results of surface profilometry regarding the layer thickness are shown in Table. S.3.1 of the supplementary information.

2.4 Optical and opto-electronic characterization

Optical properties of fabricated photoanodes were studied between 300 – 700 nm (2 nm step size) by using diffusive reflectance UV-vis spectroscopy (LAMBDA 1050+ UV/Vis/NIR spectrophotometer, UV Winlab software). Incident photon-to-electron conversion efficiency (IPCE) was also measured between 280 – 700 nm (10 nm step size) by utilizing a incident photon to current conversion efficiency (IPCE) set-up (specialized for solar cells measurement) under 1 Sun illumination (AM 1.5 standard conditions). IPCE measurement was performed by using the $BiVO_4$ photoanode as working electrode at 1 V (external bias) and a platinum wire as the counter electrode. 0.1 M Na_2SO_4 solution containing 45 µg L^{-1} of ACT was used as electrolyte for IPCE measurements. The IPCE value of the photoanode at each wavelength was calculated by the set-up software using the Eq. 1 and the short circuit current (J_{sc}) was automatically calculated by the software at the end of measurement.

$$\text{IPCE } \% = \frac{\text{I (A)}}{\text{P}_{\text{in}}\text{ (W)}} \times \frac{1240}{\lambda\text{ (nm)}} \times 100 \qquad \text{(Eq. 1)}$$

I = Photocurrent response at each wavelength.

P_{in} = Input power of the light source at each wavelength.

λ = Wavelength of incoming photons.

Linear sweep voltammetry (LSV) was carried out in a three-electrode cell (dark & light conditions: 60 W m^{-2}) between -0.2 and 1.5 V (vs Ag/AgCl) at a scan rate of 100 mV s^{-1}. Similarly, electrochemical impedance spectroscopy (EIS) under illuminated conditions (60 W

m^{-2}) was carried out in a three-electrode cell between 10,000 to 0.01 Hz with a perturbation voltage of 0.2 V, during the measurement the reaction solution was continuously stirred at 600 rpm. For LSV and EIS 0.1 M Na_2SO_4 containing 45 µg L^{-1} of ACT was used as an electrolyte. The data for Mott Schottky plot was obtained under dark conditions by measuring the capacitance of the working electrode ($BiVO_4$ photoanode) within the applied potential range of -1.1 V to 1.1 V vs Ag/AgCl in an electrolyte consisting of a 5 mM solution of $[Fe(CN)_6]^{3-/4-}$ (prepared in 0.1 M KCl) (pH 7.2).

2.5 Photoelectrocatalytic (PEC) experiments

Removal of selected OMPs by PEC based AOP with the use of the prepared photoanodes was carried out by using an Autolab potentiostat (PGSTAT128N) in three electrode cell. The experimental process was similar to our previously published research [140] A quartz reactor cell containing three electrodes and 167 mL of electrolyte solution was used for the PEC based AOP removal experiments. 0.1 M Na_2SO_4 containing ACT, BTA and PRO each with a concentration of 45 µg L^{-1} at a pH of 6.8 was used as electrolyte for the removal experiments. Demineralized water was used for the preparation of the electrolyte. Fabricated photoanodes, Ag/AgCl (3.0 M KCl) electrode and graphite plate (40 x 40 mm) were used as working electrode, reference electrode and counter electrode, respectively. A constant voltage of 1 V vs Ag/AgCl was applied during the removal experiments to minimize the rate of recombination in the fabricated photoanodes. A solar simulator SUNTEST XXL+ having three air cooled 1700 W Xenon lamps emitting 1 Sun illumination spectrum (300-900 nm) was used as light source. The intensity of emitted light between 300-400 nm was calibrated to 60 W m^{-2} and the distance between the light source and the photoanode was approximately 15 cm. The reactor cell was placed in a temperature-controlled bath at 25 ± 1°C to perform the removal experiments at constant temperature. Before turning on the simulated solar light and applying the external voltage (1 V), the three-electrode cell containing the reaction solution along with the $BiVO_4$ photoanode, Ag/AgCl reference electrode and graphite cathode was kept under dark conditions for 45 min to analyse the effect of adsorption of OMPs by the components of the reactor cell. After 45 min, the concentrations of the three OMPs were analysed by LC-MS as explained in section 2.6 and there was no significant change observed in the concentration of the selected OMPs. After 45 min of adsorption time, each removal experiment ran for 2 h with continuous stirring at 600 rpm to increase the mass transfer of OMPs from the bulk to the surface of the photoanode. Samples for the concentration analysis of each OMP were taken at intervals of 30 min. PEC based AOP removal experiments were conducted in triplicate to assess the reproducibility of the results.

Reusability experiments with $BiVO_4$ photoanode were performed by using the same photoanode for four consecutive removal experiments of 2 h each. Between successive experiments the photoanode was rinsed with demineralized water to remove any adsorbed OMP from the photoanode.

2.5.1 Quenching experiments

Quenching experiments were carried out in a similar way as the removal experiments described in section 2.4, except for the addition of quenching agent in the electrolyte. 4 mM of ethylene diamine tetraacetic acid (EDTA), p-benzoquinone (p-BZQ) and methanol were used in separate experiments to quench photo-generated holes, •OH and $^{\bullet}O_2^-$, respectively. Each experiment ran for 2 h and samples were taken at intervals of 30 min for the concentration analysis of ACT, BTA and PRO.

2.6 Analytical measurement of ACT, BTA and PRO

The concentration of three OMPs in the samples was measured by using liquid chromatography combined with tandem triple-quadrupole mass spectrometry (LC-MS). The complete measurement procedure is described in our previous publication [140]. Based on the measured concentrations of OMPs, removal efficiency of $BiVO_4$ photoanode for each OMP was calculated by using the following equation:

$$\text{Removal efficiency (\%)} = \left(1 - \frac{C_t}{C_o}\right) \times 100$$

Where C_0 = Initial concentration at time t=0 and C_t = Concentration at any time

3. Results and Discussion

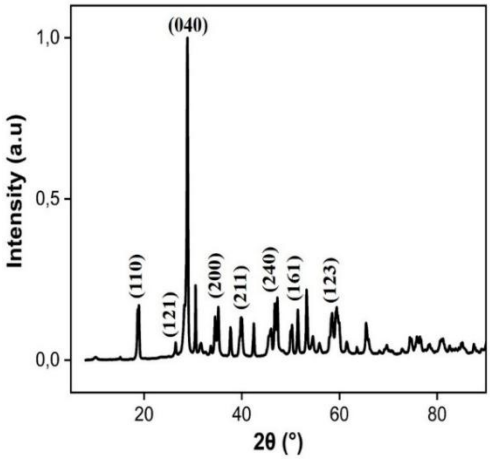


Fig. 3.1: *X-ray diffraction peaks of $BiVO_4$ photocatalytic layer showing the indexed peaks of monoclinic scheelite phase.*

3.1 Structure and morphology of photoanodes

Fig. 3.1 shows the X-ray diffraction peaks of dip-coated $BiVO_4$ photoanode. The main peaks at 18.97°, 28.89°, 30.52°, 34.55°, 35.20°, 39.87°, 42.43°, 46.74°, 47.27°, 51.46° and 59.43° as shown in Fig. 1 were assigned to monoclinic scheelite phase of $BiVO_4$ which was also confirmed by the ICDD database as shown in Fig. S.3.2 of the supplementary information. The designated peaks were in agreement with the previous literatures [19,40] and indexed as (110), (121), (040), (200), (002), (211), (015), (240), (042), (161),

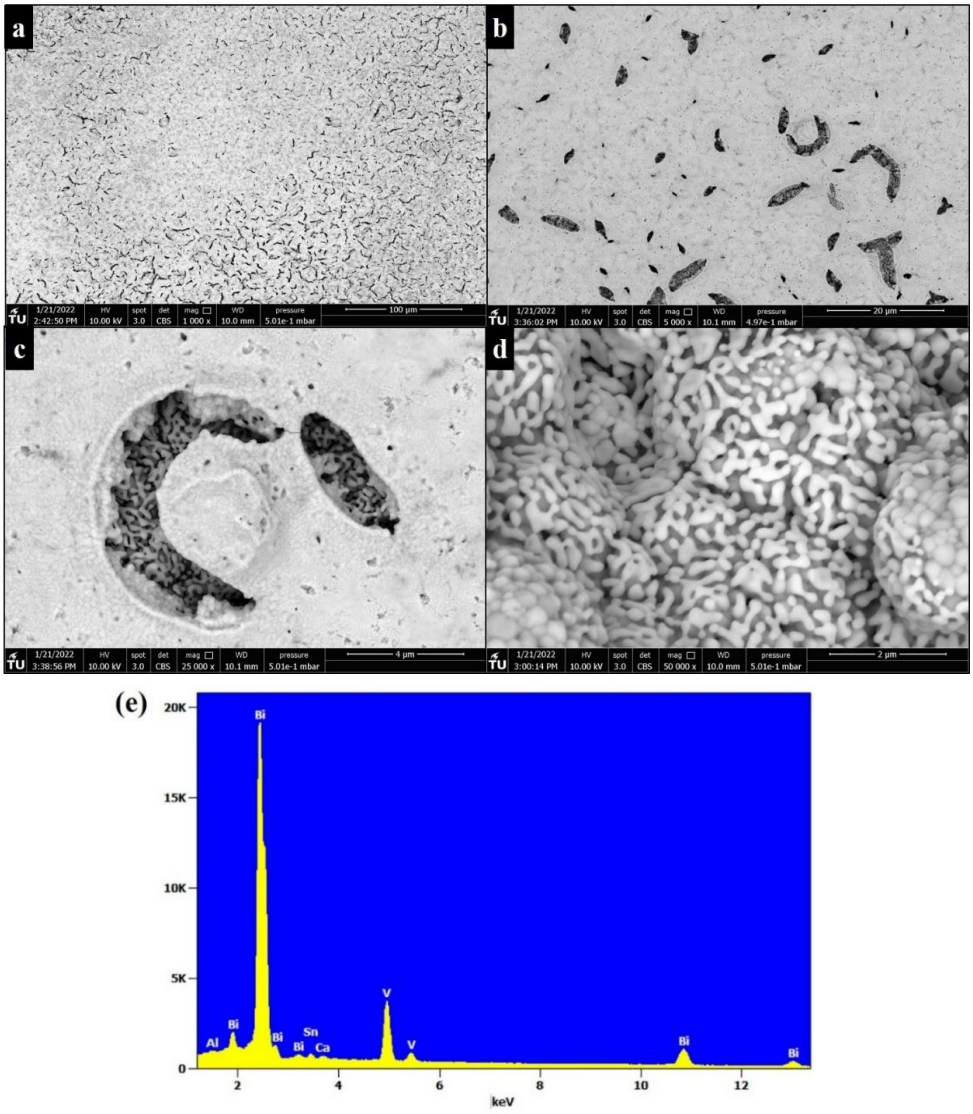


Fig. 3.2: *SEM images showing surface morphology of $BiVO_4$ photoanode at magnification of 1000 x (a) 5000 x (b) 25000 x (c) 50,000 x (d) and compositional analysis of $BiVO_4$ photoanode through EDX showing the characteristic peaks of constituent elements present in the photocatalytic layer (e)*

(321) and (123), respectively. Formation of monoclinic scheelite phase of $BiVO_4$ was desired in this research due to its relatively narrow band gap energy that enables it to have improved interfacial charge transfer properties as compared to tetragonal zircon $BiVO_4$ [67]. The XRD characterization confirmed the successful deposition of $BiVO_4$ without any impurity compound.

Fig. 3.2 shows the surface morphology of dip-coated $BiVO_4$ photoanode. In low resolution images (Fig. 3.2 (a) & (b)), the photoanode appeared to have a compact surface with micro sized cracks. These surface cracks increased the roughness and available adsorption surface area of the photoanode for the OMP molecules. The high-resolution SEM image in Fig. 3.2(c) shows the porous layer of $BiVO_4$ particles (under the cracks) that were joined together to form a 3D branch network. The magnified image (Fig. 3.2(d)) of the porous layer shows the inter-joining of deposited $BiVO_4$ particles that facilitated efficient charge transport within the photoanode. SEM result exhibited that the porous $BiVO_4$ particles possibly improved the transfer of photo-induced charges from the bulk material to the photoanode-electrolyte interface where they were utilized for the oxidants (•OH and $\cdot O_2^-$) generation. Furthermore, the cracks on the compact layer increased the adsorption surface area available for the BTA, PRO and ACT molecules and this enhanced adsorption of molecules on the surface of the photoanode resulted in a fast and efficient removal of selected OMPs either by direct oxidation through photo-generated holes or by the in-situ produced oxidants. Fig 3.2(e) shows the EDX spectrum of the fabricated photoanode which depicts the elemental analysis of $BiVO_4$ photocatalytic layer, and it is evident from EDX spectrum that only bismuth (Bi), oxygen (O) and vanadium (V) were detected as the major constituent elements in the photoanode. Fluorine doped tin oxide (FTO) was responsible for the detection of Tin (Sn) and calcium (Ca) in the EDX analysis as shown in Fig 3.2(e). The EDX analysis complemented the XRD findings and further corroborated the purity of the $BiVO_4$ deposition without the presence of any impurity element.

The survey scan of X-ray photoelectron spectroscopy (XPS) of the $BiVO_4$ photoanode is shown in Fig. S.3.3 of the supplementary information. Fig. S.3.3 in supplementary information shows that Bi, O and V were co-existing and exhibited distinct peaks at their respective binding energies. Carbon (C) detected in the XPS survey analysis was considered as an impurity that was present during the analysis. Fig. 3.3 presents the deconvoluted high-resolution spectra of Bi, V and O. In Fig. 3.3, the two asymmetric peaks at 162.97 and 157.57 eV represented Bi $4f_{5/2}$ and Bi $4f_{7/2}$ spin orbit splitting states of Bi, respectively. The difference between their binding energies was 5.4 eV, which suggested that Bi was present as Bi^{3+} in the lattice structure of $BiVO_4$ [141]. Similarly, in the case of vanadium (V), the two peaks at 528.42 and 515.22 eV were assigned to V $2p_{1/2}$ and V $2p_{3/2}$ spin orbit splitting states, respectively. Their peak positioning observed in the spectrum suggested that V was present as V^{5+} in the lattice structure of $BiVO_4$ [142]. In the case of oxygen (O) three distinct peaks were observed where each peak represented a different bonding environment around oxygen. The two peaks at 528.05 and 528.85 eV were assigned to oxygen in the lattice structure of $BiVO_4$ and was bonded to Bi and V, respectively. A relatively low intensity peak observed in the O spectrum at 529.95 eV represented the surface adsorbed oxygen [140,143]. Overall, the XPS results successfully confirmed the presence of constituent elements (Bi, O and V) of $BiVO_4$, which was in accordance with the XRD and EDX results.

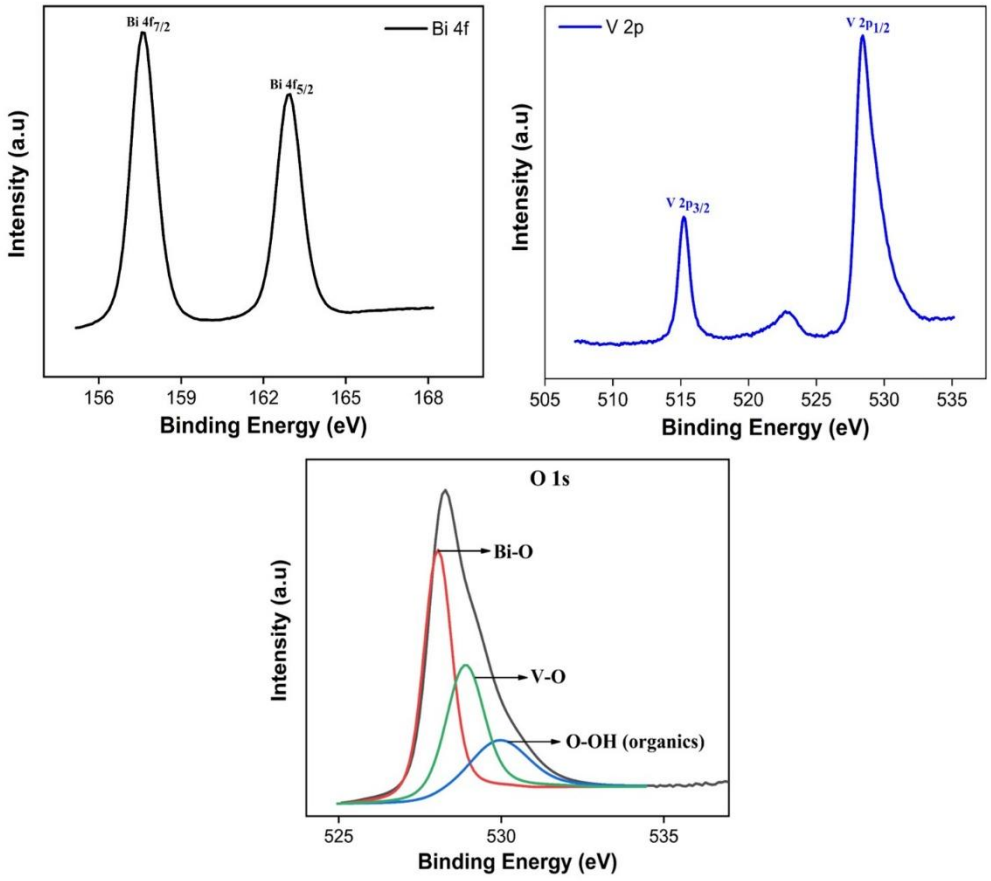


Fig. 3.3: *De-convoluted high resolution XPS spectra revealing Bi $4f_{7/2}$ and Bi $4f_{5/2}$ spin orbit splitting states for Bi, V $2p_{3/2}$ and V $2p_{1/2}$ spin orbit splitting states for V and different chemical bonding environment around O in the lattice structure of $BiVO_4$.*

3.2 Optical and opto-electronic properties of the $BiVO_4$ photoanode

The absorbance spectrum of the $BiVO_4$ photoanode was measured by using UV-vis diffusive reflectance spectroscopy. The absorbance spectrum of the fabricated photoanode is shown in Fig. 3.4(a), and it is evident from the spectrum that the photoanode showed strong absorption of incoming photons within the UV-visible range (300-550 nm) of the solar spectrum. The absorbance edge of the $BiVO_4$ photoanode was observed in the visible spectrum of solar irradiation at about 526 nm. The absorbance pattern of the $BiVO_4$ photoanode confirmed that the deposited $BiVO_4$ layer absorbs in the UV-visible range and can be applied for visible light driven PEC based AOP removal of OMPs. The absorbance spectrum in Fig. 3.4(a) was also used to determine the approximate band gap energy (E_g) of the fabricated $BiVO_4$ photoanode by using the Eq. 2 as shown below [144]:

$$\alpha hv = A(hv - E_g)^{n/2} \quad \text{(Eq. 2)}$$

The Eq. (1) is called as Tauc equation, in this equation: α, h, v, A and E_g corresponds to absorbance coefficient, Planck's constant, incident light frequency, constant and band gap energy, respectively. The exponent n is a constant, and its value depends on the optical transition behaviour of the specific semi-conducting material being used. According to literature, $BiVO_4$ is a direct transition semi-conductor and the value of n for a direct transition semi-conductor is 1 [143]. The E_g was evaluated by substituting the known values in Eq. 2 and a plot of $(\alpha hv)^2$ against hv was constructed as shown in the inset of Fig 3.4(a). The assessed E_g was found to be 2.36 eV. Result of UV-vis spectroscopy and band gap calculation showed that the dip coating method was successful in fabricating a narrow band gap and a UV-visible light absorbing $BiVO_4$ photoanode.

The calculated band gap energy (E_g) obtained from the inset of Fig. 3.4(a) was utilized to determine the valence band (E_{VB}) and conduction band (E_{CB}) edge potentials of the fabricated photoanode. Eq. (3) and Eq. (4) were used to compute E_{CB} and E_{VB} [79]:

$$E_{CB} = X - E_C - 0.5E_g \text{ (Eq. 3)}$$

$$E_{VB} = E_g + E_{CB} \text{ (Eq. 4)}$$

In Eq. (3) the variable X represents the geometric mean of the absolute electronegativities of the constituent atoms present in the photocatalyst being used, and for $BiVO_4$ its value is 6.04 eV [145]. In Eq. (3) the E_c corresponds to the energy of free electrons relative to the normal hydrogen electrode and its value is 4.50 eV. E_g in both Eq. (3) and (4) represents the band gap energy of the $BiVO_4$ photoanode that was obtained from Tauc plot (inset of Fig. 3.4(a)). After substituting the known values of E_c, E_g and X in Eq. (3) and (4), the E_{VB} and E_{CB} for the $BiVO_4$ photoanode were calculated as 2.72 and 0.36 eV, respectively. The calculated band edge potentials were found to be in consistent with the values reported in literature [79] and were able to produce the reactive species to oxidize the OMP molecules as illustrated in Fig. 3.4(b).

Linear sweep voltammetry (LSV) technique was used to investigate the influence of the applied voltage on the photo-induced current generated by the $BiVO_4$ photoanode. The LSV plot (Fig. 3.4(c)) shows that in dark conditions no photocurrent was generated within the applied potential window of -0.2 to 1.5 V. Fig 3.4(c) shows that in the absence of light, the fabricated photoanode did not act as a classical electro-catalyst for the direct oxidation of OMPs even when an external voltage was applied. In the presence of light (60 W m^{-2}), the applied voltage had a positive impact on the photocurrent of the fabricated photoanode, which confirmed that the applied external voltage decreased the recombination of photo-generated charge carriers in the $BiVO_4$ photoanode. Furthermore, the LSV plot also revealed that photocatalytic removal of OMPs was not possible as no photocurrent was observed at 0 V in the presence of light. Based on the findings of LSV, 1.0 V was selected as the suitable applied

voltage for the PEC based AOP removal of the selected OMPs because sufficient current density (0.16 mA cm^{-2}) was obtained at 1.0 V. The obtained photocurrent density current density of 0.16 mA cm^{-2} was comparable to the current densities (0.1 – 1 mA cm^{-2}) reported in the relevant literature [117,146,147] that used $BiVO_4$ based photoanodes. However, the reported light intensities used in LSV was mostly 1000 W m^{-2}, which could significantly increase the photocurrent response. The increased light intensities could be the explanation of current densities higher than 0.16 mA cm^{-2} reported in the literature. The transient photocurrent response during the removal experiment as shown in Fig. S. 4 of the supplementary information is also comparable with the value (0.16 mA cm^{-2}) obtained by the LSV characterization.

The approximate value of flat band potential (E_{fb}) and the electron donor density (N_D) of fabricated $BiVO_4$ photoanode was calculated by using the Mott-Schottky plot. The E_{fb} and N_D are important parameters to assess the charge separation efficiency not only in a photocatalyst but also in heterojunction interfaces. Mott Schottky plot was constructed by using the Eq. 5 as given below:

$$\frac{1}{C^2} = \frac{2}{e\varepsilon\varepsilon_o N_D A^2} \times \left(E_A - E_{fb} - \frac{kT}{e}\right) \quad \text{(Eq. 5)}$$

In Eq. 5, the C is the capacitance at the photoanode-electrolyte interface, e is the electron charge (1.60 x 10^{-19} C), ε is the dielectric constant (68 for $BiVO_4$ [148]), ε_o is the permittivity of vacuum, N_D is the charge carrier density (cm^{-3}), A (m^2) is the surface area of the photoanode, E_A is the applied potential, E_{fb} is the flat band potential, k is the Boltzmann constant and T is the absolute room temperature. A Mott Schottky plot ($1/C^2$ as a function of E_A (V) vs Ag/AgCl) was constructed as shown in Fig. S. 5, N_D was calculated from the slope of the linear part of the plot and the E_{fb} was determined by extrapolating the straight tangent line of the linear part of the plot to x-axis intercept as shown in Fig. S. 5 in supplementary information. The calculated value of N_D was 1.04 x 10^{23} cm^{-3} which was in agreement with the value reported in the literature [79] for the $BiVO_4$ photoanode used in water treatment. The approximate value of E_{fb} from the Mott Schottky plot was -0.534 V vs Ag/AgCl (0.088 V vs RHE), which also closely matched to the values reported in the literature [79]. The value of E_{fb} was consistent with the literature [79], where similar values of E_g, E_{CB} and E_{VB} were calculated by the UV-vis absorbance data and Eq. (3) and (4).

To assess the quantum efficiency of the $BiVO_4$ photoanode, incident photon to current conversion efficiency (IPCE) characterization was carried out. It calculated the number of incoming photons that were converted into electrons by the $BiVO_4$ layer. Fig. 3.4(d) shows the IPCE plot of the fabricated $BiVO_4$ photoanode and it is evident from the plot that the photoanode absorbed the incoming photons between 300 to 500 nm and converted them into photocurrent. The percentage of converted incoming photons to photocurrent at each wavelength varied, and a maximum IPCE of 9.23% was reached at 450 nm. The overall shape

of IPCE plot is similar to the absorbance pattern shown in Fig. 3.4(a), both the absorbance edge and the maximum IPCE were observed in the visible range (λ>400 nm) of the solar spectrum. The position of maximum IPCE in the visible range of solar spectrum (λ>400 nm) provides further evidence that dip-coating was successful in preparing a visible light absorbing $BiVO_4$ photoanode. The short circuit current (J_{sc}) of 4.60 A m^{-2} was also obtained by the IPCE characterization that represented the maximum current that can be generated by the $BiVO_4$ photoanode.

Electrochemical impedance spectroscopy (EIS) was carried out as described in section 2.3 to analyse the charge transfer dynamics at the photoanode-electrolyte interface. Fig 3.4(e) shows the Nyquist plot along with the equivalent circuit model that shows important elements in the circuit such as solution resistance (R), double layer capacitance (C or CPE), charge transfer resistance ($R_{ct)}$ and Warburg diffusion coefficient (W). Among these elements, R_{ct} is the most important one as it substantially influences the reaction kinetics. The radius of the arc in the Nyquist plot is indicative of R_{ct}, with a smaller arc radius corresponding to a lower R_{ct} [137]. The calculated value of R_{ct} in Fig 3.4(e) was 142 Ω, which was comparable to, or even smaller than, most of the values (300 Ω [137], 20426 Ω [149] and 106 Ω [150]) reported in the literature for various photo-electrochemical applications using $BiVO_4$ based photoanodes. This inferred that the dip-coating method was successful in fabricating photoanodes with good interfacial charge transfer efficiency. The overall shape of the Nyquist plot in Fig. 3.4(e) suggested that the removal rate of the OMPs in the solution was partially diffusion controlled because the tail at the end of the arc is approximately at an angle of 45° with the X-axis. This kind of shape is characteristic of mixed kinetic-diffusion controlled reactions in which the reaction rate is not only hindered by the charge transfer resistance at the electrode-electrolyte interface but also by the transport of molecules from the bulk towards the photoanode-electrolyte interface. The EIS data was also analysed with a bode phase angle plot (Fig 3.4(f)) to compute the lifetime of photo-generated electrons in the photoanode. The Bode plot relates the lifetime of the electrons with the maximum phase angle frequency of the response signal as follows [79]:

$$\tau_\varepsilon = \frac{1}{2\pi f_{max}} \quad \text{(Eq. 6)}$$

where τ_ε is the lifetime of the electrons and f_{max} is the frequency at the maximum phase angle in the bode plot. According to Fig. 3.4(f) f_{max} was 34.3 Hz, by substituting the value of f_{max} in Eq. 6 the lifetime of the photogenerated electrons was assessed to be 4.6 ms. The calculated lifetime of electrons was about 14 times higher than the lifetime reported in the literature [79], higher lifetime of electrons implied lower recombination of charge carriers in the photoanode, which will ultimately increase the removal efficiency. The increased lifetime of the photogenerated electrons was attributed to the porous structure of the $BiVO_4$ particles as discussed in section 3.1. This porous structure reduced the internal resistance for the electron mobility within the $BiVO_4$ layer and increased the charge separation efficiency.

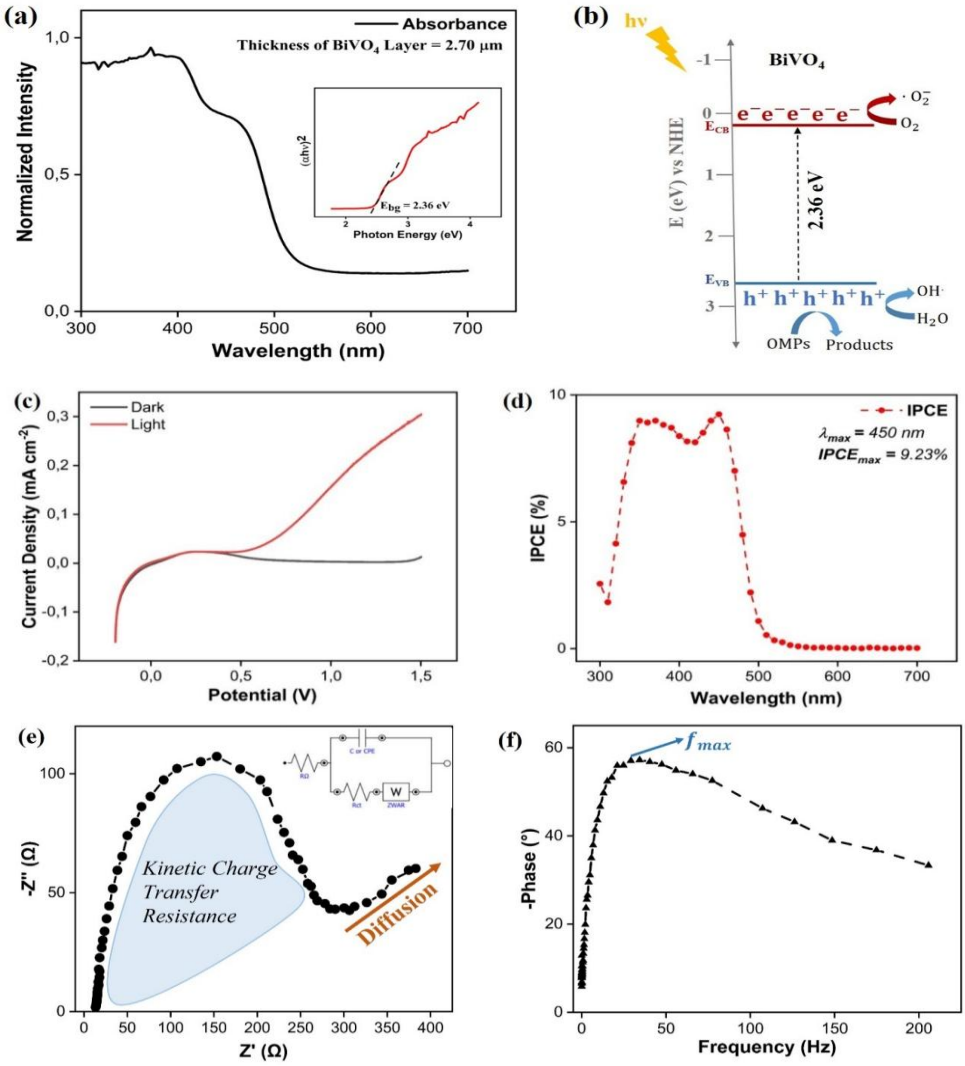


Fig 3.4: *(a) UV-Vis absorbance spectrum showing the absorbance pattern and the range of absorbance of the $BiVO_4$ photoanode (b) Illustration of interaction of solar photons with the $BiVO_4$ photoanode for the in-situ generation of oxidants (c) LSV plot of $BiVO_4$ photoanode under dark and light (60 W m^{-2}) conditions measured within the potential window of -0.2 to 1.5 V with a scan rate 100 mV s^{-1} (d) IPCE plot of $BiVO_4$ photoanode under 1 sun standard illumination and 1 V applied potential vs platinum wire as a counter electrode (e) Nyquist plot of $BiVO_4$ photoanode under illuminated conditions (60 W m^{-2}) performed between 10,000 Hz to 0.01 Hz at a perturbation voltage of 0.2 V (f) Bode phase angle plot showing the phase angle response to the applied frequency for electron lifetime determination.*

3.3 Photoelectrocatalytic based AOP removal of OMPs

Fig. 3.5(a) shows the normalized simultaneous decrease in concentration of ACT, BTA and PRO each having an initial concentration of 45 μg L^{-1} as a result of photolysis. It is evident from Fig. 3.5(a) that less than 10% of each OMP was removed as a result of the direct exposure of the reaction solution to the incoming simulated solar light. This low removal by photolysis is in accordance with the absorbance properties of ACT, BTA and PRO as all three OMPs absorb majorly in the UV range below 280 nm [132,140,151,152]. Photolysis results confirmed that removal of the selected OMPs was due of the use of the $BiVO_4$ photoanode for PEC advanced oxidation. Fig. S.3.6 (a) in supplementary information shows the normalized simultaneous removal of the selected OMPs in the absence of light (dark conditions) by using the fabricated $BiVO_4$ photoanode at an applied voltage of 1 V vs Ag/AgCl. It is evident from Fig. S.3.6 (a) in the supplementary information that in the absence of light there was minimum removal (<15%) of OMPs confirming that the removal of OMPs was due to PEC effect. Similarly, Fig. S.3.6 (b) in supplementary information shows the normalized simultaneous removal of ACT, BTA and PRO in the presence of light (60 W m^{-2}) by using the $BiVO_4$ photoanode at an applied voltage of 1 V vs Ag/AgCl. Before starting of the photo-electrocatalytic removal, 45 min of adsorption time was given to analyse the effect of OMPs adsorption by the reactor cell components (photoanode, reference electrode and counter electrode). Fig. S.3.3(b) shows that under dark conditions, less than 10% removal of OMPs were removed through adsorption. This low removal of OMPs through adsorption suggests that the selected OMPs removal occurred due to the PEC effect. Fig. S.3.5 (b) in supplementary information shows 99% removal of ACT and PRO within 2 h while approximately 70% BTA was removed after 2 h of solar simulated irradiation. Fig. 3.5(b) gives more detailed information regarding the removal efficiency of photoanode for ACT, BTA and PRO on a 30 min interval basis. It shows that more than 50% of ACT and PRO was removed by the $BiVO_4$ photoanode within 30 min of irradiation, while only 24% of BTA was removed within 30 min of irradiation. After 30 mins, the rate of removal decreased for ACT and PRO, which could have been caused by a limiting transport of ACT and PRO molecules from the bulk solution to the photoanode-electrolyte interface where the removal reaction takes place [153]. As the transport of ACT and PRO molecules towards the surface of the $BiVO_4$ photoanode became slower, the removal rate decreased, which resulted in longer times to reach 99% removal efficiencies for ACT and PRO. This observation is in agreement with the findings from the Nyquist plot (Fig 3.4(e)), showing mixed kinetic-diffusion for the removal of ACT. The decrease in (normalized) concentration of BTA remained almost constant after 30 min, suggesting that the BTA removal was not influenced by the limiting transport of molecules towards the surface of photoanode. The low removal efficiency of $BiVO_4$ photoanode for BTA in comparison to ACT and PRO was most likely due to its low reactivity with •OH. The reactivity of •OH is influenced by the presence of functional groups and the chemical structure of the compound under consideration. BTA is generally resistant to oxidation by •OH because the triazole ring in BTA is relatively stable and cannot be easily oxidized by •OH attack,

whereas the N-H bond and the aromatic ring in BTA are more prone to •OH attack for oxidation [123]. In the case of PRO, the presence of primary and secondary alcohol groups makes it highly reactive to oxidation by •OH. Moreover, the aromatic ring in PRO could also be oxidized by •OH which can further enhance the kinetics of PRO removal [154]. Similarly in ACT, the phenolic hydroxyl and the amide group are highly susceptible to oxidation by •OH, which results in its fast removal [155]. Overall, it is likely that ACT and PRO involved more reaction pathways as compared to BTA for the oxidation by •OH due to their chemical structure and attached functional groups that resulted in their higher removal. The complete reaction

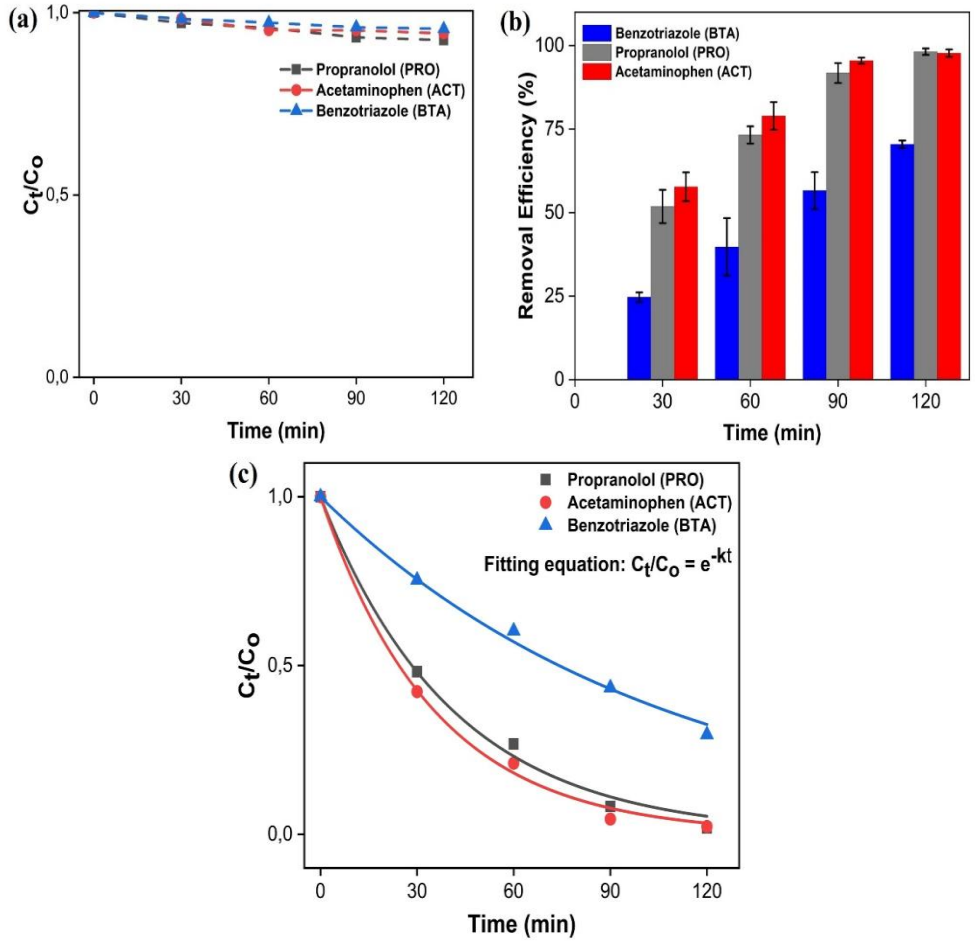


Fig. 3.5: *(a) Normalized removal of ACT, BTA and PRO in response to direct interaction of the incoming solar simulated light (60 W m^{-2}) with the reaction solution for 2 hours (b) Comparison of efficiency of removing ACT, BTA and PRO by using the $BiVO_4$ photoanode at intervals of 30 min (c) Fitting of the first order kinetic model to the normalized simultaneous removal efficiencies of ACT, BTA and PRO under illuminated condition (60 W m^{-2}) during a 120 min removal experiment.*

pathway and the ultimate fate of ACT, BTA and PRO in demineralized water could not be confirmed in this study because the intermediate products were not analysed. The identification and quantification of intermediate products of OMPs are quite challenging because of the low initial concentration of parent OMP in the reaction solution [156]. Moreover, analysing the intermediate products of more than one OMP in a solution is complex [157] and was beyond the scope of this study.

Table 3.1: *Rate coefficients of first order reaction kinetics along with R^2 values and half-life times of ACT, BTA and PRO after 2 hours of removal experiment by using $BiVO_4$ photoanode.*

	Rate Coefficient (min^{-1})	R^2	Half-life time (min)
Acetaminophen	2.84×10^{-2}	0.993	28
Propranolol	2.44×10^{-2}	0.994	24
Benzotriazole	9.35×10^{-3}	0.996	74

The kinetics of PEC based simultaneous removal of ACT, BTA and PRO during 2 h of solar simulated irradiation is shown in Fig. 3.5(c). A first order rate equation ($C_t/C_0=e^{-kt}$) was used to compute the rate coefficients of ACT, BTA and PRO removal because the normalized decrease matched the first order kinetic model. As expected, the rate coefficients of ACT and PRO were almost equal (Table 3.1) and about 67% higher than the rate coefficient of BTA. Similarly, the half-life times of PEC based simultaneous removal of ACT and PRO were also approximately 67% higher than the half-life of BTA. Rate coefficients given in Table 3.1 are similar and comparable to the previous studies using different AOPs for the removal of ACT [158,159], BTA [160] and PRO [154] having initial concentrations of more than 1 mg L^{-1}. Table 3.2 summarizes a comparison between the removal efficiency of the fabricated $BiVO_4$ photoanode used in this study with the relevant literature is presented in Table 3.2. According to Table 3.2 most of the literature studies used 1.0 V as the applied external voltage, but the resulting removal efficiencies are lower than the removal efficiency of the $BiVO_4$ photoanode used in this study.

The results of the reusability experiments are shown in Fig. S. 7 of supplementary information. In reusability experiments, a $BiVO_4$ photoanode was used for four consecutive experiments of 2 h each. The $BiVO_4$ photoanode showed good reusability performance as the removal efficiency was only 17, 22 and 32% decreased for ACT, BTA and PRO respectively after three consecutive experiments of using one and the same photoanode. After the second experiment the removal efficiency of the photoanode remained constant as shown in supplementary information Fig. S. 7, the decrease in efficiency was most likely due to the adsorption of the unoxidized OMP molecules within the surface cracks of the photoanode that decreased the active surface area available for the water oxidation to produce reactive species (•OH and $^{\bullet}O_2^-$).

Table 3.2: *Summary table showing the comparison between the removal efficiency of the BiVO4 photoanode used in this study with the relevant literature studies.*

Photoanode	Pollutant Compound	Applied Potential and Light Intensity	Removal Efficiency	Ref
$BiVO_4$	Acetaminophen, Benzotriazole and Propranolol each at a starting concentration of 45 µg L^{-1}	1 V vs Ag/AgCl and 60 W m^{-2} light intensity (calibrated between 300-400 nm)	Simultaneous Removal of Acetaminophen 99%, Propranolol 100% and Benzotriazole 70% in 120 min	This Study
$BiVO_4$	Methylene Blue at 10 mg L^{-1}	1.0 V vs Ag/AgCl and 100 mW cm^{-2} of light intensity	50% in 80 min	[161]
$BiVO_4$	Ciprofloxacin at 10 mg L^{-1}	1.0 V vs Ag/AgCl and 100 mW cm^{-2} of light intensity	50% in 120 min	[79]
WO_3/$BiVO_4$@FeOOH	Sulfamethoxazole at 25 mg L^{-1}	1.0 vs RHE and light intensity of 100 mW cm^{-2}	35% in 120 min	[162]
$BiVO_4$	Phenol at 20 mg L^{-1}	1.0 vs Ag/AgCl and light intensity of 60 W m^{-2}	65% in 240 min	[163]
$BiVO_4$/TiO_2 nanotube	Tetracycline hydrochloride at 10 mg L^{-1}	0V and light intensity of 100 mW cm^{-2}	23% in 120 min	[164]
$BiVO_4$/WO_3	Norfloxaxin at 10 mg L^{-1}	1.0 V vs SCE and light intensity of 1 mW cm^{-1}	63% in 180 min	[80]

3.3.1 Electrical energy per order

The electrical energy per order (E_{EO}) quantifies the energy required (electrical and solar) in kilowatt hours (kWh) to decrease the concentration of an OMP in 1 m^3 volume of water by a factor of 10 (1 log reduction). E_{EO} for the selected OMPs was calculated by using Eq. 7 below [165]:

$$E_{EO} = \frac{P \times t \times 1000}{V \times 60 \times \log(\frac{C_i}{C_f})} \quad \text{(Eq. 7)}$$

Where P (kW) is the total input power, t (min) is the reaction time for the OMP removal, V (L) is the treated volume, C_i and C_f are initial and final concentrations of the OMP, respectively. For a first order reaction the term $\log(C_i/C_f)$ equals 0.4343kt, therefore, the final simplified E_{EO} equation is given below in Eq. 8 [166]:

$$E_{EO} = \frac{38.4 \times P}{V \times k} \quad \text{(Eq. 8)}$$

In Eq. 6, k (min^{-1}) is the rate coefficient of the OMPs given in table 1. Variable P (kW) is the total input power including electrical power and irradiation power that is available for the absorption by the $BiVO_4$ photoanode within its total absorbance area (300-550 nm). The total light intensity measured by a photodiode between 300-550 nm for 16 cm^2 surface area of photoanode was 1.09 x 10^{-3} kW. The applied electrical power was 1.6 x 10^{-6} kW based on 1 V external bias and 1.6 mA photocurrent. Therefore, the total input power of the system was 1.0916 x 10^{-3} kW, the E_{EO} values for each OMP are given in Fig. 6 (a) by substituting the values of V (0.167 L), P (1.0916 x 10^{-3} kW) and rate coefficients (k) in Eq. 8. The E_{EO} value for BTA in Fig. 3.6 (a) is higher than the E_{EO} values of ACT and PRO due to its slow removal kinetics. The total energy consumption (including both light intensity and electrical power) of the removal process of 2 hr was calculated as 13.07 kWh m^{-3}.

3.3.2 Quenching of reactive species

Quenching experiments were performed by using $BiVO_4$ photoanodes for the simultaneous removal of the selected OMPs in the presence of a quenching agent. EDTA, methanol and p-BZQ were used in separate experiments to quench photogenerated holes, hydroxyl and super-oxide radicals, respectively. Fig 3.6 (b), (c) and (d) show the removal efficiency of $BiVO_4$ photoanode for the selected OMPs in the presence of selected quenching agents. In the presence of EDTA (Fig. 3.6(b)), the removal efficiency of all OMPs decreased but the most pronounced effect was observed for BTA where the removal efficiency decreased from 70% (without quenching) to 29%. This substantial decrease in the removal of BTA suggested that photogenerated holes have the potential to directly oxidize the BTA molecules at the surface of the $BiVO_4$ photoanode. EDTA quenched the photogenerated holes thereby decreasing the in-situ generation of •OH, which could be another explanation for the decrease in the removal of all three OMPs because less •OH would be available for the oxidation. In the presence of methanol, all three OMPs showed substantial decrease in the removal efficiency as shown in Fig. 3.6(c). The decrease in the removal efficiency of ACT and BTA was higher compared to PRO which implies that •OH were the dominating reactive species for ACT and BTA. In the presence of p-BZQ, the removal efficiency of PRO decreased (Fig 3.6(d)) from 98% (without quenching) to 51%, whereas negligible decrease in the removal efficiency of ACT and BTA was observed. The substantial decrease in the removal efficiency of all three OMPs in the presence of methanol suggested that •OH were the dominating reactive specie for the oxidation

of all three OMPs. Similarly, the quenching results exhibited that the oxidation of PRO and BTA was partially influenced by $^{\bullet}O_2^-$ and photogenerated holes, respectively.

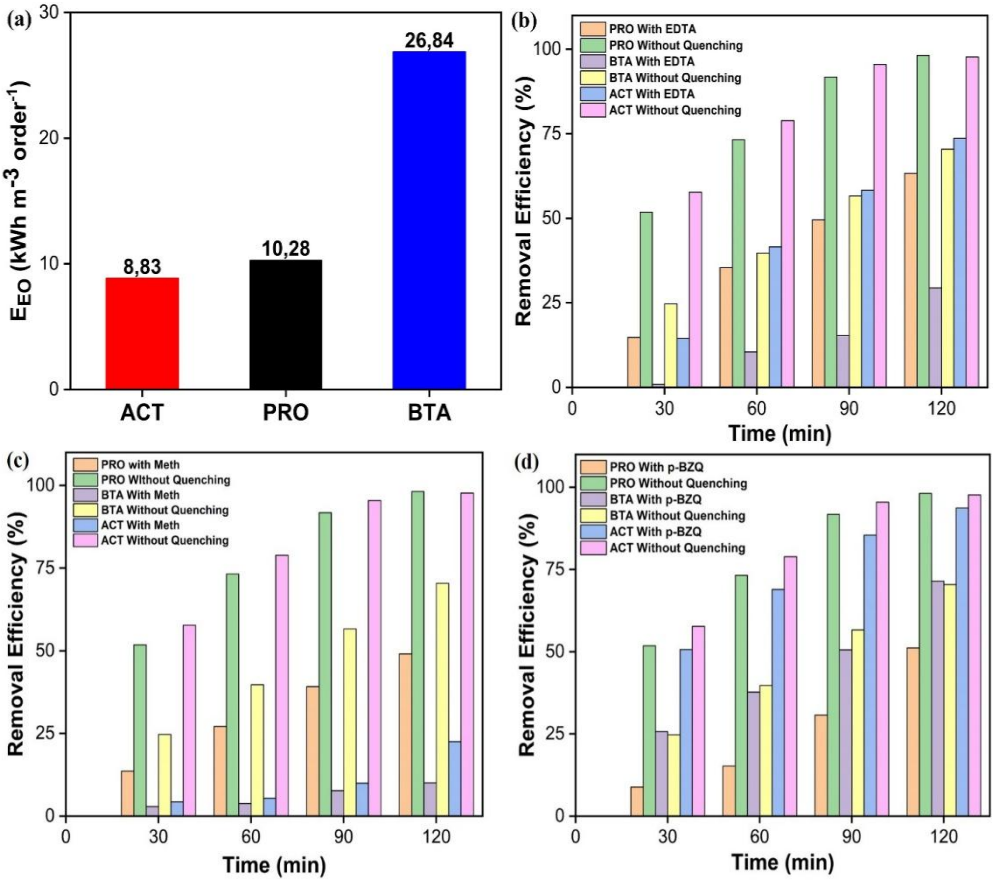


Figure 3.6: *(a) E_{EO} values for the complete removal of ACT, BTA and PRO (b) Removal efficiency of $BiVO_4$ photoanode for the removal of ACT, BTA and PRO in the presence of 4 mM EDTA, (c) 4 mM methanol and (d) 4 mM p-BZQ as quenching agents.*

4. Conclusions

A $BiVO_4$ photoanode was successfully fabricated by using a simple and effective dip-coating method to deposit a $BiVO_4$ photocatalytic layer on FTO glass slides. SEM characterization showed a rough surface morphology of the fabricated photoanode that was favourable for the adsorption of OMP molecules. The rough and porous surface morphology of the $BiVO_4$ photoanode played an important role for the generation of reactive species at the photoanode-electrolyte interface. Similarly, UV-Vis spectroscopy and IPCE measurements confirmed that the fabricated photoanode absorbed light in the visible spectrum of the solar irradiation for the in-situ generation of oxidants. The dip-coated $BiVO_4$ photoanode, used in the PEC-based AOP

removal, simultaneously removed more than 70% of the selected OMPs from the solution after 2 h. However, during the simultaneous removal, ACT and PRO showed faster removal kinetics than BTA. The faster removal of ACT and PRO was most likely due to their chemical structures and the presence of functional groups that facilitate multiple oxidation pathways for the attack of reactive species at the photoanode-electrolyte interface. Consequently, BTA required about 67% more energy for its removal from the solution than ACT and PRO. Findings of the quenching study revealed that •OH radicals were the dominating reactive species in our research for the PEC based simultaneous oxidation of the selected OMPs. The results obtained in this study are promising and could be considered as a foundation step towards the PEC-based simultaneous removal of multiple OMPs in WWTP effluents.

Acknowledgement

This research study was financed under the InnovEOX project that has received funding from the European Union's EU Framework Programme for Research and Innovation Horizon 2020 under Grant Agreement No 861369.

Supplementary Information

1. Effect of $BiVO_4$ layer on the removal efficiency

Fig. S. 1 shows the effect of deposited layers of $BiVO_4$ on the removal performance of the photoanodes for ACT (45 µg L^{-1}) removal. Each photoanode was tested for ACT removal in a similar way as described in section 2.4 of the main manuscript. Photoanodes with 1, 2, 3, 4 and 5 $BiVO_4$ layers were tested to find the optimum thickness of $BiVO_4$ layer. Fig. 1 shows that the photoanode with three layers achieved the fastest removal of ACT compared to the other photoanodes. Hence the photoanode with three layers was selected for further characterization and application for the simultaneous removal of ACT, PRO and BTA.

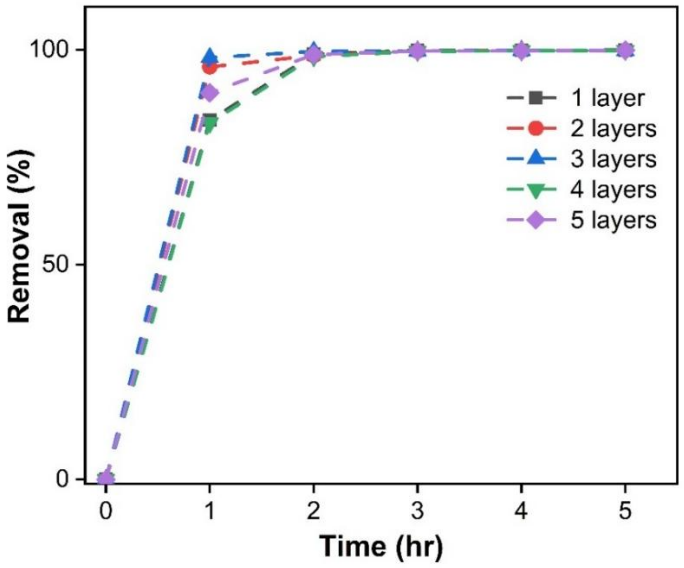


Fig. S.3.1: *Removal efficiency of ACT (C_0 = 45 µg L^{-1}) during 5 hours of removal experiment by using the fabricated photoanodes having 1, 2, 3, 4 and 5 layers of $BiVO_4$ at an external voltage of 1 V vs Ag/AgCl*

Table. S.3.1: *Thickness of $BiVO_4$ layers measured by surface profilometery.*

Number of $BiVO_4$ layers	Thickness (µm)
1	1.61
2	2.25
3	2.70
4	3.07
5	3.34

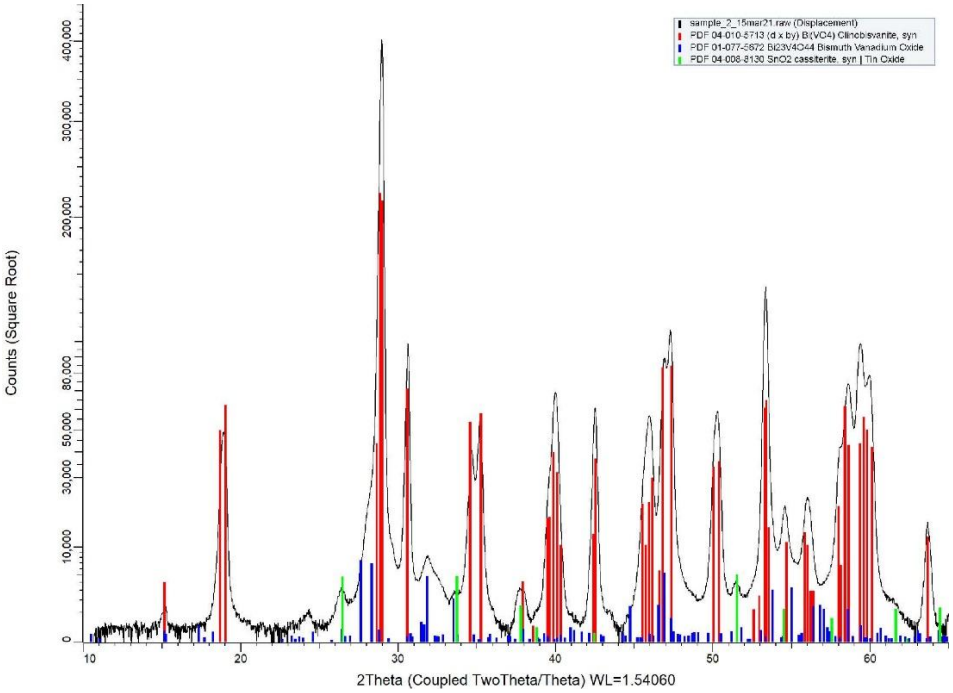


Fig. S.3.2: *XRD peaks of $BiVO_4$ sample (black) and ICDD database reference peaks of $BiVO_4$ (red) bismuth vanadium oxide (blue) and FTO (green)*

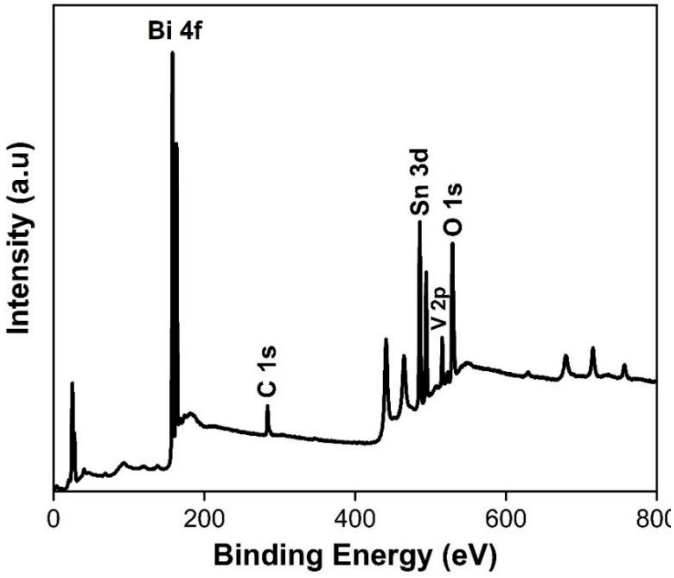


Fig. S.3.3: *XPS survey scan of $BiVO_4$ photoanode showing distinct peaks of Bi, V, O and Sn at their respective binding energies*

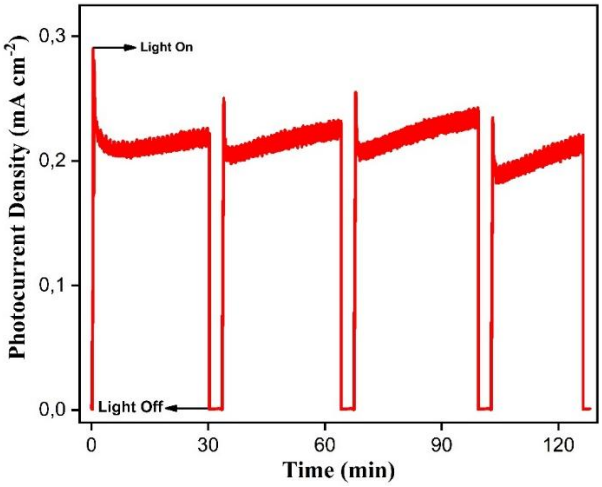


Fig. S.3.4: *Transient photocurrent response of the $BiVO_4$ photoanode during the PEC removal experiment at 1.0 V vs Ag/AgCl with 0.1 M Na_2SO_4 electrolyte having ACT, BTA and PRO each at a starting concentration of 45 ug L^{-1}.*

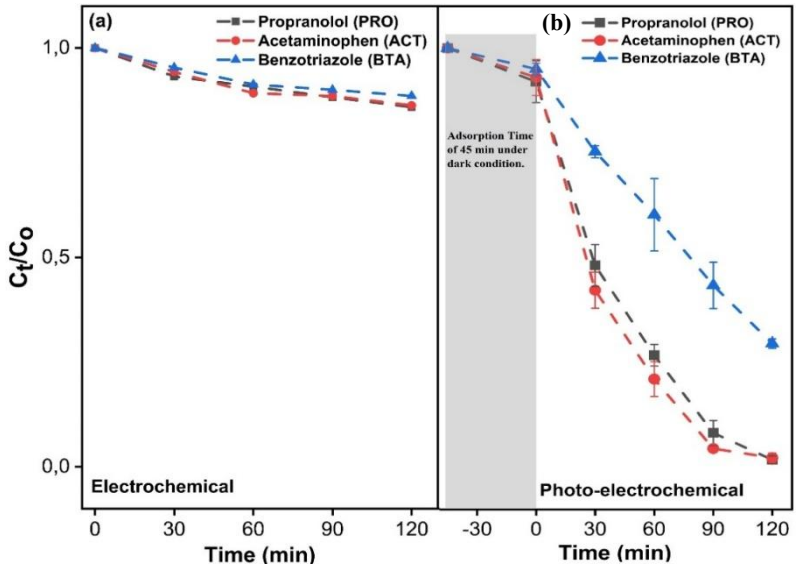


Fig. S.3.5: *Normalized removal of ACT, BTA and PRO during 120 min of removal experiment by using $BiVO_4$ photoanodes in the absence of light (dark) corresponding to an electrochemical reaction at 1 V as external applied voltage (a) and in the presence of light (60 W m^{-2}) corresponding to a photo-electrochemical reaction at 1 V as external applied voltage (b)*

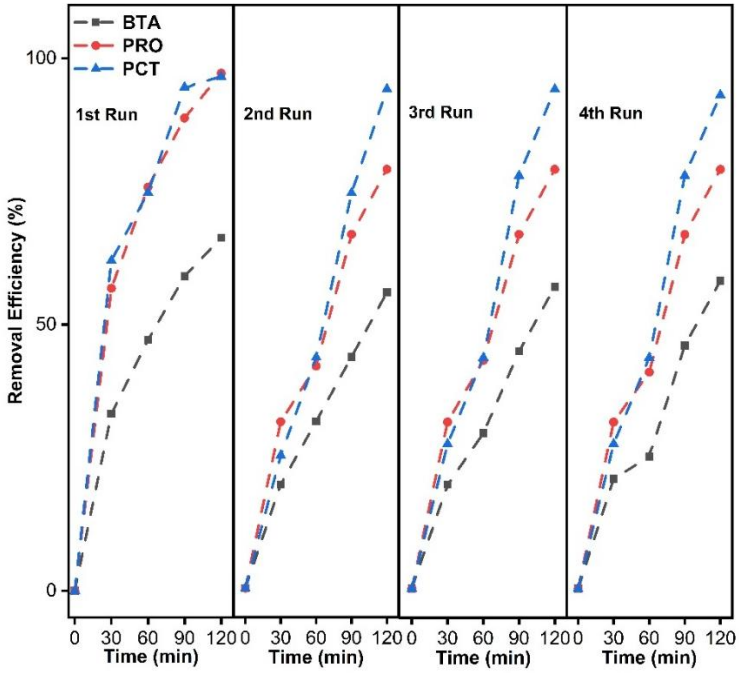


Fig. S.3.6: *Removal efficiency of a $BiVO_4$ photoanode during 2 hours of four consecutive experimental runs. The removal experiments were performed in a three-electrode set-up in which the $BiVO_4$ photoanode was the working electrode, Ag/AgCl was the reference electrode and graphite plate was the counter electrode.*

Chapter 4

Photoelectrocatalytic based removal of acetaminophen: Application of visible light driven heterojunction based $BiVO_4$/BiOI photoanode

This chapter is based on the following publication:

Agha Zeeshan Ali, Yiqian Wu, Yasmina-Doekhi Bennani, Henri Spanjers, Jan Peter van der Hoek, Photo-electrocatalytic based removal of acetaminophen: Application of visible light driven Heterojunction based $BiVO_4$/BiOI photoanode, Chemosphere, Volume 324, 2023, 138322, https://doi.org/10.1016/j.chemosphere.2023.138322.

Abstract

The presence of organic micro-pollutants (OMPs) in wastewater treatment effluents is becoming a major threat to the water safety for aquatic and human health. Photo-electrocatalytic based advanced oxidation process (AOP) is one of the emerging and effective techniques to degrade OMPs through oxidative mechanism. This study investigated the application of heterojunction based $BiVO_4$/BiOI photoanode for acetaminophen (40 μg L^{-1}) removal in demineralized water. Photoanodes were fabricated by electrodeposition of $BiVO_4$ and BiOI photocatalytic layers. Optical (UV-vis diffusive reflectance spectroscopy), structural (XRD, SEM, EDX) and opto-electronic (IPCE) characterization confirmed the successful formation of heterojunction for enhanced charge separation efficiency. The heterojunction photoanode showed incident photon to current conversion efficiency of 16% (λ_{max}=390 nm) at an external voltage of 1 V under AM 1.5 standard illumination. The application of the $BiVO_4$/BiOI photoanode in the removal of acetaminophen at 1 V (external bias) vs Ag/AgCl under simulated sunlight showed 87% removal efficiency within the first 120 min compared to 66% removal efficiency of the $BiVO_4$ photoanode. Similarly, combining $BiVO_4$ and BiOI exhibited 57% increase in first order removal rate coefficient compared to $BiVO_4$. The photoanodes also showed moderate stability and reusability by showing 26% decrease in overall degradation efficiency after three cycles of each 5 h experiment. The results obtained in this study can be considered as a stepping stone towards the effective removal of acetaminophen as an OMP present in wastewater.

Keywords: Organic micro-pollutants, Advanced oxidation process, photoelectrocatalysis, heterojunction photoanodes, $BiVO_4$/BiOI, acetaminophen.

1. Introduction

Water pollution is a major environmental concern due to various factors among which increase in industrial growth, population growth and water scarcity are the most important [3]. Owing to the importance of water safety, The United Nations (UN) also included access to clean water and sanitation in its sustainable development goals list [167]. Keeping the surface water bodies safe for use is imperative because major part of the drinking water supply comes from surface water resources [168]. The majority of the research efforts within wastewater treatment domain is focused on ensuring that the wastewater treatment plant's (WWTP) effluent is safe for aquatic and human life [169]. Apart from resource recovery from the wastewater (Puyol et al., 2017; Solon et al., 2019), using the treated wastewater for different practical purposes is also becoming increasingly important within the circular economy domain [171]. Conventional treatment plants only remove carbon (C), nitrogen (N) and phosphorous (P) from the wastewater [105]. However, over the past several decades analysis of WWTP effluents has shown that some chemical compounds mainly belonging to the industrial and pharmaceutical compounds category [172] are still present in the effluent within the range of 1-10 μg L^{-1} [173]. The compounds that are present in the water resources in the ng L^{-1} to μg L^{-1} range are called

micro-pollutants (MPs), and MPs that are organic are called organic micro-pollutants (OMPs) [174].

Advanced oxidation processes (AOPs) are becoming increasingly important for the complete removal of OMPs from industrial or municipal wastewater. Among various types of AOPs, photoelectrocatalytic (PEC) based AOP is gaining importance due to the use of solar energy to activate photocatalytic materials for the generation of reactive species. PEC based AOP involves the use of semiconducting anode materials for the in-situ production of oxidants that are mainly hydroxyl (•OH) and superoxide radicals ($^{\bullet}O_2^-$). The in-situ oxidants unselectively oxidize the organic pollutants to remove them from the wastewater [175]. Metal oxide based photocatalysts such as titanium dioxide (TiO_2) [111], tungsten trioxide (WO_3) [112], zinc oxide (ZnO) [61], zirconium dioxide (ZrO_2) [113] and iron oxide (Fe_2O_3) [110] are widely reported in literature for the removal of pharmaceuticals and industrial dyes (1-10 mg L^{-1}) in aqueous solution. However, these photocatalysts have an intrinsic drawback that due to their large band gap energy (3.0 – 3.5 eV) they can only absorb photons in the UV range of solar irradiation. Bismuth vanadate ($BiVO_4$) in its monoclinic scheelite phase is a small band gap (~2.4 eV) visible light driven photocatalyst and, due to its stability and non-toxicity, $BiVO_4$ is used as anodic material for the PEC based removal of organic micro-pollutants in aqueous solution [176,177]. However, PEC activity of pristine $BiVO_4$ is hindered due to poor charge transport and high rate of recombination of photo-generated electron-hole pairs [178]. The PEC activity corresponds to the removal efficiency of the $BiVO_4$ photoanode for the removal of pollutants from aqueous solution. Combining monoclinic scheelite $BiVO_4$ with other photocatalysts to make a heterojunction is one of the effective strategies to improve the PEC activity of $BiVO_4$ [178]. Depending on the band gap alignment of the photocatalysts under consideration, the heterojunction between them can be of two types, either type I or type II [45]. Photogenerated holes and electrons in type I heterojunction are transferred to the electrode-electrolyte interface, whereas in type II heterojunction the photogenerated charge carriers are transferred in opposite directions thereby effectively enhancing the charge separation in the photoanode [45] (illustrated in Fig. 4.1). Various heterojunction structures that are mostly type II such as WO_3/$BiVO_4$ [80], CuO/$BiVO_4$ [148], CdS/$BiVO_4$ [179], $BiVO_4$/Ag_2S [79] and $BiVO_4$/Ag_3PO_4 [180] are reported in literature that have shown enhanced PEC based removal of dyes and pharmaceutical compounds compared to pure $BiVO_4$.

Bismuth oxyiodide (BiOI) is also a bismuth based small band gap (~1.9 eV) photocatalyst that can be used for visible-light applications. Combining $BiVO_4$ with BiOI is also possible as $BiVO_4$/BiOI heterojunction-based nanoparticles are used to remove dyes. The heterostructure based $BiVO_4$/BiOI nanoparticles shows improved PEC activity compared to pristine $BiVO_4$ and BiOI due to enhanced charge separation efficiency [181,182]. Only one application of

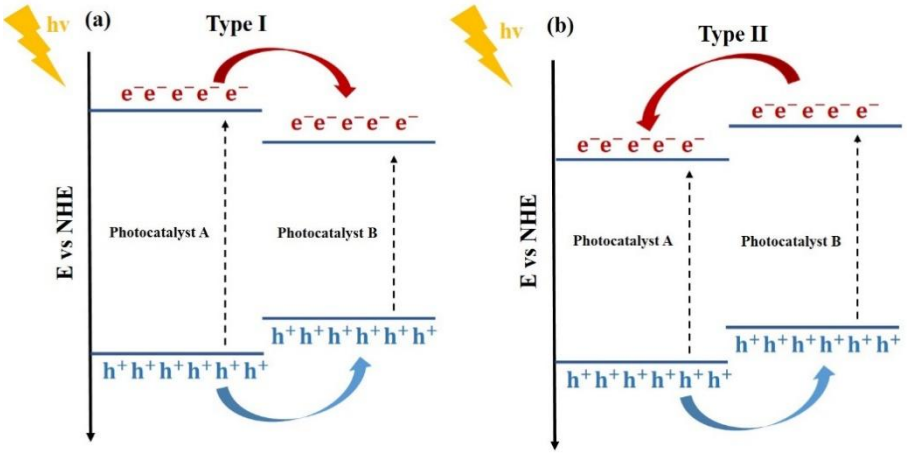


Fig. 4.1: *Illustration showing the transfer of photogenerated holes and electrons in type I and type II heterojunction after the interaction of incoming solar photons with the BiVO4 heterojunction photoanode.*

$BiVO_4$/BiOI photoanode is reported in literature for the degradation of pharmaceuticals [137], however, the concentration of pharmaceuticals was 10 mg L^{-1}, which is much higher than actual concentration of OMPs present in the aquatic environment [174]. At lower concentrations (<100 µg L^{-1}) the removal kinetics of organic micro-pollutants would be different as there will be chances of lack of diffusion of organic molecules from bulk solution to the surface of the photoanode. To the best of our knowledge and based on a literature review [45], there is a lack of knowledge regarding the use of $BiVO_4$ and $BiVO_4$/BiOI photoanode for the removal of organic micro-pollutants in the concentration range of 0-100 µg L^{-1}.

Acetaminophen (ACT) belongs to the non-steroidal anti-inflammatory drugs (NSAIDs) category that can be purchased as over the counter (OTC) drug without any specific prescription [134]. Due to the excessive use of ACT for pain and fever reduction [183], it is one of the most commonly found OMP in wastewater, surface water and drinking water [7]. Eco-toxic effects of ACT and its transformation products on aquatic and human life have been widely investigated and now ACT is recognized as an environmental and human health concern [184]. Conventional WWTPs are unable to completely remove ACT from the influent and a concentration between 0-20 µg L^{-1} is still present in the WWTPs effluent in many European countries [135]. Electrochemical AOP (eAOP) has been widely employed to remove ACT from secondary effluents of WWTPs and simulated wastewater within the range of 1-10 mg L^{-1} [136]. However, there is a lack of information available on the removal kinetics of ACT at lower concentrations (<100 µg L^{-1}) using photo-electrocatalysis (PEC).

The objective of this study was to successfully fabricate a visible light driven heterojunction $BiVO_4$/BiOI photoanode and to employ it for ACT (40 µg L^{-1}) removal in demineralized water.

Removal kinetics of ACT by using the $BiVO_4$/BiOI photoanode was also compared with pristine $BiVO_4$ and BiOI photoanodes. $BiVO_4$, BiOI and $BiVO_4$/BiOI photoanodes were fabricated by electrodeposition. Fabricated photoanodes were characterized by using structural, morphological, optical and opto-electronic characterization techniques to analyse and confirm the formation of heterojunction between $BiVO_4$ and BiOI. Lastly, the fabricated photoanodes were used to remove ACT in demineralized water in a three electrode PEC set-up. Quenching experiments were also performed by using methanol and p-benzoquinone (p-BZQ) to evaluate the role of reactive species ($^{\bullet}OH$ and $^{\bullet}O_2^-$) in $BiVO_4$/BiOI photoanode based ACT removal.

2. Materials and Methods

Three different kinds of photoanodes (BiOI, $BiVO_4$ and $BiVO_4$/BiOI) were prepared in the first stage and their fabrication processes are described below.

2.1 Fabrication of BiOI photoanode

As previously reported, electrodeposition [178,185] with minor adjustments was used to deposit BiOI on fluorine doped tin oxide (FTO) glass (40 mm x 40 mm x 2.2 mm). To prepare the electrolyte for electrodeposition, 0.04 M bismuth nitrate pentahydrate ($Bi(NO_3)_3 \cdot 5H_2O$) was added to 50 mL of 0.4 M potassium iodide (KI) solution and the pH was adjusted to 1.5 – 1.6 by using 1M HNO_3. This solution was mixed with 20 mL of ethanol (100 %) containing 0.23 M p-benzoquinone and sonicated afterwards for 10-15 min. To electrodeposit the BiOI layer on the FTO glass, a cathodic bias of -0.2 V was applied for 5 min to the working electrode in a three electrode electrochemical cell. FTO glass, Ag/AgCl (3.0 M KCl) electrode and a platinum wire were used as the working electrode, reference electrode and counter electrode, respectively. After 5 min the working electrode was taken out from the cell and was rinsed with de-ionized water. After drying, a bright red coloured BiOI photoanode (shown in supplementary Fig. S.4.2) was stored for further use.

2.2 Preparation of $BiVO_4$ photoanode

A $BiVO_4$ photoanode was prepared by converting the BiOI layer to $BiVO_4$. First the BiOI layer on the surface of FTO glass (40 mm × 40 mm x 2.2 mm) was electrodeposited in the same way as described in the above section (2.1). To convert the BiOI layer to $BiVO_4$ a 0.15 - 0.2 mL of Dimethyl Sulfoxide (DMSO) solution containing 0.2 M Vanadyl-Acetylacetonate was drop casted on the BiOI layer. Then, the electrode was placed in a furnace for annealing treatment at 450°C for 2 h (ramping rate at 5°C/min). After annealing treatment, the electrode was taken from the furnace and as a last step the electrode was soaked in 1.0 M NaOH for 15 min under gentle stirring to remove the excess vanadium oxide (V_2O_5). After removing excess V_2O_5, the bright yellow coloured electrode (shown in supplementary Fig. S.4.2) was kept in a dry place under normal atmosphere for further use.

2.3 Fabrication of $BiVO_4$/BiOI heterojunction photoanode

To fabricate a heterojunction photoanode, first $BiVO_4$ photoanode was fabricated in the same way as described in section 2.2. To electrodeposit a BiOI layer on top of the $BiVO_4$ photoanode same procedure was followed as described in section 2.1. The only change was that the $BiVO_4$ photoanode replaced FTO as the working electrode in the three-electrode electrochemical set-up. After the electrodeposition process, the $BiVO_4$/BiOI photoanode was washed with deionized water and after drying the $BiVO_4$/BiOI photoanode (shown in supplementary Fig. S.4.2) was stored in a dry place under normal atmosphere for further use.

Fig. S.4.1 in the supplementary information explains why 5 min was selected as the deposition time for the fabrication of the $BiVO_4$ photoanode and for the deposition of BiOI on the BiVO4 photoanode.

2.4 Structural and morphological characterization

Morphological and micro/nano-structure analysis of fabricated photoanodes was carried out by using field emission scanning electron microscopy (SEM) (FEI, Quanta F650) coupled with an Inca 250 SSD XMax20 detector for energy-dispersive X-ray spectrometer (EDS) analysis. The degree of crystallinity and purity of the photoanodes were determined with X-ray diffraction (XRD) using Cu Kα radiation within a range of 2 θ = 10° - 130°, a step size of 0.040° 2 θ, and a counting time of 2 seconds per step. X-ray photoelectron spectroscopy (XPS) analysis was carried out with a Thermo Fisher K-Alpha surface analysis machine (Thermo Fisher Scientific, USA).

2.5 Optical and Opto-electronic characterization

Optical properties of fabricated photoanodes were studied between 300 – 700 nm (5 nm step size) by using diffusive reflectance UV-vis spectroscopy (The LAMBDA 1050+ UV/Vis/NIR spectrophotometer, UV Winlab software). Incident photon-to-electron conversion efficiency (IPCE) was also measured between 280 – 700 nm by using a customized incident photon to current conversion efficiency (IPCE) set-up under 1 sun illumination (AM 1.5 standard conditions). Each IPCE measurement was carried out by using the $BiVO_4$/BiOI, $BiVO_4$ and BiOI photoanode each time as working electrode at 1 V (external bias) and a platinum wire as the counter electrode. 40 μg L^{-1} ACT dissolved in 0.1 M Na_2SO_4 solution was used as electrolyte for IPCE measurements. Linear sweep voltammetry (LSV) was carried out in a three-electrode arrangement between -0.2 to 1.5 V (vs Ag/AgCl) at a scan rate of 100 mV s^{-1} in 0.1 M Na_2SO_4.

2.6 Photo-electrocatalytic (PEC) experiments

PEC based removal of ACT by using the prepared photoanodes was carried out by using Autolab potentiostat (PGSTAT128N) in three electrode configuration set-up. A quartz reactor

cell containing three electrodes and 167 mL of electrolyte solution was used for the PEC removal experiments. 0.1 M Na_2SO_4 containing 40 µg L^{-1} ACT having a pH of 6.8 was used as electrolyte for the removal experiments and demineralized water was used for the preparation of the electrolyte. Fabricated photoanodes, Ag/AgCl (3.0 M KCl) electrode and graphite plate (40 x 40 mm) were used as working electrode, reference electrode and counter electrode, respectively. A constant voltage of 1 V vs Ag/AgCl was applied during the removal experiment to minimize the rate of recombination in the fabricated photoanodes. Solar simulator SUNTEST XXL+ having three air cooled 1700 W Xenon lamps emitting 1 sun illumination spectra was used as light source. The intensity of emitted light between 300-400 nm was calibrated to 60 W/m^2 and the distance between the light source and the photoanode was 13 cm. Each experiment ran for 5 h and samples were taken at an interval of 1 h for the analysis of ACT. Reusability experiments with $BiVO_4$/BiOI photoanode were performed by using same photoanode for three consecutive removal experiments of each 5 h experiment. Between successive experiments the photoanode was rinsed with demineralized water to remove any adsorbed acetaminophen on the photoanode.

2.6.1 Quenching experiments

Quenching experiments were carried out in a similar way as the removal experiments described in section 2.6, except the addition of quenching agents in the electrolyte. To quench the $^{\bullet}OH$ reactive species 5 mM methanol was added in the electrolyte because methanol has a high reaction rate constant of 9.7 x 10^8 $M^{-1}s^{-1}$ with $^{\bullet}OH$ [186], whereas in a separate experiment 5 mM p-BZQ [79] was added in the electrolyte to quench $^{\bullet}O_2^-$. Each experiment ran for 5 h and samples were taken at an interval of 1 h for the quantification of ACT.

2.7 Analytical measurement of ACT

The concentration of ACT in the samples was measured by using liquid chromatography combined with tandem triple-quadrupole mass spectrometry (LC-MS). Acquity UPLC BEH C18 column from Waters was used in LC-MS to measure ACT in the samples. All Samples were first filtered with 0.2 µm glass fibre filters (GF-75, ADVANTEC®, Japan) and then 495 µL of filtered sample solution and 5 µL of internal standard (ACT-ring D4) calibration solution were added to the LC-MS sample vials. After mixing, the quantification of the target compound (ACT) in the samples was accomplished by the LC-MS device. Based on the concentration values of ACT, removal efficiency of each photoanode was calculated by using the following equation:

$$\textbf{Removal efficiency (\%)} = \left(1 - \frac{C_0}{C_t}\right) \times 100$$

Where C_0 = Initial concentration at time t=0 and C_t = Concentration at any time

3. Results and Discussion

3.1 Structure and morphology of photoanodes

Fig. 4.2 shows the X-ray diffractograms of $BiVO_4$, BiOI and $BiVO_4$/BiOI photoanodes. In the case of $BiVO_4$, the characteristic peaks at 18.8°, 19.1°, 29.03°, 30.64°, 34.63°, 35.32°, 39.95°, 42.5°, 46.83°, 47.39°, 51.54°, 59.7° and 60.08° corresponded to monoclinic scheelite phase of $BiVO_4$ (JCPDS no. 75-1866). These characteristic peaks were in accordance with previous studies [79,164] indexed as (110), (011), (121), (040), (200), (002), (211), (015), (240), (042), (161), (321) and (123), respectively [187].Main peaks of BiOI at 30.01°, 32.19°, 45.89°, 51.95° and 55.65° are previously reported in literature [188] and were indexed as (102), (110), (200), (114) and (212), respectively [189]. The XRD pattern of $BiVO_4$/BiOI photoanode contains the characteristic peaks of both monoclinic scheelite $BiVO_4$ and BiOI [181], which confirms the successful deposition of BiOI on top of the $BiVO_4$ layer.

The scanning electron microscopy (SEM) images in Fig. 4.3 show the surface morphology of pristine $BiVO_4$ and heterojunction $BiVO_4$/BiOI photoanode. Fig. 4.3a shows homogenous distribution of $BiVO_4$ particles over FTO substrate after electrodeposition. The fabrication process proved to be effective in producing $BiVO_4$ particles of similar shape and size. Fig. 4.3b shows the magnified image of $BiVO_4$ particles that were inter-connected to form a branched network. This branched network could facilitate an effective charge transfer at the interface of heterojunction. Fig. 4.3c shows the surface morphology of the $BiVO_4$/BiOI photoanode, which exhibited a homogeneous deposition of needle-like BiOI particles on top of the $BiVO_4$ layer. The magnified image in Fig. 4.3d shows the interaction of needle-like BiOI particles with the branched $BiVO_4$ particles. The interaction shows that there was an interfacial contact between the photocatalytic layers that will hold the potential to enhance the charge separation in the photoanode [190]. The energy dispersive X-Ray (EDX) spectrum shown in 4.3 (e) gives the compositional analysis of the heterojunction photoanode, and it consisted of only Bi, I, O and V. The element tin (Sn) in the EDX spectra came from the fluorine doped tin oxide (FTO) substrate. The EDX result also confirmed the purity of the deposited photocatalytic layers without any major impurity element present.

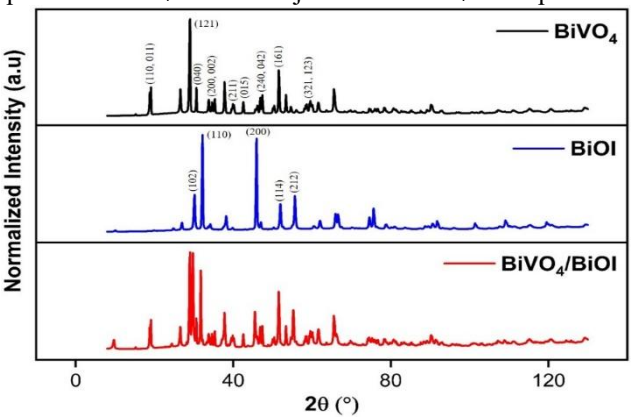


Fig. 4.2: *XRD patterns of $BiVO_4$, BiOI and $BiVO_4$/BiOI photoanodes showing indexed characteristic peaks.*

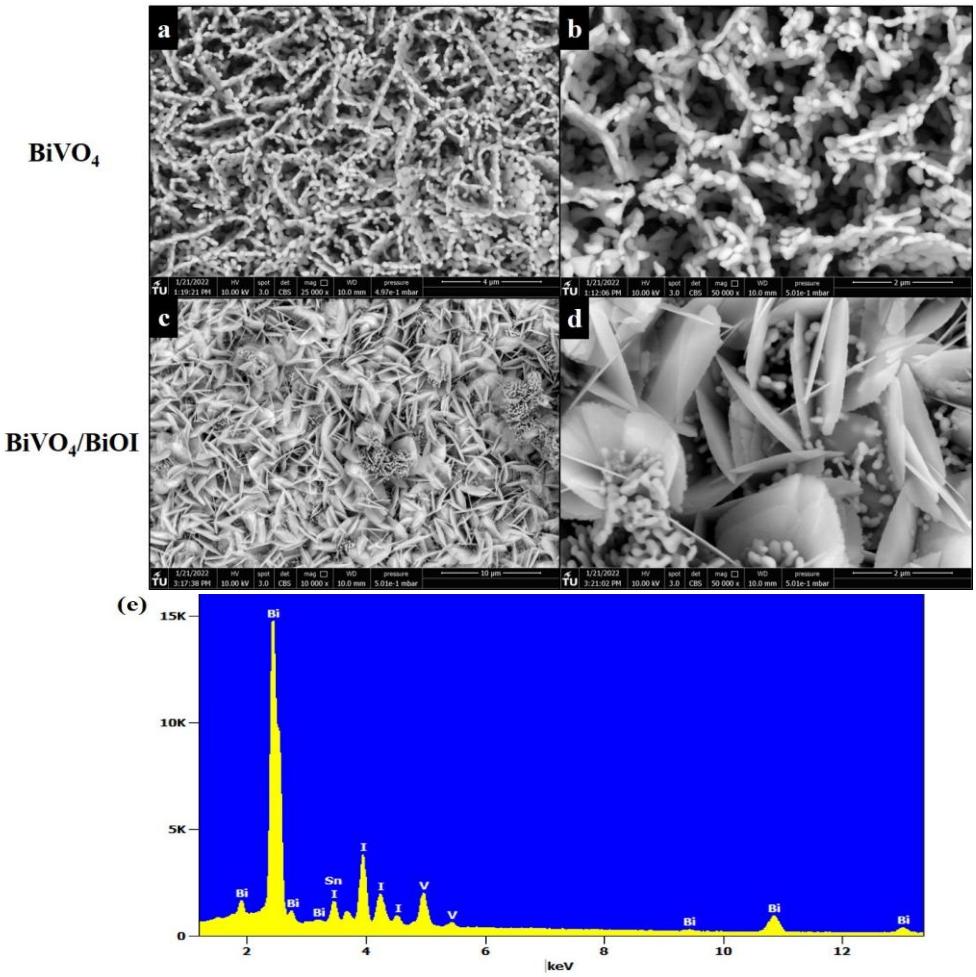


***Fig. 4.3**: SEM surface morphology images of $BiVO_4$ (a) (b), $BiVO_4$/BiOI (c) (d) and EDX spectra of $BiVO_4$/BiOI showing the peaks of elements present in the photoanode (e)*

X-Ray photoelectron spectroscopy (XPS) survey results are shown in supplementary Fig. S.4.3. The survey confirmed that only Bi, V, O, I, and C were present in the photoanodes and showed distinct peaks at their respective binding energies. The survey of $BiVO_4$/BiOI in particular confirmed the co-existence of Bi, V, O, I and C, which indicated the formation of a heterojunction. Carbon (C) is considered as impurity element and came from the atmosphere during the measurement. The de-convoluted high-resolution spectra of elements (Bi, V, I, O) present in the photoanodes are also shown in Fig. 4.4. Starting with the Bi, two asymmetric peaks with different binding energies corresponded to two different spin orbit splitting states ($4f_{5/2}$ & $4f_{7/2}$) of Bi4f. The peaks at 162.85 , 157.48 eV in $BiVO_4$ and 163.98, 158.58 eV in BiOI were related to $Bi4f_{5/2}$ and $Bi4f_{7/2}$ respectively (Meng et al., 2020; Ni et al., 2018, p. 4).

These characteristic peaks of Bi4f also suggest that Bi was present in the form of Bi^{3+} in the crystal lattice. The peak positions of $Bi4f_{5/2}$ and $Bi4f_{7/2}$ in $BiVO_4$/BiOI photoanode were at 163.58 and 158.28 eV, respectively. The slight increase in binding energies of Bi4f in $BiVO_4$/BiOI photoanode compared to pristine $BiVO_4$ could be due to a loss of surface bound oxygen and hydroxyl groups, which decreased the electron concentration around Bi [181]. Vanadium was also present in two different spin orbital states as $V2p_{1/2}$ and $V2p_{3/2}$ in both $BiVO_4$ and $BiVO_4$/BiOI photoanode. Two distinct peaks at 528.28 and 515.08 eV corresponded to $V2p_{1/2}$ and $V2p_{3/2}$ in $BiVO_4$, whereas the peaks at 529.08 and 515.98 eV were related to $V2p_{1/2}$ and $V2p_{3/2}$ in $BiVO_4$/BiOI photoanode. The peak positions of $V2p_{1/2}$ and $V2p_{3/2}$ suggest that V was present as V^{5+} in both photoanodes [87,142]. Two relatively sharp peaks at 629.98 and 618.48 eV are attributed to $I3d_{3/2}$ and $I3d_{5/2}$ in BiOI electrode. The peaks at 629.68 and 618.18 eV corresponded to $I3d_{3/2}$ and $I3d_{5/2,}$ respectively, in the $BiVO_4$/BiOI photoanode. The peak positions of I3d in both photoanodes indicated that I was present in -1 oxidation state in the lattice structure [191]. Furthermore, there was no significant shift in the binding energies of $I3d_{3/2}$ and $I3d_{5/2}$ in $BiVO_4$/BiOI photoanode compared to BiOI, confirming that the chemical environment around I was the same in both photoanodes. In $BIVO_4$, O1s peaks observed at 528.18 and 528.98 eV corresponded to lattice oxygen bonded to Bi and V, respectively, whereas a diminishing peak at 530.8 eV was attributed to surface adsorbed O-OH molecules. In case of BiOI, the strong peak observed at 529.38 eV was related to lattice oxygen bonded to Bi, and a small peak at 530.88 eV that was also observed in $BiVO_4$ corresponded to surface absorbed O-OH molecules [181]. In the heterojunction photoanode, the O1s peak at 529.08 eV corresponded to lattice oxygen whereas the peak at 530.28 eV was attributed to surface adsorbed O-OH molecules. Because the binding energy of O1s in heterojunction photoanode was closer to the binding energy of the BiOI O1s peak, it can be inferred that the Bi-O interaction was stronger in heterojunction photoanode than pristine $BiVO_4$ photoanode. Overall, the XPS results show that both $BiVO_4$ and BiOI co-existed in heterojunction photoanode, which was in accordance with the XRD and SEM results.

3.2 Optical and Opto-electronic properties of prepared photoanodes

UV-Vis diffusive reflectance spectroscopy was used to analyse the optical properties of the fabricated photoanodes. Fig. 4.5a shows the absorbance pattern of $BiVO_4$, BiOI and $BiVO_4$/BiOI photoanodes and it is evident from the Fig. 5a that all three photoanodes absorbed in the UV-Visible range. As BiOI absorbed strongly in the visible range, combining it with $BiVO_4$ gave an increase in the absorbance edge of heterojunction photoanode as is shown in Fig. 4.5a. The absorbance edges of $BiVO_4$, BiOI and $BiVO_4$/BiOI photoanodes were around 501, 636 and 647 nm, respectively. The absorbance results confirmed that combining $BiVO_4$ and BiOI increased the absorbance range of the heterojunction photoanode. Furthermore, the absorbance data was used to estimate the band gap energies of the $BiVO_4$ and BiOI photoanodes using the Tauc equation as given below: [144].

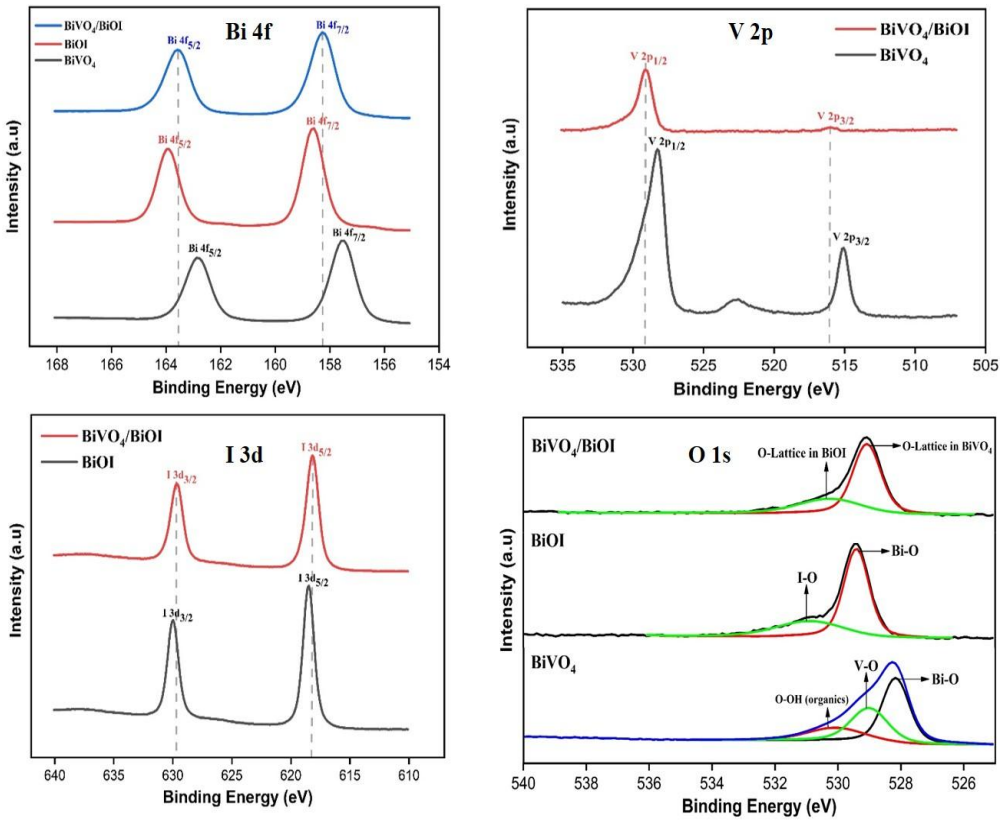


Fig. 4.4: *De-convoluted and high resolution elemental XPS spectra of Bi4f, V2p, I3d and O1s showing different orbital states, bonding environment and their respective binding energies.*

$$\alpha hv = A(vh - E_g)^{n/2} \text{ (Eq. 1)}$$

where α, h, v, A and E_g correspond to absorbance coefficient, Planck's constant, incident light frequency, constant and band gap energy, respectively in Eq. (1). The exponent n is a constant whose value is dependent on the optical transition behaviour of the photocatalyst under consideration. The value of n for a direct transition semiconductor such as $BiVO_4$ is 1 [192]. Therefore, a plot of $(\alpha hv)^2$ versus photon energy (hv) was made as shown in supplementary Fig. S.4.4 to estimate the band gap energy, which was 2.49 eV. Similarly, BiOI is an indirect optical transition semiconductor whose n value is 4 [193]. After substituting the value of n=4 in the Tauc equation a plot between $(\alpha hv)^{1/2}$ versus photon energy (hv) is made from which a band gap energy of 1.80 eV was obtained. The calculated values of band gap energies for $BiVO_4$ and BiOI photoanodes were very close to previously reported values in the literature). UV-vis absorbance results clearly showed that the absorbance region of $BiVO_4$/BiOI

photoanode was broader compared to $BiVO_4$ and BiOI, which confirmed the successful formation of a heterojunction.

Calculated band gap energies (E_g) were used to calculate the valence band (E_{VB}) and conduction band (E_{CB}) potentials of $BiVO_4$ and BiOI. Following equations were used to calculate E_{VB} and E_{CB} [137].

$$E_{CB} = X - E_C - 0.5E_g \text{ (Eq. 2)}$$

$$E_{VB} = E_g + E_{CB} \text{ (Eq. 3)}$$

wherein X is the geometric mean of the absolute electronegativities of all the constituent atoms present in the photocatalyst. The value of X for $BiVO_4$ is 6.04 eV, whereas for BiOI it is 6.10 eV [145]. E_c corresponds to the energy of free electrons with respect to hydrogen scale (NHE) and its value is 4.50 eV. E_g corresponds to the band gap energies of the respective photoanodes that were calculated using Tauc plots. By substituting the values of X, E_c and E_g in the above equations, the band edge potentials of $BiVO_4$ and BiOI were calculated. For BiOI the values of E_{CB} and E_{VB} were 0.7 and 2.5 eV, respectively, whereas for $BiVO_4$ the values of E_{CB} and E_{VB} were 0.29 and 2.78 eV, respectively. These band edge potential values show that the heterojunction that was formed between $BiVO_4$ and BiOI was of type I. In type I heterojunction both photogenerated charge carriers are transferred to the electrode-electrolyte interface [45] as shown in Fig. 4.5b. One intrinsic drawback of type I heterojunction is that there is a high chance of recombination if the photogenerated charge carriers are not consumed at the electrode electrolyte interface [45]. Application of a positive bias (applied potential >0) in type I heterojunction enhances the charge separation efficiency by creating an electric field at the heterojunction that pulls apart electrons and holes). Furthermore, in PEC based water treatment processes, the photogenerated holes and electrons are used to produce $^{\bullet}OH$ and $^{\bullet}O_2^-$ radicals which oxidize the organic pollutants [79]. Therefore, chances of recombination are reduced if photogenerated holes and electrons are consumed for the generation of $^{\bullet}OH$ and $^{\bullet}O_2^-$.

Linear sweep voltammetry (LSV) was carried out to study the effect of applying external voltage on the photocurrent generated by the photoanodes. In Fig. 4.5c, as expected the photocurrent generated by $BiVO_4$/BiOI photoanode in the presence of simulated solar light was higher compared to pristine $BiVO_4$ and BiOI. In illuminated conditions, the increase in the application of external voltage yielded a positive impact on the photo-current of all three types of photoanodes, confirming that the application of external bias reduced the rate of recombination. 1.0 V was chosen as the optimum potential to be applied for the PEC removal of ACT because at this potential sufficient current was generated. Increase in photocurrent of $BiVO_4$/BiOI photoanode implied that more charges (electrons and holes) were available at the electrode-electrolyte interface for the generation of reactive oxygen species (ROS). As a result, the formation of heterojunction will increase the removal kinetics of ACT in demineralized

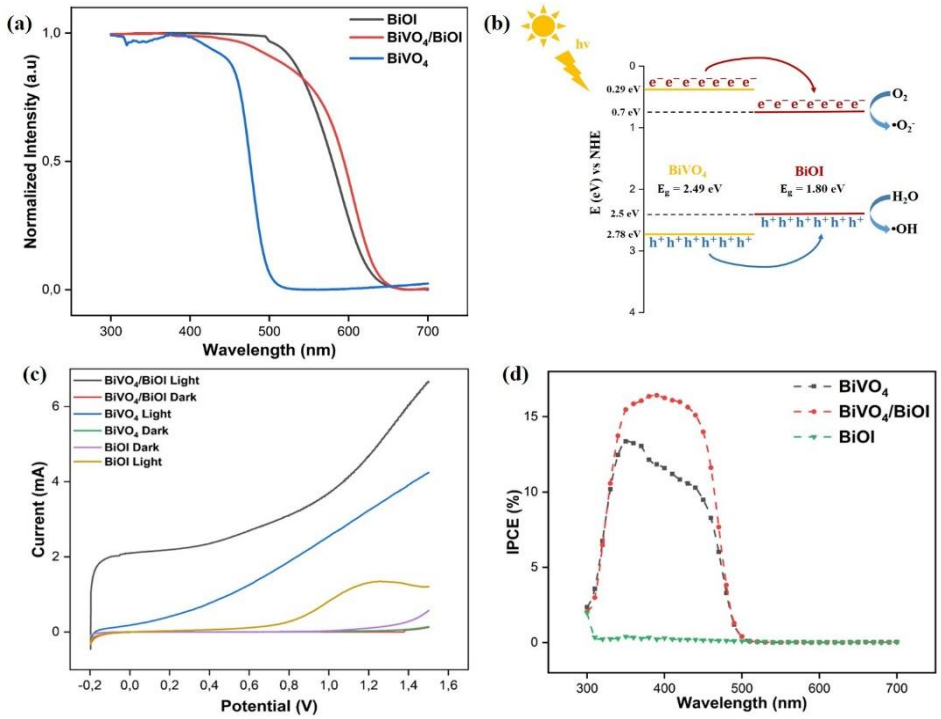


Fig. 4.5: *(a) UV-Visible diffusive reflectance spectra of $BiVO_4$, BiOI and $BiVO_4$/BiOI photoanodes showing the absorbance range (b) Illustration of photogenerated holes and electrons for the generation of $^{\bullet}OH$ and $^{\bullet}O_2^-$ radicals after the interaction of solar photons with $BiVO_4$/BiOI photoanode (c) LSV curves for $BiVO_4$, BiOI and $BiVO_4$/BiOI photoanodes under dark and illuminated conditions performed from -0.2 to 1.5 V at 100 mV s^{-1} scan rate (d) IPCE plots for $BiVO_4$, BiOI and $BiVO_4$/BiOI photoanodes under 1 sun illumination at 1V external bias vs platinum wire as counter electrode.*

water because of the increased in-situ generation of $^{\bullet}OH$ and $^{\bullet}O_2^-$. There is negligible current in the absence of light (dark), which means that applying an external voltage to the photoanodes in the absence of light will be of no use for the removal of ACT.

Incident photon to current conversion efficiency (IPCE) measurements were performed to study the quantum efficiency of fabricated photoanodes. Quantum efficiency measures the amount of electrons generated in response to the incident photons absorbed by the photoanode. Fig. 5d shows the IPCE plots of BiOI, $BiVO_4$ and BiVO4/BiOI photoanodes. The Fig. 5d clearly shows that $BiVO_4$ and heterojunction photoanode exhibits high incident photon to current conversion efficiency in UV-visible range. In case of $BiVO_4$, the maximum IPCE yield was 13%, and it occurred at 350 nm (λ_{max}), whereas after the formation of heterojunction the maximum IPCE yield increased to 16% at λ_{max}=390 nm. Pristine BiOI photoanode showed negligible IPCE yield which corresponded to its intrinsic high rate of recombination. Overall,

the IPCE result illustrates that the formation of heterojunction not only increased the incident photon to current conversion efficiency by 23% but it also shifted the λ_{max} further in the visible region. The IPCE measurement also gives the value of short circuit photo-current (J_{sc}), which corresponds to the maximum current that can be drawn from the photoanode [195]. The $BiVO_4$ photoanode yielded a J_{sc} of 4.88 A m^{-2}, whereas $BiVO_4$/BiOI photoanode yielded a J_{sc} of 7.05 A/m^2. This increase in IPCE and J_{sc} values as compared to $BiVO_4$ and BiOI was attributed to the interface of $BiVO_4$ and BiOI photocatalyts that increased the charge separation efficiency and thus reduced the rate of recombination in the heterojunction photoanode.

3.3 Photoelectrocatalytic removal of ACT

Fig. 4.6a shows the normalized decrease in concentration of ACT in demineralized water by using $BiVO_4$, BiOI and $BiVO_4$/BiOI photoanodes at an applied external voltage of 1 V vs Ag/AgCl (reference electrode). Direct irradiation with simulated sunlight from the solar simulator (photolysis) of the ACT solution had limited effect as it only removed 7% ACT in 5 hr. PEC based removal of ACT by using BiOI photoanode showed 24% removal in 5 hr. Fig. 4.6a shows that formation of heterojunction had a positive impact on the ACT removal. Although both $BiVO_4$ and $BiVO_4$/BiOI removed 100% ACT after 5 hr, the evolution of the removal efficiency is different. Fig. 4.6b provides more detailed insight on the removal efficiency of ACT on hourly basis. Fig. 4.6b shows that $BiVO_4$/BiOI photoanode removed more than half of the ACT within the first hour, which was a 22% increase in removal efficiency compared to $BiVO_4$. This increasing trend in the removal efficiency continued till 2 h and after that the removal efficiency of both photoanodes were similar. It can be observed in Fig. 4.6b that the removal efficiency increased with time, however, its rate of increment decreased with time. This was explained by the decrease in ACT concentration in the bulk solution, therefore, the reaction became partially diffusion controlled in which the diffusion of ACT molecules from bulk towards the surface of the photoanode became slower. The diffusion of ACT molecules to the surface is important because the oxidation reaction takes place within the vicinity of photoanode-electrolyte interface due to the short lifetime of ROS ($^{\bullet}OH$ and $^{\bullet}O_2^-$ radicals) [153]. According to previous studies related to ACT degradation suggest that three initial oxidation/hydroxylation reactions compete with each other [196,197]. In these reactions the reactive species ($^{\bullet}OH$ and $^{\bullet}O_2^-$ radicals) attack the aromatic ring of ACT to form ortho-, para- or meta-hydroxylation products of ACT [197]. Nuclear magnetic resonance (NMR) studies have shown that the meta-position is relatively favourable for further degradation of ACT [196], however, the complete mechanism of ACT degradation cannot be proposed in this study because the intermediates/transformation products of ACT were not analysed.

Kinetic plots for $BiVO_4$, BiOI $BiVO_4$/BiOI are shown in Fig. 4.6c. Because the normalized removal followed a classical first order reaction, first order rate equation ($C/C_0=e^{-k/t}$) was used to determine the rate coefficients of $BiVO_4$, BiOI and $BiVO_4$/BiOI photoanodes. As expected, the rate coefficient of $BiVO_4$/BiOI photoanode (shown in Table 4.1) compared to $BiVO_4$ is

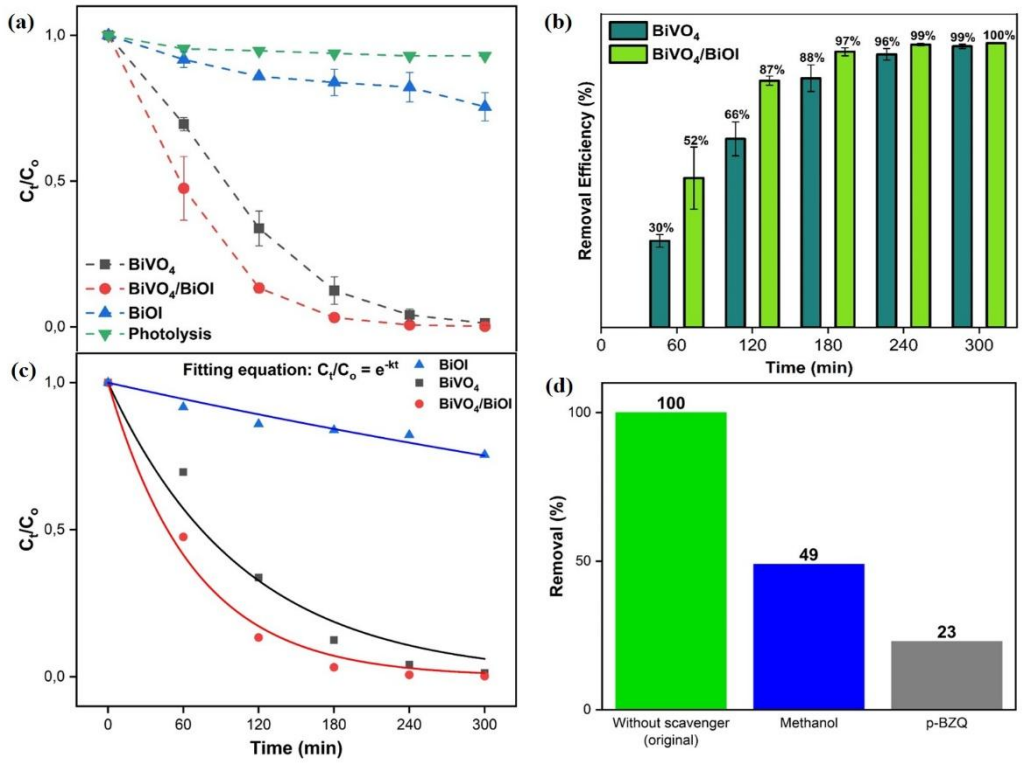


Fig. 4.6: *(a) Normalized decrease in concentration of ACT during 5 h of removal experiment by using the fabricated photoanodes at an external bias of 1 V vs Ag/AgCl (b) Comparison of removal efficiency of $BiVO_4$ and $BiVO_4$ /BiOI photoanode on hourly basis (c) Determination of first order rate coefficients of $BiVO_4$, BiOI and $BiVO_4$/BiOI photoanodes during 5 h of removal experiments (d) Removal efficiency of $BiVO_4$/BiOI photoanode in the presence of quenching agent. 5 mM methanol was used to quench $^{\bullet}OH$ radicals and 5mM p-BZO was used to quench $^{\bullet}O_2^-$ radicals.*

57% higher. The overall superior performance of $BiVO_4$/BiOI in removing ACT from demineralized water is attributed to the formation of heterojunction that facilitated the charge separation efficiency. Similarly, the applied external voltage of 1 V (vs Ag/AgCl) further decreased the rate of recombination by diverting the electrons from the conduction band to the external electrical circuit.

Table 4.1: *First order rate coefficients of BiOI, $BiVO_4$ and $BiVO_4$/BiOI photoanodes after 5 h of illumination.*

Photoanode	Rate coefficient (min^{-1})	R^2
BiOI	9.50×10^{-4}	0.928
$BiVO_4$	9.32×10^{-3}	0.967
$BiVO_4$/BiOI	1.46×10^{-2}	0.928

The removal rate coefficient of the $BiVO_4$/BiOI photoanode given in Table 4.1 is similar or higher than the rate coefficients reported in literature that applied $BiVO_4$ based photoanodes for the removal of different pharmaceuticals such as phenol (20 mg L^{-1}; k = 0.5 x 10^{-2} min^{-1}) [72], bisphenol A (10 mg L^{-1}; k = 4.1 x 10^{-2} min^{-1}) [74], norfloxacin (10 mg L^{-1}; k = 0.268 x 10^{-2} min^{-1}) [80], tetracycline hydrochloride (10 mg L^{-1}; k = 0.51 x 10^{-2} min^{-1}) [164] and dyes such as methyl orange (10 mg L^{-1}; k = 2.9 x 10^{-2} min^{-1}) [73] and rhodamine B (10 mg L^{-1}; k = 0.92 x 10^{-2} min^{-1}) [94]. Although, these studies report first order removal kinetics and the pollutant concentrations vary between 8 and 20 mg L^{-1}, the reported rate coefficients are not drastically higher than those of the $BiVO_4$/BiOI photoanode given in Table 4.1. In terms of applied external potential (electrical energy input) most studies used between 1 and 2 V vs Ag/AgCl as an external bias for an average reaction time of around 2.5 h with approximately 80% removal of organic compounds from aqueous solution [72,73,75,78,79]. In this study PEC based ACT removal showed faster removal kinetics than in most of the studies reported in literature with a similar electrical energy input.

Quenching studies are normally performed to gain information about the main oxidants involved in the removal reaction of organic pollutants [79]. According to previous studies [79], hydroxyl radicals ($^{\bullet}OH$) and super oxide radicals ($^{\bullet}O_2^-$) are the two main oxidising species responsible for the removal of organic micro-pollutants. Quenching experiments were carried out for $BiVO_4$/BiOI photoanode by using methanol and p-benzoquinone (p-BZQ) to quench $^{\bullet}OH$ and $^{\bullet}O_2^-$, respectively, in the reaction solution of ACT. The results of the quenching experiments after 5 h of illumination are shown in Fig. 6d. The figure shows that the removal efficiency of $BiVO_4$/BiOI photoanode in the presence of both quenching agents was lower than without quenching agents, which confirmed the effect of $^{\bullet}OH$ and $^{\bullet}O_2^-$ radicals on the removal of ACT.

Removal in the presence of methanol was higher than in the presence of p-BZQ, which indicates that the $^{\bullet}O_2^-$ was the main reactive specie in our research, because the $BiVO_4$/BiOI photoanode only removed 23% ACT in the presence of p-BZQ. Overall, the results of the quenching study suggest that both $^{\bullet}OH$ and $^{\bullet}O_2^-$ were responsible for the ACT removal as the removal efficiency also decreased in the presence of methanol. This joint attack of both reactive species was due to the formation of type I heterojunction as mentioned in section 3.2, where both reactive species ($^{\bullet}OH$ and $^{\bullet}O_2^-$) were generated within the vicinity of photoanode surface. The finding of the quenching study is in accordance with the literature where researchers have reported different photocatalysts for the in-situ oxidation of organic compounds and dyes through $^{\bullet}O_2^-$ as the main oxidant [198]. The results of reusability experiments are shown in the supplementary information. Fig. S.4.5 in the supplementary information shows the removal efficiency of a $BiVO_4$/BiOI photoanode that was used for 3 consecutive removal experiments of each 5 h. The removal efficiency after the third run dropped down from 100% to 74%, meaning a decrease of 26% after 15 h of using the same photoanode. This drop in efficiency could be because of the adsorption of ACT molecules

within the surface pores of $BiVO_4$/BiOI photoanode that reduced the available surface area for the ROS generation.

In summary, the formation of heterojunction enhanced the kinetics of the ACT removal as shown in Fig. 4.6c and this enhancement was attributed to type I heterojunction that generated both $^{\bullet}OH$ and $^{\bullet}O_2^-$ radicals at the photoanode-electrolyte interface. The generated $^{\bullet}OH$ and $^{\bullet}O_2^-$ radicals unselectively attacked the molecules of ACT to remove them from the electrolyte.

4. Conclusions

Successful fabrication of $BiVO_4$, BiOI and $BiVO_4$/BiOI photoanodes was achieved by using electrodeposition. Fabricated photoanodes were characterized by using structural, morphological, optical and opto-electronic characterization techniques. Successful and effective formation of $BiVO_4$/BiOI heterojunction was confirmed with diffusive reflectance UV-Vis spectroscopy and IPCE characterization. Band edge potential calculations showed that a type I heterojunction was formed that enhanced the kinetics of ACT removal in demineralized water. BiOI, $BiVO_4$ and $BiVO_4$/BiOI photoanodes showed removal efficiency of 24, 99 and 100 %, respectively. Although the removal efficiency of $BiVO_4$ and $BiVO_4$/BiOI after 5 h were almost the same, the first order rate coefficient of $BiVO_4$/BiOI photoanode showed a 57% higher value as compared to $BiVO_4$ photoanode. Furthermore, the quenching study demonstrated that $^{\bullet}O_2^-$ radicals were the main reactive species in the removal of ACT. In conclusion, our research demonstrated the successful formation of $BiVO_4$/BiOI heterojunction photoanode that enhanced the removal kinetics of ACT (40 μg L^{-1}) in demineralized water compared to $BiVO_4$ and BiOI photoanodes.

Acknowledgement

This research study was part of InnovEOX project that has received funding from the European Union's EU Framework Programme for Research and Innovation Horizon 2020 under Grant Agreement No 861369.

Supplementary Information

Photo-electrocatalytic based removal of acetaminophen: Application of visible light driven heterojunction based $BiVO_4$/BiOI photoanode.

Figure 1 shows the effect of deposition time on the removal performance of $BiVO_4$ and $BiVO_4$/BiOI photoanodes for ACT (40 µg L^{-1}) removal. Each photoanode was tested for ACT removal in the same way as described in section 2.6 of main manuscript. Five deposition times (2, 5, 7, 10 and 15 min) were tested to find the optimal time for depositing $BiVO_4$ and BiOI layers. Figure 1(a) clearly shows that the $BiVO_4$ photoanode fabricated with 5 min deposition time performed the fastest removal of ACT than rest of the photoanodes. That's why 5 min was selected as the optimal deposition time for the fabrication of $BiVO_4$ photoanode. Similarly for $BiVO_4$/BiOI photoanode as shown in figure 1(b), 5 min was selected as the optimal deposition time for the BiOI deposition on $BiVO_4$ photoanode because it showed the fastest removal of ACT than rest of the photoanodes.

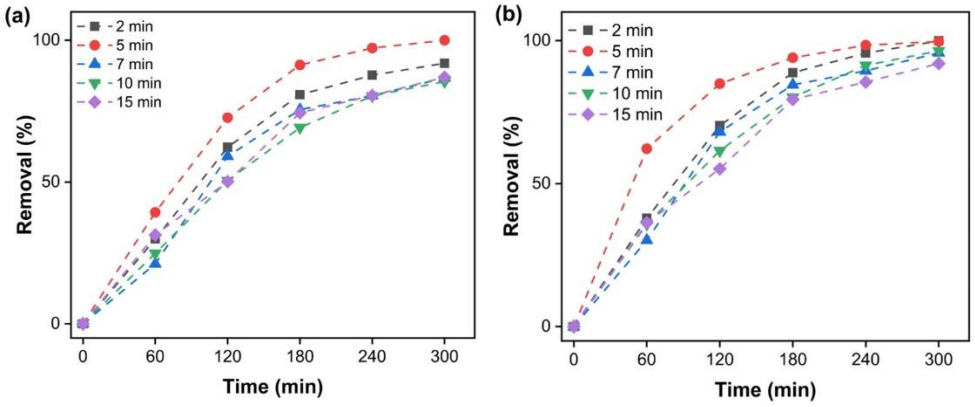


Fig. S.4.2: *Removal percentage of ACT (C_0=40 µg L^{-1}) during 5 hours of removal experiment by using the fabricated (a) $BiVO_4$ and (b) $BiVO_4$/BiOI at an external bias of 1 V vs Ag/AgCl.*

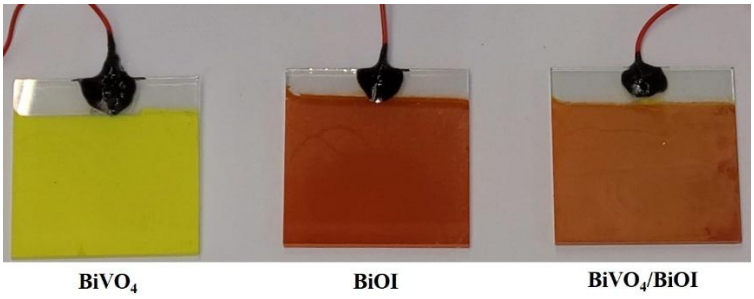


Fig. S.4.3: *Three different types of photoanodes fabricated by electrodeposition, showing distinct colours of BiVO4, BiOI and $BiVO_4$/BiOI photoanodes.*

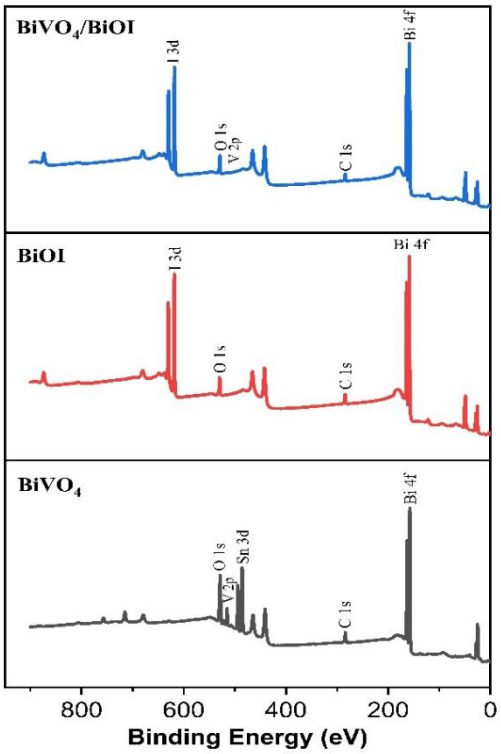


Fig. S.4.4: *XPS survey spectra of BiVO4, BiOI, $BiVO_4$/BiOI photoanodes showing distinct peaks of Bi, V, I, O and Sn at their respective binding energies in BiVO4, BiOI, BiVO4/BiOI photoanodes.*

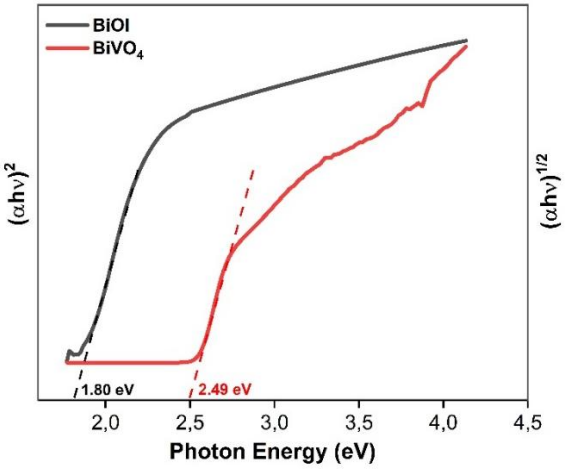


Fig. S.4.5: *Tauc plot showing band gap measurement of BiOI and $BiVO_4$ photoanode by using Tauc equation.*

Reusability of $BiVO_4$/BiOI

Fig. 1 shows the removal efficiency of a $BiVO_4$/BiOI photoanode that was used for three consecutive ACT removal experiments. The duration of each experiment was 5 hours, and they were performed in the same way as mentioned in section 2.6 of the main manuscript. Three reusability experiments were designated as 1st run, 2nd and 3rd run, respectively.

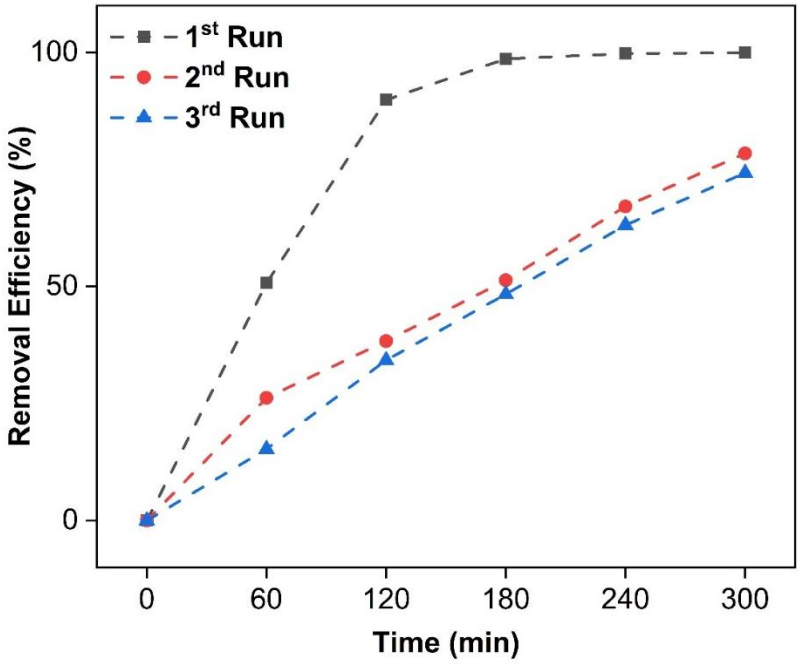


Fig. S.4.5: *Removal efficiency of a $BiVO_4$/BiOI photoanode during 5 hours of three experimental runs. The removal experiments were performed in a three-electrode set-up in which the $BiVO_4$/BiOI photoanode was the working electrode, Ag/AgCl was the reference electrode and graphite plate was the counter electrode.*

Chapter 5

Simultaneous removal of multiple organic micropollutants via UV-visible light driven $BiVO_4/TiO_2$-GO photoanode: Experimental and CFD study

This chapter is based on the following publication:

Agha Zeeshan Ali, Yuhao Wu, Bas Wols, Mohamad Zeidan, Henri Spanjers, Jan Peter van der Hoek, Simultaneous removal of multiple organic micropollutants via UV-visible light driven BiVO4/TiO2-GO photoanode: Experimental and CFD study, Chemical Engineering Journal Advances, Volume 22, 2025, 100721, https://doi.org/10.1016/j.ceja.2025.100721

Abstract

In this study, we investigated the use of $BiVO_4/TiO_2$-GO heterojunction photoanode in a PEC based AOP to simultaneously remove four organic micropollutants (OMPs): benzotriazole (BTA), carbamazepine (CBZ), caffeine (CAF) and diclofenac (DIC) from demineralized water. Each OMP had an initial concentration of 40 μg L^{-1}. Ultrasonic spray pyrolysis (USP) was used to deposit $BiVO_4$ and TiO_2-GO layers on fluorine doped tin oxide (FTO) electrodes. The heterojunction photoanode at an applied voltage of 1 V (vs Ag/AgCl) achieved simultaneous removal efficiencies of 100% for DIC, 54% for CBZ, 36% for BTA and 33% for CAF under simulated solar light. Compared to the pristine $BiVO_4$ photoanode, the heterojunction photoanode showed 50% higher removal efficiency for BTA, CBZ and CAF. The reaction kinetics revealed that the first order rate coefficient for DIC removal was about nine times higher than that of CBZ and fifteen times higher than those of BTA and CAF. To assess scalability, a computational fluid dynamics (CFD) model incorporating the experimentally determined reaction kinetics was developed for a conceptually designed up-scaled PEC reactor. The model analysed the effect of reactor design and fluid flow conditions on the removal of OMPs. Under turbulent flow conditions, enhanced removal efficiency was observed for all four OMPs, which was attributed to the effects of eddy diffusion and convective mixing. The optimized reactor design under turbulent flow condition achieved an 80% removal efficiency for all four OMPs within 25 min under a light intensity of 400 W m^{-2}. The findings highlight the potential of $BiVO_4/TiO_2$-GO heterojunction photoanodes for efficient and scalable PEC water treatment, showing a promising approach for the elimination of OMPs from wastewater.

Keywords: Photoelectrocatalysis, advanced oxidation process, heterojunction photoanode, bismuth vanadate, organic micro-pollutants, computational fluid dynamics model.

1. Introduction

Organic micropollutants (OMPs) belong to an expanding range of organic pollutants that are present in water bodies due to industrial and human activities [199]. OMPs consist of a variety of organic compounds, which include pharmaceutical drugs, corrosion inhibitors, pesticides, surfactants and personal care products [200]. Depending on the geographical location and source of origin, OMPs are typically present within the range of ng L^{-1} and μg L^{-1} in the surface water [201]. Industrial and municipal wastewater treatment plant (WWTP) effluents are becoming a major contributor to the release of OMPs in the surface water [202]. Conventional wastewater treatment technologies are ineffective to completely remove OMPs from the wastewater [203], therefore, research efforts are increasing to enhance the existing technologies to remove OMPs or to convert them into less harmful compounds.

Advanced oxidation processes (AOPs) and related technologies are effective for eliminating OMPs from industrial and municipal WWTP effluents [107,204]. Different AOPs such as

ozonation [205], electrochemical oxidation [206], persulfate oxidation [207] and Fenton reactions [208] have been studied in the literature for the removal of organic pollutants (primarily pharmaceuticals) from aqueous solutions. However, these processes have several disadvantages including high power consumption, high chemical cost (particularly in persulfate oxidation, which requires a continuous supply of persulfate salts), short lifetime of reactive species, incomplete mineralization of pollutants leading to the formation of toxic byproducts, and pH dependency (as observed in both ozonation and Fenton reactions) [209]. Photoelectrocatalytic (PEC) based AOP is in its early stage of development. In PEC-based AOPs, semiconducting photocatalytic materials are used as anodes, facilitating the generation of hydroxyl radicals (•OH) and superoxide radicals ($^{\bullet}O_2^-$) as primary oxidants in water [109]. The anode in a PEC cell, the photoanode, coated with a photocatalytic material is in direct contact with the water containing the OMPs, and the removal reaction usually takes place within the close vicinity of the anode-electrolyte interface [137]. When solar light interacts with the photoanode, electron-hole pairs are generated. The holes oxidize water molecules to form •OH, while the electrons reduce dissolved oxygen, yielding $^{\bullet}O_2^-$. These photoinduced •OH and $^{\bullet}O_2^-$ react with the OMP molecules through oxidative mechanisms and either completely oxidize them or convert them into less harmful products [109]. The main advantages of PEC based AOP over other AOPs are enhanced pollutant mineralization, lower energy consumption through the integration of solar energy, and efficient removal of emerging contaminants such as antibiotics and pesticides.

UV driven photocatalysts including titanium dioxide (TiO_2) [111], tungsten trioxide (WO_3) [112] and zinc oxide (ZnO) [61] have been extensively used for the removal of industrial dyes and pharmaceuticals (1-10 mg L^{-1}) in aqueous solution through PEC based AOP. A major drawback of using UV driven photocatalysts is that they have a wide band gap energy ranging from approximately 3.0 to 3.5 eV, which allows them to absorb only less than 10% (180 – 400 nm) of the solar spectrum. Bismuth vanadate ($BiVO_4$), a photocatalyst activated by visible light, is emerging as an alternative to UV driven photocatalysts for PEC water treatment applications [74]. Studies have explored $BiVO_4$ based photoanodes for removing dyes and pharmaceuticals (concentrations ranging from 1 to 10 mg/L) from aqueous solutions via PEC based AOPs [45,210]. However, the effectiveness of $BiVO_4$ photoanodes is hindered by the rapid recombination of photoinduced holes and electrons, which limits charge transport to the anode surface and reduces the formation of •OH and $^{\bullet}O_2^-$ [116]. Applying a suitable external voltage to $BiVO_4$ photoanode is one of the ways to reduce the rate of recombination and ultimately increase its removal efficiency. Combining $BiVO_4$ with a different UV or visible light driven photocatalyst and thereby creating a heterojunction is also an effective way to reduce rate of recombination in $BiVO_4$. In heterojunction photoanode, the photo-generated holes and electrons are separated from each other by travelling in opposite direction within the photocatalytic layers and increasing their lifetime to produce •OH and $^{\bullet}O_2^-$ [114]. Graphene oxide (GO) is a photo active semi-conducting material with high specific area [211]. It is also

used for water treatment applications either as a heterojunction photocatalyst with TiO_2 or mixed in the TiO_2 layer [212]. GO helps to increase the charge separation efficiency in heterojunction photoanodes and also increases the specific surface area for the adsorption of molecules of OMPs [211].

Benzotriazole (BTA) is a corrosion inhibitor mostly used in anti-icing fluids and dishwashing detergents [120]. Within the European Union, BTA is an emerging OMP that is frequently detected in surface water resources at concentrations ranging from 10 to 50 μg L^{-1} [122]. Due to its low biodegradability and weak adsorption to organic matter, BTA is only partially removed during biological treatment in WWTPs [122]. UV/H_2O_2 [125] and photocatalytic [127] based AOPs have been employed to remove BTA (1-10 mg L^{-1}) from WWTP effluents. Carbamazepine (CBZ) is an anticonvulsant medicine that is a frequently detected OMP in surface water and WWTP effluents [213]. CBZ is resilient to chlorination and UV photolysis based water treatment processes, which is why it is only partially removed from the wastewater [214]. As a result of its partial removal in a WWTP, CBZ is released into the surface water through the WWTP effluent discharge. UV/chlorine [215] and electrochemical based AOP [216] have been applied to remove CBZ (1-10 mg L^{-1}) from water. Caffeine (CAF) is a central nervous system stimulant that is extensively used to increase focus and reduce body fatigue [217]. CAF is also an emerging OMP in surface water resources because it is only partially removed by the conventional wastewater treatment technologies [218]. Chemical oxidation, ozonation [218] and photocatalytic based AOP [219] have been applied in some studies for the removal of CAF (5-50 mg L^{-1}) from water. Diclofenac (DIC) is an anti-inflammatory drug and it is frequently detected as an OMP in the aquatic environment [220]. It is only partially removed during conventional wastewater treatment due to its low biodegradability [221], hence it is also released in the environment through WWTP effluent. Adsorption and UV-A based treatment [222] have been used for the removal of DIC (10-50 mg L^{-1}) from water. A previous study conducted by the Dutch Ministry of Water and Infrastructure reported the presence of BTA, CBZ and DIC in WWTP effluents at concentrations below 5 μg L^{-1} [223]. The presence and accumulation of BTA, CBZ, CAF and DIC in the surface water will become a major threat to human health and aquatic life. To the best of our knowledge, there is no publication available on the simultaneous removal of BTA, CBZ, CAF and DIC from either demineralized water or WWTP effluent through PEC based AOP.

In this study, we investigated the application of $BiVO_4/TiO_2$-GO heterojunction photoanode for the simultaneous removal of BTA, CBZ, CAF and DIC from demineralized water. A starting concentration of 40 μg L^{-1} was used in this study because it was comparable to typical concentrations of the selected OMPs in surface water. Demineralized water was used in this study because it provided a controlled environment in which we could investigate the effect of photoanode on the removal kinetics. The treated wastewater effluent may contain ions that can inhibit the production of reactive species and interfere with the PEC based AOP removal,

therefore, demineralized water was used to determine the effectiveness of $BiVO_4/TiO_2$-GO heterojunction photoanode for the removal of selected OMPs. Pristine $BiVO_4$ photoanodes and $BiVO_4/TiO_2$-GO photoanodes were fabricated by using ultrasonic spray pyrolysis (USP) method. The optical properties of fabricated photoanodes were analysed to confirm the successful deposition of photocatalytic layers and the formation of heterojunctions, which enhance photocatalytic activity. The photoanodes, specifically fabricated for this research, were used in a three electrode PEC cell. The removal reaction rate coefficient (k) of each OMP was determined by applying a suitable reaction kinetics model. Then the rate coefficient of each OMP was used in computational fluid dynamic (CFD) model to assess the removal of BTA, CBZ, CAF and DIC in an up-scaled PEC water treatment reactor (shown in the supplementary information Fig. S. 1). CFD is a valuable tool for assessing the flow behaviour of water in wastewater treatment processes [224]. CFD models are also used for assessing the removal of organic pollutants through a photocatalytic reaction, however, most models are based on the removal of only one organic pollutant with a relatively high starting concentration (>10 mg L^{-1}) [225–227]. There is a lack of literature available on the CFD modelling of a PEC based AOP removal of multiple OMPs. This study used a novel approach of using CFD simulation for simultaneous removal of BTA, CBZ, CAF and DIC in a PEC water treatment reactor.

2. Materials and methods

2.1 $BiVO_4/TiO_2$-GO photoanode preparation

The $BiVO_4$ and TiO_2-GO photocatalytic layers were deposited on an FTO glass surface (40 mm x 40 mm, 7 Ω/square, Luoyang Guluo glass Co., Ltd., China) by ultrasonic spray pyrolysis (USP) method. The FTO glass was first ultra-sonicated in acetone for 5 minutes and then rinsed with demineralized water to clean the surface. The spray precursor solution for $BiVO_4$ layer was prepared as follows. 0.02 M bismuth nitrate pentahydrate ($Bi(NO_3)_3.5H_2O$ (99% Sigma Aldrich)) was dissolved in 10 mL acetic acid (CH_3COOH (98% Sigma Aldrich)) and an equimolar amount of vanadyl acetylacetonate ($VO(AcAc)_2$ (99% Sigma Aldrich)) was dissolved in 20 mL demineralised 1:1 (v:v) water-ethanol mixture. The precursor solution was then made by mixing above solutions together slowly to form a clear blue homogenous solution. The spray coating process was carried out by an ultrasonic spray system (MSK-USP-ST1, MTI Corporation, USA). A multistage X-Y axis CNC controller was used in this system to control the progressive scanning motion of the nozzle using a set of programmed X–Y linear motion stages. The distance between the titanium alloy cylindrical spray nozzle and the substrate was 10 cm and the FTO substrate was kept at 300°C on a hot plate (EQ-HP-1515-LD, MTI Corporation, USA) in an open atmosphere. The nozzle was fixed to a 0.05 W digital ultrasonic generator (MSK-SP-01A, MTI Corporation, USA) and the feeding rate of the precursor solution was set at 0.3 mL/h by a syringe pump (NE-1010, ProSense B.V., the Netherlands). The pressure of the compressed air acting as a carrier gas was fixed at 0.25 bar.

The spray coating process was conducted twice to form the homogeneous nanostructured $BiVO_4$ film. Subsequently, the prepared $BiVO_4$ photoanodes were annealed at 460 °C for 2 h with a ramping rate of 2 °C per minute. To prepare the spray precursor solution for TiO_2-GO film on previously prepared $BiVO_4$ photoanodes, 0.001 M nano GO powder (Suzhou Tanfeng Graphene Technology Co., Ltd., China) was first dispersed in 30 mL demineralised 1:9 (v:v) water and ethanol mixture and ultra-sonicated for 1 h. Then 0.02 M P25 TiO_2 nano powder (Tianjin Baima Technology Co., Ltd., China) was added into the above mixture and then stirred for 2 h and ultra-sonicated again for 1 h. The spray coating method was the same as for the $BiVO_4$ film, except that the temperature of the heating plate was 150 °C. Finally, the prepared electrodes were annealed at 500 °C for 1 h in the oven with ramp rate of 5 °C per minute and used for further characterizations and degradation experiments.

2.2 Structural characterization

The phase composition of the fabricated photoanodes was identified using X-Ray diffraction (XRD) technique. A detailed description of the XRD parameter is provided in our previous publication [228].

2.3 Optical characterization

The absorbance spectra of the fabricated photoanodes were obtained between 300 and 700 nm (5 nm step size) by using diffusive reflectance UV-vis spectroscopy (The LAMBDA 1050+ UV/Vis/NIR spectrophotometer, UV Winlab software).

2.4 Photo-electrocatalytic (PEC) experiments

Photo-electrocatalytic (PEC) based simultaneous removal of four OMPs (BTA, CBZ, CAF and DIC) was carried out by using the prepared photoanodes in combination with a Autolab potentiostat (PGSTAT128N) in a three electrode configuration set-up. A quartz reactor cell containing three electrodes and 167 mL of electrolyte solution was used for the PEC experiments. A 0.1 M Na_2SO_4 solution was prepared with demineralized water and used as the electrolyte for the experiments. Each OMP was then added to the electrolyte to achieve a concentration of 40 µg L^{-1}. The starting pH of the electrolyte was set at 5.1 by adding 0.2 mL of 0.5 M nitric acid (HNO_3) to facilitate a higher in-situ production of hydroxyl radicals ($^{\bullet}OH$). The experimental setup included fabricated photoanodes as the working electrode, an Ag/AgCl (3.0 M KCl) electrode as the reference electrode, and a graphite plate (40 x 40 mm) as the counter electrode. During the removal experiments, a constant voltage of 1 V vs. Ag/AgCl was applied to reduce the recombination rate in the photoanodes. Solar simulator (SUNTEST XXL+) equipped with three air-cooled 1700 W Xenon lamps, which produced a light spectrum equivalent to 1 sun was used as the illumination source. The intensity of emitted light between 300 and 400 nm was 60 W/m^2 and the distance between the light source and the photoanode was 23 cm. During the experiments the reaction solution was constantly stirred at 600 rpm with the help of a magnetic stirrer to enhance the transport of OMPs molecules from the bulk

towards the surface of the photoanode. During the Pec experiment, the temperature of the quartz reactor cell was maintained at 25°C (±2°C) by using a temperature controlling bath. Each experiment ran for 3 h and samples were taken at an interval of 30 min for the measurement of DIC, BTA, CAF and CBZ concentration. Photolysis experiments were conducted to investigate the simultaneous removal of OMPs in demineralized water as a result of direct irradiation in the absence of a photoanode. For the photolysis experiment, the total duration was 3 hr and the starting concentration of each OMP was 40 µg L^{-1} in demineralized water. Reusability experiments were conducted using a $BiVO_4/TiO_2$-GO heterojunction photoanode over three consecutive removal experiments of 3 hours each. Each OMP had an initial concentration of 40 µg L^{-1} in demineralized water. Between each experiment, the photoanode was rinsed with demineralized water to remove any adsorbed OMPs from its surface.

2.5 Analytical measurement of OMPs

The concentrations of OMPs in the samples were determined using liquid chromatography coupled with tandem triple quadrupole mass spectrometry (LC-MS). A Waters Acquity UPLC BEH C18 column was used for the analysis of BTA, CAF, CBZ, and DIC. Prior to analysis, all samples were filtered through 0.2 µm glass fiber filters (GF-75, ADVANTEC®, Japan). Subsequently, 495 µL of the filtered sample solution was combined with 5 µL of an internal standard calibration solution in LC-MS sample vials. After thorough mixing, the LC-MS system quantified the target compounds in the samples. The removal efficiency of the photoanodes, based on the concentrations of the target compounds, was determined using the following equation:

$$\text{Removal efficiency (\%)} = \left(1 - \frac{C_t}{C_0}\right) \times 100 \quad \text{(Eq. 1)}$$

where C_0 = Initial concentration at time t=0 and C_t = Concentration at time t.

2.6 CFD modelling of photoelectrocatalytic (PEC) water treatment reactor

A CFD model was used to simulate a full-scale reactor by using the results from the lab-scale reactor cell discussed in section 3.3. A conceptually designed photo-electrocatalytic water treatment reactor, as shown in Fig. S.5.1 of the supplementary information, was used for the CFD simulation by using COMSOL multi-physics software. The reactor was conceptually designed to remove BTA, CBZ, CAF and DIC from water, with the target of at least 80% removal. In this design, the water stored in a storage tank is pumped into the reactor, where the photo-electrocatalytic oxidation reaction (OMP removal reaction) takes place in the vicinity of the photoanode surface. The reactor is cylindrical and made up of a transparent material (i.e quartz) so that the incoming solar light can reach the photoanode. The photoanode inside the reactor has also a hollow cylindrical shape and is made up of heterojunction $BiVO_4/TiO_2$-GO to minimize the rate of recombination and enhance photoelectrocatalytic

removal. Graphite is used as cathode in the reactor and a solar trough (aluminium or silver) is used to concentrate the solar light towards the reactor to achieve maximum absorbance of photons by the heterojunction photoanode. A recirculation loop after the outlet of the reactor is provided to ensure sufficient reaction time while maintaining a higher velocity to have a better mixing and minimize the partial diffusion controlled reaction [229,230]. In the recirculation loop, the outgoing water is recirculated with same initial flow rate from the inlet of the reactor, the recirculation is carried out until the removal efficiency of the photoanode for each OMP is 80%. The CFD model was used to calculate the removal efficiency after the first circulation of water in the reactor, the removal efficiency (percentage removal) in each recirculation was regarded the same as of the first circulation, assuming a perfect mixing in the recirculation piping and first-order reactions (removal efficiency independent of the initial concentration of OMP). Furthermore, a current density of 2.82 A m^{-2} was applied to the photoanode to enhance the kinetics of the removal reaction and to minimize the rate of recombination in the heterojunction photoanode. The value of 2.82 A m^{-2} was chosen because it corresponds to the current density at 1 V (vs Ag/AgCl) in the laboratory removal experiments.

COMOL Multiphysics software (v6.2)[1] was used to calculate the simultaneous removal of BTA, CBZ, CAF and DIC having a starting concentration of 40 µg L^{-1} in water. The following surface reaction flux equation was derived from the lab experiments (k values in Table 5.1) to calculate the removal of OMPs in CFD simulations [231].

$$N_{surf} = K^*_{surf} \times I_c \times I_L \times C \ (\mathrm{mol.\,m^{-2}.\,s^{-1}}) \quad \text{(Eq. 2)}$$

Where

N_{surf} = Surface reaction flux used to calculate the removal of OMPs at the surface of photoanode.

K^*_{surf} = experimental removal kinetic coefficient including the effect of current density and light intensity (m^5 .A^{-1}. W^{-1}. s^{-1})

I_c = Current density (A m^{-2})

I_L = Solar light intensity (W m^{-2})

C = Concentration of OMPs at the surface of the photoanode (mol m^{-3})

Laminar flow and turbulent flow multiphysics packages were used in COMSOL to simulate the flow of water inside the reactor in laminar and turbulent flow conditions. Transport of dilute species (tds) package was used to calculate the removal of OMPs. At the cathode, photoanode and outer walls no slip wall conditions with default wall equations were used as boundary conditions in both laminar and turbulent flow. Similarly, normal inflow velocity with

[1] COMSOL Multiphysics v.6.2. ww.comsol.com. COMSOL AB, Stockholm, Sweden.

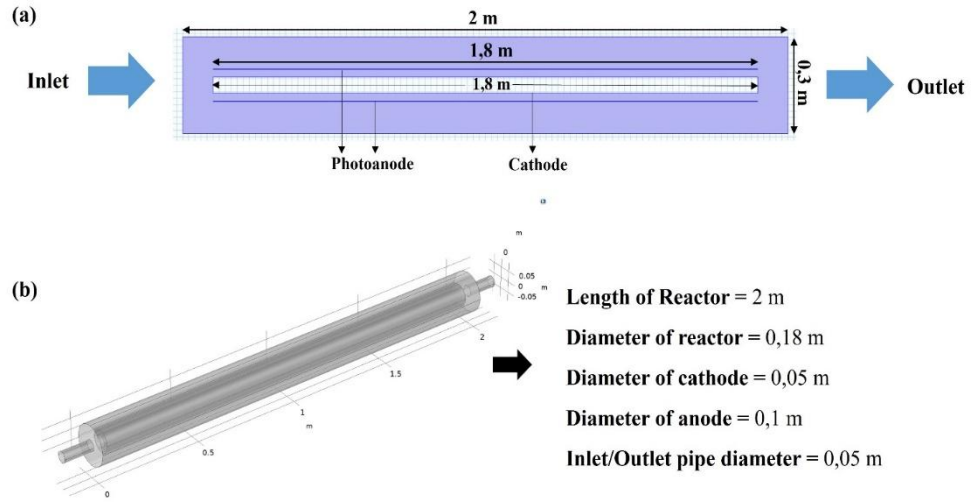


Fig. 5.1: *Geometrical shape of the photo-electrocatalytic reactor used in 2D (a) and 3D (b) CFD simulations.*

default settings were used at the inlet for both turbulent and laminar flow. Normal static pressure flow (value = 0 Pa) was used as a boundary condition for the outlet in turbulent and laminar flow conditions. For transport of dilute species (tds), at the cathode and outer walls, concentration constraint was used as a boundary condition. At the photoanode surface reaction flux given in Eq. 2 was used as condition. At the inlet, the starting concentration of the OMPs were set as boundary conditions. The important parameters used in the CFD simulations are listed in Table S.5.1 of the supplementary information. The 2D geometrical shape shown in Fig. 5.1(a) was used for 2D simulations. The length of photoanode and cathode were both 1.8 m, the height of cathode was set at 0.05 m. The 3D geometrical shape shown in Fig. 5.1(b) was used for 3D simulations. The photoanode thickness was set at 0.005 m, with a total available reaction surface area (including both inner and outer surfaces) of 1.07 m^2. The overall reactor volume was 0.050 m^3, whereas the effective flow volume, excluding the solid cylindrical cathode, was 0.046 m^3. The resulting surface area to volume ratio was calculated as 23.2. Mesh element size was set as normal for both 2D and 2D simulations, the number of mesh elements for 2D configuration was around 50,000 and for 3D configuration it was around 2 million mesh elements.

3. Results and discussion

3.1 Structural characterization

The crystallinity and phase composition of all the fabricated photoanodes were characterized using XRD. The XRD patterns of GO, $BiVO_4$, TiO_2-GO and $BiVO_4/TiO_2$-GO photoanodes are shown in Fig. 5.2. The diffraction pattern of pristine $BiVO_4$ photoanode showed fourteen broad

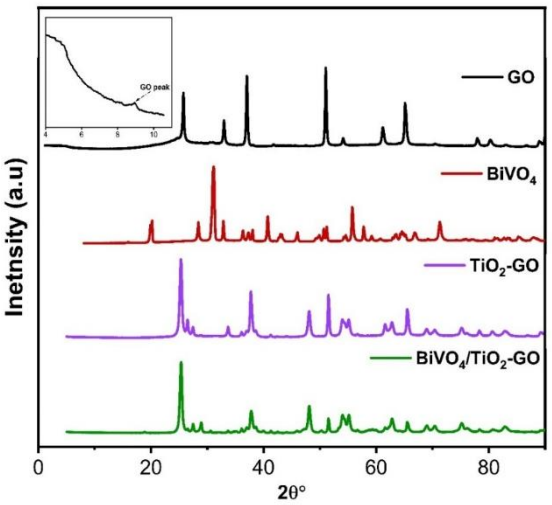


Fig. 5.2: *XRD patterns of $BiVO_4$, GO, TiO_2-GO and $BiVO_4/TiO_2$-GO photoanodes showing characteristic diffraction peaks.*

peaks with 2θ value at 18.8°, 19.1°, 29.0°, 30.6°, 34.6°, 35.3°, 39.9°, 42.5°, 46.9°, 47.4°, 50.4°, 53.4°, 58.6° and 59.5°, which corresponds to the monoclinic scheelite phase of $BiVO_4$ (JCPDS Card No. 75-1867) [232]. The XRD pattern of the TiO_2-GO photoanode showed peaks at 25.3°, 37.7°, 48.1°, 53.9°, 55.1°and 62.7°, which are characteristic peaks of anatase TiO_2 (JCPDS Card No. 88–1175). Additionally, the diffraction peaks at 27.4°, 36°, 41.2°and 56.6° are related to rutile TiO_2 (JCPDS Card No. 84–1286) [233]. The XRD pattern of the pure GO sample showed a minor peak at 9° (inset of Fig. 5.2), which is in accordance with a previous study [234]. The XRD pattern of $BiVO_4/TiO_2$-GO photoanode showed diffraction peaks of both $BiVO_4$ and TiO_2, however, the intensity of $BiVO_4$ was decreased because TiO_2-GO was deposited on top of the $BiVO_4$ photocatalytic layer. The GO diffraction peak in $BiVO_4/TiO_2$-GO photoanode could not be detected due to the lower concentration of GO in the TiO_2 matrix.

3.2 Optical properties of the fabricated photoanodes

The optical properties of the fabricated photoanodes were characterized using UV visible diffuse reflectance spectroscopy. Fig. 5.3 presents the absorbance spectra of $BiVO_4$, TiO_2, TiO_2-GO and $BiVO_4/TiO_2$-GO photoanodes. We observed that both the pristine $BiVO_4$ photoanode and the heterojunction $BiVO_4/TiO_2$-GO photoanode absorbed photons within the UV-visible range of the solar spectrum. In contrast, pristine TiO_2 and TiO_2-GO photoanodes showed absorption limited to the UV region, consistent with literature studies that attribute this behaviour to the intrinsic bandgap of TiO_2 and GO, which restricts photon absorption to the UV spectrum [235,236]. The combination of UV absorbing TiO_2 with $BiVO_4$ resulted in a heterojunction photoanode capable of absorbing both UV and visible light. This configuration demonstrated a lower recombination rate of photogenerated charge carriers compared to the pristine $BiVO_4$ photoanode [237]. Overall, the UV visible reflectance spectroscopy results confirmed the successful fabrication of the $BiVO_4/TiO_2$-GO heterojunction photoanode, which is driven by UV-visible light. Combining UV light absorbing TiO_2 and $BiVO_4$ layer resulted in the UV-visible absorbing heterojunction photoanode, which has lower rate of recombination of photogenerated charge carriers as compared to pristine $BiVO_4$ layer [237]. Overall, the results of UV visible reflectance

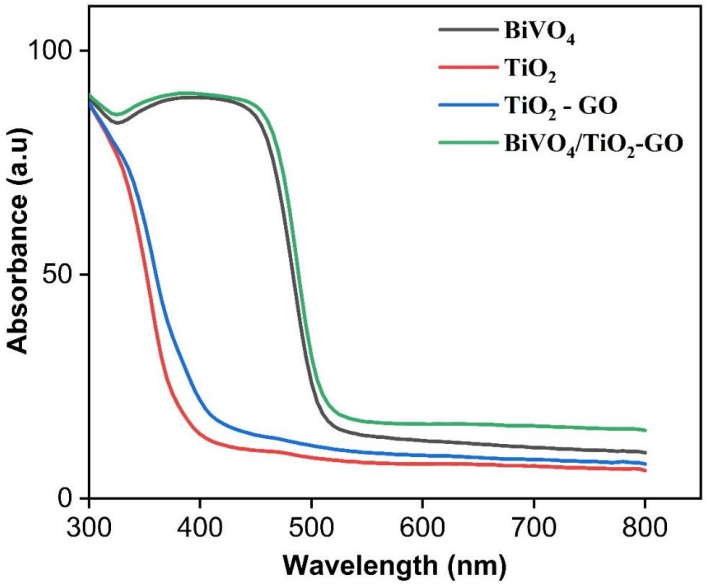


Fig. 5.3: *UV-Visible absorbance spectrums of $BiVO_4$, TiO_2, TiO_2-Go and $BiVO_4/TiO_2$-GO photoanodes showing absorbance pattern of the fabricated photoanodes.*

spectroscopy results confirmed the successful fabrication of the $BiVO_4/TiO_2$-GO heterojunction photoanode, which is driven by UV-visible light.

3.3 Photoelectrocatalytic removal of selected OMPs

Fig. S.5.2 in the supplementary information shows the removal efficiencies of the selected OMPs as a result of photolysis under simulated solar light. After 3 hr of photolysis, removal efficiency of BTA, CBZ and CAF was less than 10% and DIC showed a removal efficiency of 60%. The higher removal efficiency of DIC after photolysis is consistent with the literature because it absorbs photons within the UV range of the solar spectrum [222]. The low removal efficiency of BTA, CBZ and CAF is also in line with the literature because their removal reaction kinetics is very slow under simulated solar light [238,239]. Fig. 5.4(a) shows the removal efficiency of pristine $BiVO_4$ and heterojunction $BiVO_4/TiO_2$-GO photoanodes for the simultaneous PEC removal of BTA, CBZ, CAF and DIC in demineralized water. Compared to the pristine $BiVO_4$ photoanode, the $BiVO_4/TiO_2$-GO photoanode showed 50% higher removal efficiency for BTA, CBZ and CAF. This difference in the removal efficiency was attributed to the formation of a heterojunction between the $BiVO_4$ and TiO_2-GO photocatalytic layers, which resulted in a reduction in the recombination rate of photogenerated electron-hole pairs. The coupling of photocatalytic layers of $BiVO_4$ and TiO_2-GO resulted in a built-in electric field in the $BiVO_4/TiO_2$-GO heterojunction [240]. After the irradiation of the photoanode under UV-visible light, the photogenerated electrons in the conduction band of $BiVO_4$ were

transferred to the conduction band of TiO_2 under the influence of the heterojunction. At the same time, the high energy holes in the valence band of the TiO_2 were transferred to the valence band of $BiVO_4$ [66]. This improved separation of photogenerated charge carriers reduced the recombination rate and increased the in-situ production of reactive species ($^{\bullet}OH$ and $^{\bullet}O_2^-$), which ultimately enhanced the overall removal of OMPs.

Fig. S.5.3 in the supplementary information shows the average removal efficiency of the heterojunction $BiVO_4/TiO_2$-GO photoanode for all four OMPS based on triplicate experiments, along with the corresponding standard errors. Fig 5.4(b) shows the fitting of the first order reaction rate equation ($C/C_0=e^{-kt}$) for the selected OMPs to determine the rate coefficient (k) for the selected OMPs. The first order rate coefficients of BTA, CBZ, CAF and DIC are shown in Table 5.1. The rate coefficient of DIC was higher than that of CBZ, CAF and BTA. Fig. 5.4(b) also shows the normalized removal of BTA, CBZ, CAF and DIC in demineralized water by using heterojunction $BiVO_4/TiO_2$-GO photoanode at an applied voltage of 1 V (vs Ag/AgCl as the reference electrode). Fig. 5.4(b) shows that the pattern of normalized removal of the selected OMPs varies, DIC showed a faster removal compared to the other OMPs. The removal kinetics of CAF and BTA were almost equal whereas the removal kinetics of CBZ was higher compared to CAF and BTA. DIC showed faster removal kinetics compared to other OMPs because of the combination of photolysis and PEC based AOP removal reaction. The difference in the normalized removal of the selected OMPs was probably due to the chemical structure of the selected OMPs. Diclofenac (DIC) has a secondary amine group that serves as an electron donating group, making it susceptible to the attack by $^{\bullet}OH$ and $^{\bullet}O_2^-$ radicals. The oxidation reaction is likely initiated by the C-N bond cleavage due to radical ($^{\bullet}OH$ and $^{\bullet}O_2^-$) attack, resulting in the formation of 2,6-dichloroaniline as a primary intermediate [241]. Similarly, the presence of amine groups and olefinic bonds in CBZ made it more susceptible to the attack by $^{\bullet}OH$ and $^{\bullet}O_2^-$ radicals compared to CAF and BTA, which have a deficiency of electron donating functional groups. The degradation pathway of benzotriazole (BTA) is likely influenced by hydroxylation, addition, and cleavage of the phenyl ring, facilitated by •OH [242]. The process could be initiated by hydroxyl radicals (•OH) attacking the regions of high electron density within the BTA molecule, leading to the formation of hydroxylated intermediates. Subsequently, ring opening reactions can occur, resulting in the generation of aldehyde- and carboxyl- containing intermediates, ultimately leading to complete mineralization [243]. In CBZ, the olefinic double bond is most likely the primary reactive site that initiates the radical ($^{\bullet}OH$ and $^{\bullet}O_2^-$) attack on the CBZ molecule [244]. This initial reaction triggers a series of oxidative transformations, leading to the breakdown of CBZ into short-chain fatty acids or other small organic intermediates until its complete mineralization [245]. For the removal of CAF, the oxidation is most likely initiated by the •OH attack on the carbon-carbon double bond [246]. After a series of successive hydroxylation and oxidation reactions, dimethylparabanic acid and di (hydroxymethyl) parabanic acid can be formed as the main intermediates [247]. These intermediates can undergo further oxidation

and gradually be completely mineralized. This difference in the chemical characteristics and degradation pathways of the OMPs led to the difference in reaction rate coefficient of reactive species ($^{\bullet}OH$ and $^{\bullet}O_2^-$ radicals) with the OMPs, which ultimately resulted in different removal kinetics of the OMPs during 3 hr of treatment time. Based on literature, the reaction rate coefficients ($K_{\cdot OH}$) of the $^{\bullet}OH$ with the selected OMPs are different for each OMP. DIC has the highest $K_{\cdot OH}$ (8.38 x 10^9 L mol^{-1} s^{-1}) followed by CBZ (8.02 x 10^9 L mol^{-1} s^{-1}), BTA (7.6 x 10^9 L mol^{-1} s^{-1}) and CAF (6.40 x 10^9 L mol^{-1} s^{-1}) [248,249]. Moreover, there is also a possibility of direct oxidation of OMPs by the photogenerated holes generated in the heterojunction photoanode [109]. The difference in the chemical structure could also influence the direct oxidation of the selected OMPs by the photogenerated holes [45]. Similarly, the difference in the K values of the OMPs was attributed to the difference in their chemical structures, which affected their reactivity with the $^{\bullet}OH$, $^{\bullet}O_2^-$ and photo-generated holes.

Table 5.1: *First order rate coefficients (k) of DIC, CBZ, BTA and CAF after 3 hr of treatment.*

OMP	k (x 10^{-2} min^{-1})	Standard Error	R^2
Diclofenac (DIC)	3.90	1.18 x 10^{-4}	0,9997
Carbamazepine (CBZ)	0.430	1.41 x 10^{-4}	0,9697
Benzotriazole (BTA)	0.260	2.00 x 10^{-4}	0,9477
Caffeine (CAF)	0.240	5.10 x 10^{-4}	0,9571

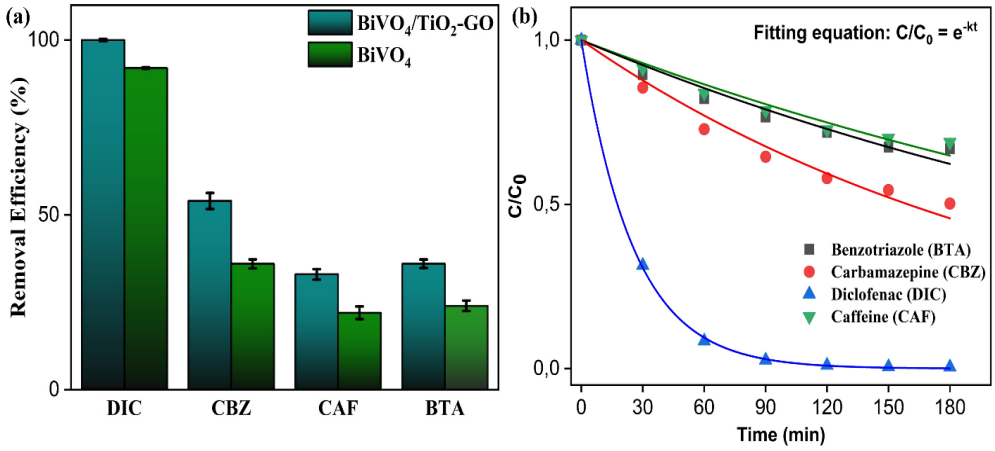


Fig. 5.4: *(a) Comparison of removal efficiencies achieved by $BiVO_4$ and $BiVO_4/TiO_2$-GO photoanode for DIC, CBZ, CAF and BTA after 3 hr of removal experiments (b) Normalized removal profiles of DIC, CBZ, CAF and BTA using $BiVO_4/TiO_2$-GO photoanode, along with the corresponding fit to a first order reaction model.*

The rate coefficients presented in Table 5.1 are comparable to, or higher than, those reported in previous studies using PEC based AOP for the removal of different pharmaceuticals such as

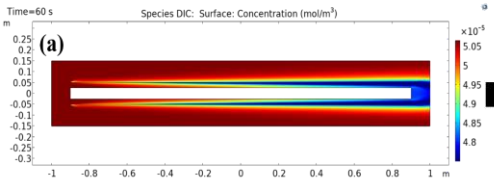
sulfamethoxazole (10 mg L^{-1}; k = 7.40 x 10^{-3} min^{-1}) [250], bisphenol A (10 mg L^{-1}; k = 4.1 x 10^{-2} min^{-1}) [74], norfloxacin (10 mg L^{-1}; k = 6.41 x 10^{-3} min^{-1}) [251], tetracycline hydrochloride (20 mg L^{-1}; k = 6.42 x 10^{-2} min^{-1}) [164], ciprofloxacin (10 mg L^{-1}; k = 6.05 x 10^{-3} min^{-1}) [252] and dyes such as orange II (20 mg L^{-1}; k = 1.40 x 10^{-2} min^{-1}) [253] and rhodamine B (10 mg L^{-1}; k = 7.32 x 10^{-3} min^{-1}) [251]. Although these studies used pollutant concentrations ranging from 8 and 20 mg L^{-1}, the corresponding first order rate coefficients are not significantly higher than those in our work. Furthermore, most studies used an external bias between 1 and 2 V vs Ag/AgCl and achieved approximately 80% removal of pollutants within an average time of about 2.5 hours. In this study PEC based simultaneous removal of BTA, CAF, CBZ and DIC showed similar removal kinetics to those reported in the literature under comparable electrical energy inputs. The results of the reusability experiments are shown in Fig. S.5.4 of the supplementary information. Heterojunction photoanode showed good reusability performance as the removal efficiency was only 12% lower for CBZ and 8% for BTA, CAF and DIC after the three consecutive experiments. This decrease in the efficiency was most likely due to the adsorption of unoxidized intermediate product molecules within the surface cracks of the photoanode, reducing the active surface area available for the production of reactive species ($^{\bullet}OH$ and $^{\bullet}O_2^-$).

3.4 CFD simulation

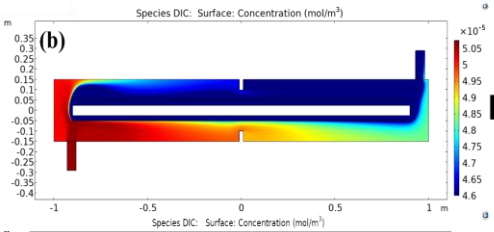
The CFD simulations were first carried out in 2D geometry by constructing a geometry as shown in Fig. 5.1(a). In this geometry, water entered from the inlet (left side), and the removal reaction took place at the photoanode. The distance between the anode and cathode was fixed at 5 cm, and the distance between the photoanode and the outer wall of the reactor was fixed at 10 cm. Laminar flow regime (28 L/min) and turbulent flow regime (61.6 L/min) were tested in the 2D geometry to assess the effect of flow conditions on the overall removal of the OMPs. The Reynolds number (Re) for the system was calculated using the reactor diameter as the characteristic length and the inlet velocity, with the properties of the working fluid taken into account. For the laminar flow regime, the Re was calculated as 1415, while for the turbulent flow regime, it was 3112. Further details on the Re calculations are provided in the supplementary information (Fig. S.5.5, Fig. S.5.6). In our CFD simulations, the selection of boundary conditions was based on both the physical principles controlling the fluid flow and established modelling practices [254]. No-slip wall conditions were applied to the cathode, photoanode and outer walls to accurately capture boundary layer formation and shear stress effects. The inlet velocity and outlet pressure conditions were specified based on experimental and design parameters to ensure realistic flow field development. These carefully chosen conditions played a critical role in determining mass transfer rates, reaction kinetics and overall reactor performance. These boundary conditions played a major role in minimizing numerical errors and enhancing simulation reliability.

Fig. 5.5(a) shows the concentration profile of DIC in turbulent flow regime after a single pass. The concentration profile in laminar flow regime indicated that the DIC concentration only decreased within the vicinity of the photoanode, removal efficiency of DIC in laminar flow regime was 11% as shown in table next to Fig. 5.5(a). The concentration profiles of other OMPs were similar in the vicinity of the photoanode, indicating that there was no removal in the bulk solution due to the short lifetime of $^{\bullet}OH$ and $^{\bullet}O_2^-$ radicals further away from the photoanode. In turbulent flow regime the removal of OMPs was enhanced as shown in table next to Fig. 5.5(a) likely due to better mixing and diffusion of OMP molecules from the bulk towards the surface of the photoanode. The residence time in turbulent flow conditions was lower compared to laminar flow due to higher flow rate. In turbulent flow conditions, the removal of OMPs after two circulations are shown in the tables next to Fig. 5.5(a),(b) and (c) to compare the removal in laminar flow conditions within same residence time. To increase the diffusion of OMP molecules from the bulk to the surface of the photoanode, a different design with inlet in the bottom, as shown in Fig. 5.5(b), was tested in both laminar and turbulent flow regimes. Again, the turbulent flow regime showed better removal of OMPs compared to laminar flow conditions as shown in table next to Fig. 5.5(b). To confirm the positive effect of mixing on the removal efficiency of OMPs, a design as shown in Fig. 5.5(c) with increased obstacles was tested in both laminar and turbulent flow regimes. The design shown in Fig. 5.5(c) was tested to observe the effect of additional mixing on the reactor's removal efficiency. The practical implementation of that design for the construction of the reactor would be quite challenging. The enhanced OMPs removal under turbulent flow regime is due to different factors, which include convective mass transfer, diffusion rates, hydrodynamic conditions and surface interactions [255]. Mass transfer is a critical factor in PEC based AOPs, as OMP removal is dependent on the transport of OMP molecules to the photoanode surface where the oxidation reaction occurs [209]. In laminar flow, mass transport was controlled by molecular diffusion, resulting in the formation of a thick concentration boundary layer at the photoanode-electrolyte interface. This boundary layer could have acted as a barrier to the transport of OMP molecules, thereby limiting reaction rates. The turbulent flow induced eddy diffusion and convective mixing, which reduced the thickness of the concentration boundary layer. The ratio of convective to diffusive mass transfer increases under turbulent conditions, which results in a higher mass transfer coefficient [256]. As a result, the OMP removal was enhanced due to the increased mass transfer of OMPs reaching the photoanode surface. Moreover, the diffusion of reactive species ($^{\bullet}OH$ and $^{\bullet}O_2^-$) is also enhanced under turbulent flow condition [254]. Turbulent flow could also prevent the excessive accumulation of reaction intermediates at the photoanode surface, thereby maintaining the high catalytic activity of the photocatalysts. Fig. 5.5(d) shows a more practical design for the construction of the reactor, and it was tested to investigate the effect of decreasing the distance between the outer wall of the reactor and the photoanode (referred to as depth) of the reactor on the residence time and removal of OMPs under turbulent flow regime. Table 5.2 shows the effect of changing the depth of the reactor on the removal of

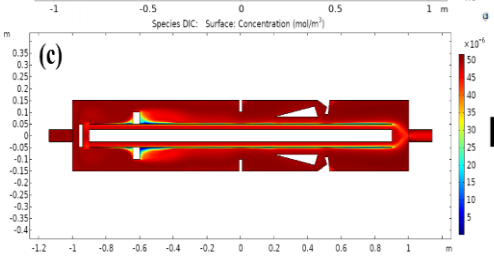
OMPs. By decreasing the depth of the reactor, the velocity increased, and residence time (treatment time) decreased, without affecting the removal of OMPs after a single treatment pass. The removal remained unchanged because the shorter residence time is compensated by a decreasing bulk zone (without reaction), allowing more surface reaction at the photoanode. The number of recirculations to achieve 80% removal was not reduced by decreasing the depth of the reactor. However, the total treatment time for 80% removal was reduced by 60% when the depth was changed from 0.10 m to 0.02 m, because the velocity increases when the depth decreases. Achieving a depth of 0.02 m would be quite challenging during the construction of



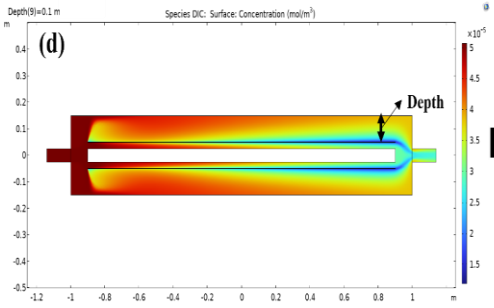
Flow Condition	Residence Time (min)	CAF Removal (%)	BTA Removal (%)	CBZ Removal (%)	DIC Removal (%)
Laminar	4.2	2.5	2.5	4.2	11
Turbulent	4 (2 circulations)	5.1	5.2	9.6	20



Flow Condition	Residence Time (min)	CAF Removal (%)	BTA Removal (%)	CBZ Removal (%)	DIC Removal (%)
Laminar	4.2	3.5	3.6	6.7	12
Turbulent	4 (2 circulations)	7.2	7.2	11.6	24



Flow Condition	Residence Time (min)	CAF Removal (%)	BTA Removal (%)	CBZ Removal (%)	DIC Removal (%)
Laminar	4.2	4.2	4.2	7.8	16
Turbulent	4 (2 circulations)	8.3	8.3	14.6	30



Flow Condition	Residence Time (min)	CAF Removal (%)	BTA Removal (%)	CBZ Removal (%)	DIC Removal (%)
Turbulent	2	5.0	5.4	8.5	30

Fig. 5.5: *Different designs tested using CFD in 2D geometry along with the removal performance (tables on right) in turbulent and laminar flow conditions.*

the reactor. Nevertheless, a depth in the range of 0.05 – 0.06 m would be more practical for the construction of the reactor.

Tabel 5.2: *Effect of depth of reactor (as shown in Fig. 3 (d)) on the residence time and removal performance of the reactor towards 80% removal of DIC, CBZ, CAF and BTA.*

Depth (m)	Residence Time (min)	CAF Removal (%)	BTA Removal (%)	CBZ Removal (%)	DIC Removal (%)	No. Of Circulations For 80% Removal	Total Time For 80% Removal
0.1	1.94	5.0	5.4	8.6	30	32	61 min
0.09	1.78	5.0	5.4	8.6	30	32	57 min
0.08	1.63	5.0	5.4	8.6	30	32	52 min
0.07	1.48	5.0	5.4	8.6	30	32	47 min
0.06	1.33	5.0	5.4	8.6	30	32	42 min
0.05	1.17	5.0	5.4	8.6	30	32	37 min
0.04	1.02	5.0	5.4	8.6	30	32	33 min
0.03	0.87	5.0	5.4	8.6	30	32	28 min
0.02	0.71	5.0	5.4	8.6	30	32	23 min

For the 3D simulation, the design shown in Fig. 5.1(b) was used and it was based upon the design in 2D shown in Fig. 5.5(d). Turbulent flow regime (61.6 L/min) was used to simulate photo-electrocatalytic removal of OMPs. The simulated results are depicted in Fig. 5.6(a) as a cross-sectional view through the central axis of the cylindrical reactor, displaying the concentration profile of DIC along its length. It was observed in Fig. 5.6(a) that the concentrations of OMPs are higher at the inner side of the photoanode. This limited removal of OMPs at the inner side of photoanode was attributed to the high flow velocity at the inner side compared to the outer side of photoanode, as shown in the velocity profile (Fig. 5.6(b)). To achieve a more uniform velocity profile in the reactor, the inlet pipe diameter was increased and set equal to the diameter of the reactor. Fig. 5.6(c) shows the concentration profile of DIC with the inlet pipe diameter equal to the diameter of the reactor. Increasing the diameter of the inlet pipe had a negative impact on the removal efficiency of the reactor because the flow velocity (Fig. 5.6(d)) was higher at the outer side of the photoanode, leading to lower removal of OMPs at the outer side of the photoanode compared to the inner side. The removal of all OMPs was lower and the number of recirculations for 80% removal along with the total treatment time also increased compared to the first configuration (Fig. 5.6(a)), as shown in Table 5.3. In the next step, the diameter of the photoanode was increased to 0.14 m to allow for a more uniform distribution of flow and to increase the surface area of the photoanode. The diameter of the inlet pipe was set equal to the diameter of the reactor. Fig. 5.6(e) shows the sliced concentration profile of DIC with increased diameter of photoanode. This had a positive

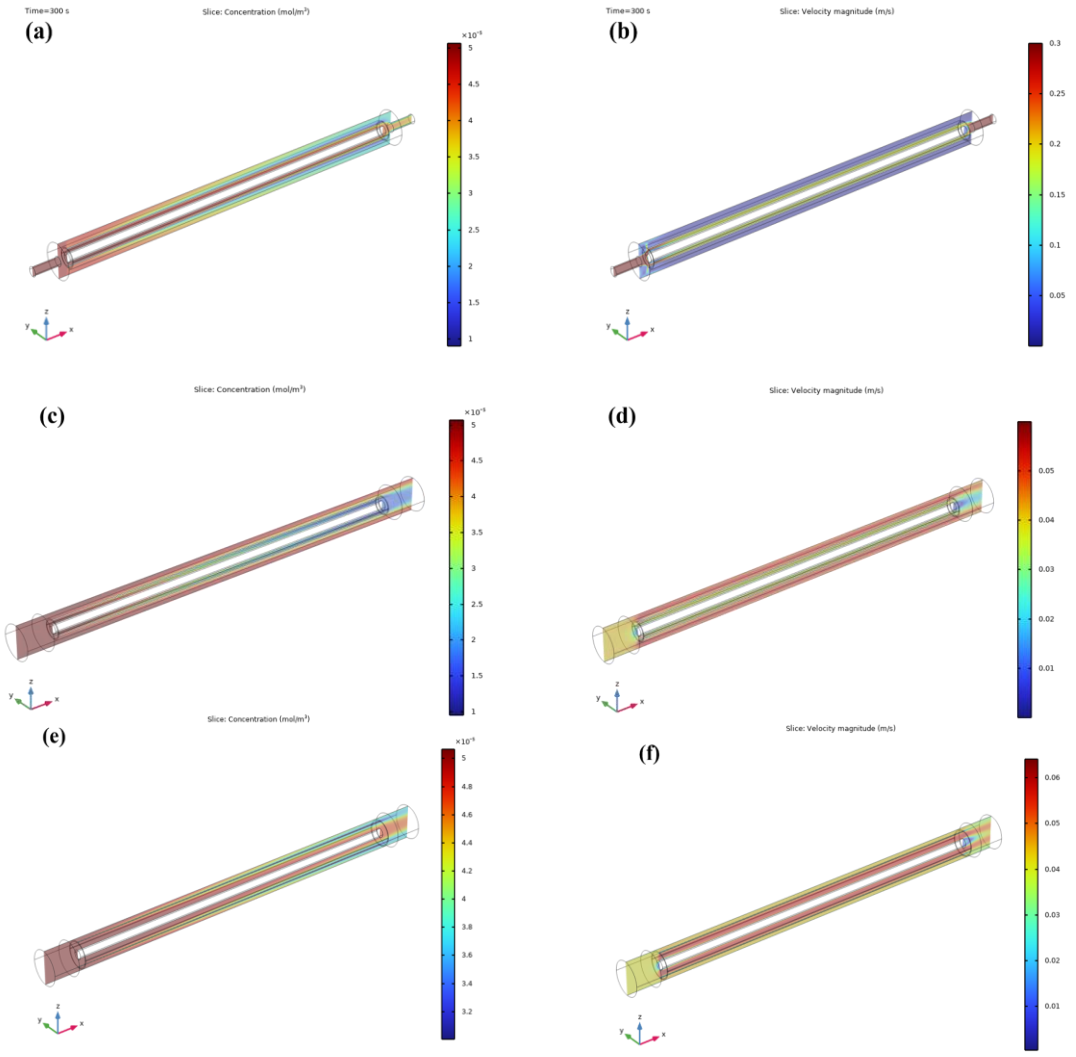


Fig. 5.6: *3D CFD simulations of photoelectrocatalytic reactor, showing the effect of inlet pipe diameter (a,b,c,d) and photoanode diameter (e,f) on the concentration profile and velocity magnitude profile of DIC.*

impact on the removal performance (Table 5.3) of the reactor as the total treatment time was reduced by 43%, compared to the previous two configurations (Fig. 5.6(a) and Fig. 5.6(c)). Moreover, the flow velocity (Fig. 5.6(f)) was more uniform inside the reactor compared to first (Fig. 5.6(a)) and second configuration (Fig. 5.6(c)). Therefore, the results of the third configuration were regarded as more efficient and applicable for pilot testing and experimental validation. The effect of light intensity on the optimized configuration was also tested in 3D

simulation. Table S.5.2 in the supplementary information highlights the impact of light intensity on the removal efficiency of the PEC reactor. A notable reduction in the removal of OMPs was observed when the light intensity was lowered from 400 W m^{-2} to 100 W m^{-2}. At lower intensity, the production yield of $^{\bullet}OH$ and $^{\bullet}O_2^-$ is decreased, therefore, the removal kinetics also slows down which decreases the removal [45]. With lower light intensity of 100 W m^{-2}, the total time for 80% removal of OMPs was also more than three times higher compared to 400 W m^{-2}. This effect of light intensity on the removal efficiency of the reactor could be regarded as a limitation of the PEC based AOP removal.

In our study, the CFD simulations primarily considered fluid flow conditions, reactor depth and light intensity as the main variables in the model. Incorporating additional variables such as electrode arrangement, light intensity distribution, and chemical reaction kinetics into the model would provide deeper insights into reactor optimization. These factors could be crucial for maximizing removal efficiency and scalability. However, their inclusion would require the development of coupled multi-physics models, which is beyond the scope of the current study. For the CFD simulations, our primary objective was to simulate the photo-electrochemical environment and hydrodynamic conditions. We suggest that future work should address these additional variables to enhance model robustness and further optimize reactor design.

Several challenges must be addressed to translate CFD simulations into practical larger scale applications. The prolonged use of the heterojunction photoanode can lead to material degradation, particularly during the time of high intensity solar irradiation and high flow rate. Strategies such as the development of (porous) protective coatings are crucial to enhance the long-term stability of the photoanode. Similarly, the photoanode in the PEC reactor would be susceptible to fouling (including biofilm growth) and organic matter deposition. The effective use of hydrodynamic shear forces, periodic electrode cleaning and antifouling coatings is necessary to address these issues. The energy consumption of large-scale PEC reactors is a critical factor in assessing their environmental impact and sustainability. Renewable energy integration and process optimization can minimize environmental impacts. Moreover, the stability of photoanodes in large scale reactors under long term operation must be evaluated to prevent secondary pollution from photocatalyst degradation.

Tabel 5.3: *Removal performance in 3D CFD simulations, showing the effect of photoanode diameter and inlet pipe diameter.*

Inlet pipe diameter (m)	Photoanode diameter (m)	Residence time (s)	CAF Removal (%)	BTA Removal (%)	CBZ Removal (%)	DIC Removal (%)	No. Of Circulations For 80% Removal	Total Time For 80% Removal
0.05	0.1	43	4	4	6	33	40	29 min
0.18	0.1	43	3	4	6	28	53	40 min
0.18	0.14	43	5	5	8	41	32	23 min

4. Conclusions

In this investigation, a heterojunction $BiVO_4/TiO_2$-GO photoanode was successfully fabricated using an ultrasonic spray pyrolysis (USP) process. Characterization via XRD and UV-visible diffusive reflectance spectroscopy confirmed the formation of UV-visible light absorbing heterojunction photoanodes. The heterojunction photoanode at an applied voltage of 1 V (vs Ag/AgCl) achieved simultaneous removal efficiencies of 100% for DIC, 54% for CBZ, 36% for BTA and 33% for BTA under simulated solar light. The heterojunction photoanode demonstrated a 50% increase in the removal efficiency for BTA, CBZ, and CAF compared to the pristine $BiVO_4$ photoanode. This increase in the removal efficiency was attributed to the improved charge separation in the heterojunction photoanode.

CFD simulations provided further insight into the reactor performance by elucidating the effects of flow dynamics on mass transport phenomena. Specifically, the simulations revealed that a turbulent flow regime substantially enhanced the diffusion of OMP molecules from the bulk solution to the photoanode surface, compared to a laminar flow regime. Under a uniform flow velocity profile and at a light intensity of 400 W m^{-2}, the optimized configuration achieved simultaneous removal efficiencies of 80% for BTA, CBZ, CAF, and DIC within 25 minutes. This result highlighted the critical influence of flow-induced mass transfer on the kinetics of OMP degradation. The CFD analysis also indicated that increasing flow velocity positively impacted the removal kinetics, offering a promising approach for scaling up the PEC reactor from laboratory to pilot scale. The integration of CFD with experimental results facilitated the optimization of reactor design. This optimization is expected to yield considerable reductions in operational time and cost during practical implementation. A key limitation of this study is the absence of uncertainty analysis of the CFD simulations. The primary objective was to establish a fundamental understanding of fluid flow effects on OMP removal and validate the model against experimental data. We acknowledge that CFD simulations involve uncertainties due to model assumptions, numerical discretization, boundary conditions and parameter estimations. Conducting a comprehensive uncertainty analysis requires additional computational resources and extensive sensitivity studies, which were beyond the scope of our study. Future research will integrate uncertainty quantification techniques such as global sensitivity analysis to improve the predictive reliability and robustness of CFD based reactor design under varying conditions. Additionally, long term investigation into the stability and durability of the photoanode under prolonged operational conditions is essential to assess the viability of PEC reactors in large scale applications. Future work will address these limitations, thereby advancing the development of robust PEC based AOPs for efficient and sustainable wastewater treatment.

Acknowledgements

This research was supported with a grant from the Topsector Water & Maritime TKI Water Technology Program (grant 2023TUD001) of the Ministry of Economic Affairs and Climate

Change, and supported by water utility Waternet (Amsterdam, the Netherlands) and Nijhuis Saur Industries.

Supplementary Information

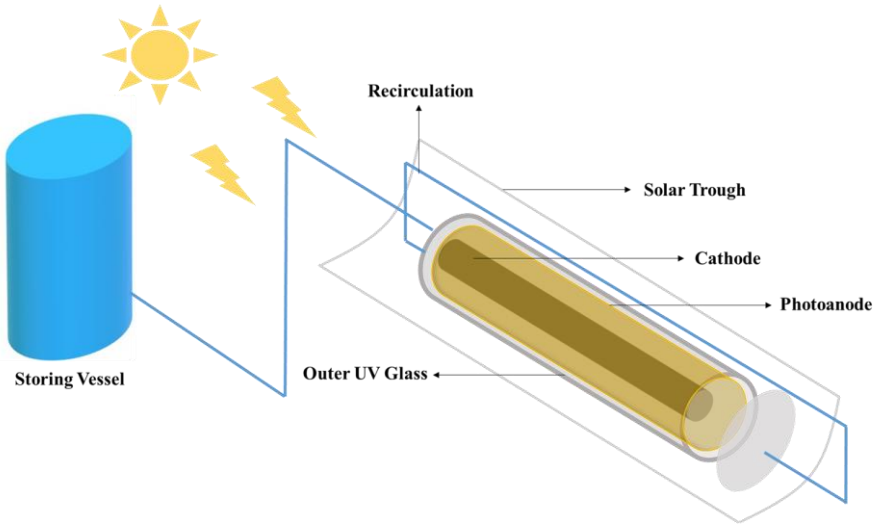


Fig. S.5.1: *Conceptual design of a photoelectrocatalytic reactor for the removal of OMPs from water.*

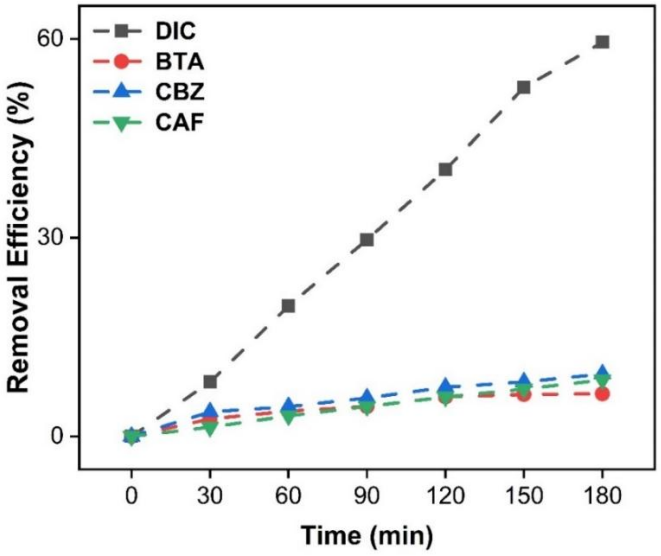


Fig. S.5.2: *Photolysis based removal of BTA, CBZ, CAF and DIC (each at C_0 = 40 µg L^{-1}) in demineralized water under solar simulated light for 3 hr reaction time.*

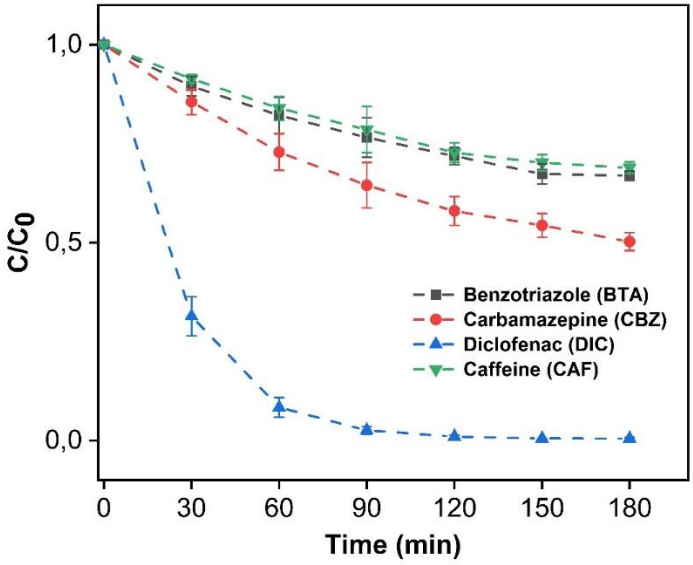


Fig. S.5.3: *Average simultaneous removal efficiency of heterojunction photoanode for BTA, CAF, CBZ and DIC based on triplicate experiments.*

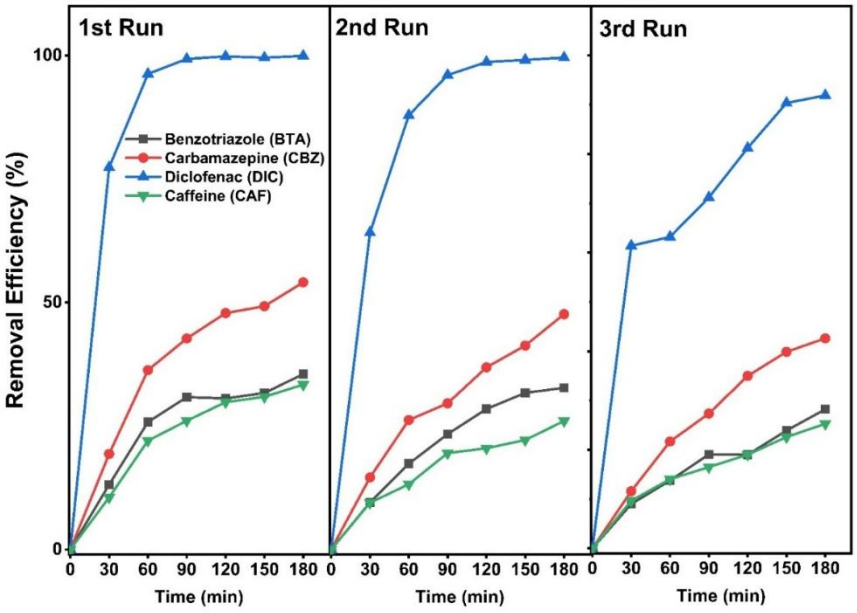


Fig. S.5.4: *Removal efficiency of a heterojunction photoanode for the simultaneous removal of BTA, CBZ, DIC and CAF during 3 hours of three consecutive removal experiments.*

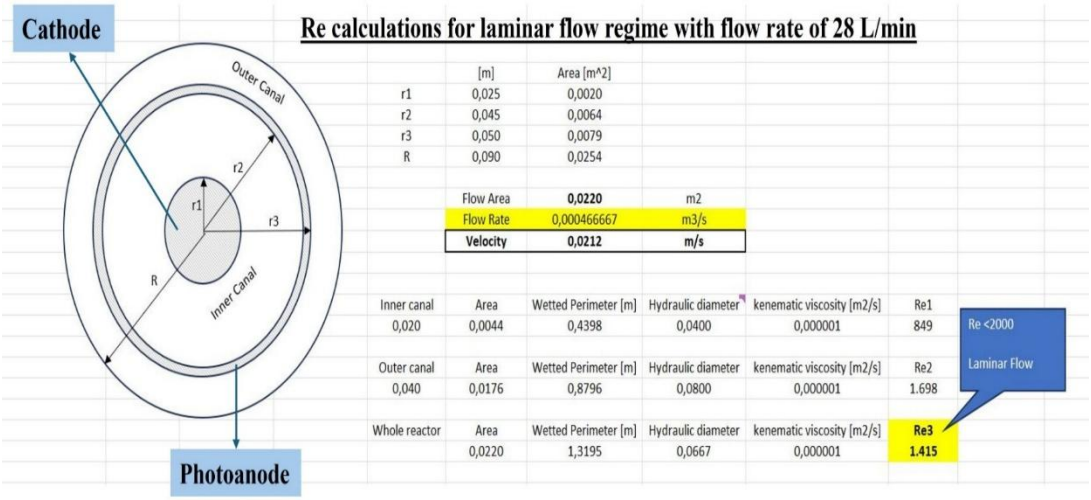


Fig. S.5.5: *Reynolds number (Re) calculations for laminar flow regime at a flow rate of 28 L/min.*

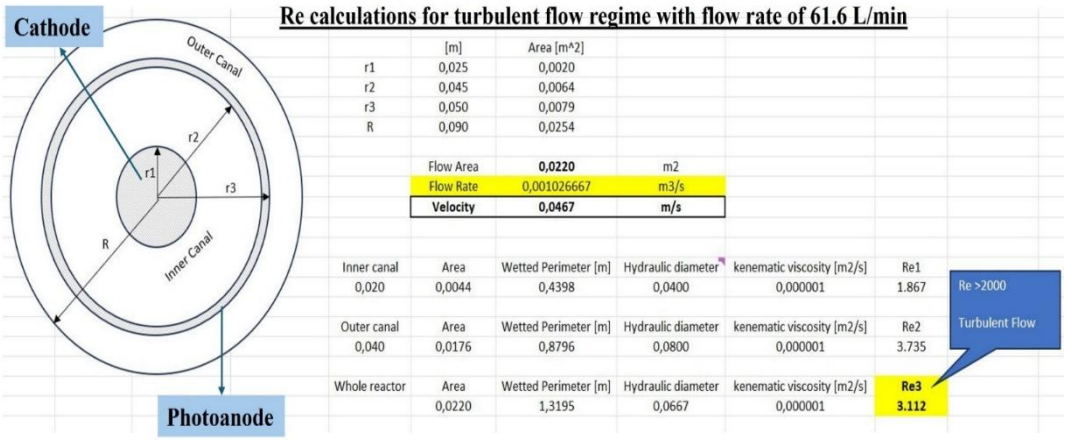


Fig. S.5.6: *Reynolds number (Re) calculations for turbulent flow regime at a flow rate of 61.6 L/min.*

Calculation of wetted perimeter of inner canal channel = $2\pi r1 + 2\pi r2 = 0{,}4398$ m

Calculation of hydraulic diameter of inner canal channel = 4 x (area of inner canal/wetted perimeter of inner canal) = 0,0400 m

Calculation of wetted perimeter of outer canal channel = $2\pi r3 + 2\pi R = 0{,}8796$ m

Calculation of hydraulic diameter of outer canal channel = 4 x (area of outer canal/wetted perimeter of outer canal) = 0,0800 m

$$\textbf{Reynolds number} = \frac{\textbf{Velocity} \times \textbf{hydraulic diameter}}{\textbf{kinematic viscosity of wtaer}}$$

Table S.1: *Parameters used in the CFD simulations.*

Parameter	Value
Light Intensity (I_{UV})	400 W m^{-2}
Current density (I_c)	2.827 A m^{-2}
Surface reaction flux for caffeine (K^*_{surf}_CAF)	2.80 x 10^{-8} m^5 W^{-1} A^{-1} s^{-1}
Surface reaction flux for benzotriazole (K^*_{surf}_BTA)	3.03 x 10^{-8} m^5 W^{-1} A^{-1} s^{-1}
Surface reaction flux for carbamazepine (K^*_{surf}_CBZ)	5.02 x 10^{-8} m^5 W^{-1} A^{-1} s^{-1}
Surface reaction flux for diclofenac (K^*_{surf}_DIC)	4.56 x 10^{-7} m^5 W^{-1} A^{-1} s^{-1}
Initial concentration of caffeine (C_CAF)	7.72 x 10^{-5} mol m^{-3}
Initial concentration of benzotriazole (C_BTA)	1.259 x 10^{-4} mol m^{-3}
Initial concentration of carbamazepine (C_CBZ)	5.698 x 10^{-5} mol m^{-3}
Initial concentration of diclofenac (C_DIC)	5.065 x 10^{-5} mol m^{-3}
Flow rate for turbulent conditions	61.6 L min^{-1}
Reynolds number (Re) for turbulent conditions	3112
Flow rate for laminar flow condition	28 L min^{-1}
Reynolds number (Re) for turbulent conditions	1415
Diffusion coefficients of OMPs	1 x 10^{-8} m^{-2} s^{-1}
Velocity scale in turbulent flow condition	1 m s^{-1}
Length scale factor in turbulent condition	0.035

Table S.2: *Effect of light intensity on the removal of BTA, CBZ, CAF and DIC.*

Light Intensity ($W\ m^{-2}$)	Residence time (s)	CAF Removal (%)	BTA Removal (%)	CBZ Removal (%)	DIC Removal (%)	No. Of Circulations For 80% Removal	Total Time For 80% Removal
400	43	5	5	8	41	32	23 min
100	43	1	1	2	17	>90	>65 min

Chapter 6

Conclusions and Outlook

6.1 Main conclusions

Overall, this dissertation met its main objective of $BiVO_4$ based photoanodes removing organic micropollutants (OMPs) mixtures at trace level under a 1V bias and simulated solar light. Although batch tests required 2-3 h for the removal of OMPs, computational fluid dynamics (CFD) modelling indicated that an optimized turbulent flow reactor operating at a light intensity of 400 W m^{-2} can reach 80% simultaneous removal of four OMPs in 25 min. The current technology readiness level (TRL) is between 3 and 4 and validation in real effluents is still required. The study responded to the defined research questions, as outlined below:

RQ 1: What is the current state of knowledge on the application of $BiVO_4$ based photoanodes for the removal of organic pollutants from aqueous solutions?

Chapter 2 highlighted that $BiVO_4$ is a visible light-driven photoanode offering distinct advantages over UV-driven alternatives, such as a relatively low band gap (~2.4 eV) and good chemical stability. However, prior research has largely focused on the removal of single OMPs at relatively high concentrations (1–10 mg L^{-1}), which does not reflect environmentally relevant concentrations. The review also revealed that pristine $BiVO_4$ suffers from rapid charge carrier recombination, which limits its photocatalytic efficiency. To address this limitation, heterojunction strategies involving materials such as Ag_3PO_4, CuO, and g-C_3N_4 have been explored, showing improved charge separation and enhanced removal efficiency. A critical knowledge gap identified was the limited research on the removal of OMP mixtures at environmentally relevant concentrations (<50 µg L^{-1}), a scenario more representative of real-world water matrices.

RQ 2: What is the removal efficiency of $BiVO_4$ photoanodes in the simultaneous removal of multiple OMPs from water?

Chapter 3 demonstrated that pristine $BiVO_4$ photoanodes can simultaneously remove acetaminophen, benzotriazole, and propranolol, each at a concentration of 45 µg L^{-1} in demineralized water. The photoanodes were fabricated using a simple and effective dip-coating method. Under simulated solar irradiation and an applied voltage of 1 V (vs Ag/AgCl), the $BiVO_4$ photoanode achieved removal efficiencies of 99% for acetaminophen and propranolol, and 70% for benzotriazole within 2 hours. Quenching experiments identified •OH as the primary reactive species responsible for OMP degradation in the photoelectrocatalytic (PEC) process. A first-order reaction kinetics model was applied to determine rate coefficients and half-lives, revealing that the degradation rates of acetaminophen and propranolol were approximately three times higher than that of benzotriazole. To assess the reusability and stability of the photoanodes, a $BiVO_4$ photoanode was used in four consecutive photo-PEC experiments, each lasting 2 hours. The photoanode demonstrated good reusability performance, with removal efficiencies decreasing by only 17%, 22%, and 32% for acetaminophen, benzotriazole, and propranolol, respectively.

RQ 3: What is the removal efficiency of a $BiVO_4$/BiOI heterojunction photoanode for a single OMP in water, and how does the heterojunction affect the rate of recombination in BiVO4?

Chapter 4 focused on the application of a $BiVO_4$/BiOI heterojunction photoanode for the removal of acetaminophen (40 μg L^{-1}) from demineralized water and investigated the role of the heterojunction in mitigating charge recombination in $BiVO_4$. The photoanodes were fabricated using an electrodeposition method and operated at an applied voltage of 1 V (vs Ag/AgCl) under simulated solar irradiation. The $BiVO_4$/BiOI heterojunction achieved a removal efficiency of 87% for acetaminophen within 2 hours, compared to 66% by the pristine $BiVO_4$ photoanode. This improvement was attributed to the heterojunction's ability to reduce charge recombination and enhance charge separation, thereby increasing the availability of reactive species. Quenching experiments identified $^{\bullet}O_2^-$ as the primary reactive species responsible for OMP degradation in the PEC process. The heterojunction photoanode demonstrated moderate stability and reusability, with a 26% decrease in overall removal efficiency observed after three consecutive 5-hour cycles.

RQ 4: What is the removal efficiency of a $BiVO_4$/TiO_2-GO heterojunction photoanode for the simultaneous removal of multiple OMPs in water?

Chapter 5 addressed this research question by evaluating the performance of a $BiVO_4$/TiO_2-GO heterojunction photoanode for the simultaneous removal of four OMPs: benzotriazole, carbamazepine, caffeine, and diclofenac, each at an initial concentration of 40 μg L^{-1} in demineralized water. The heterojunction photoanodes were fabricated via ultrasonic spray pyrolysis (USP) and operated at an applied voltage of 1 V (vs Ag/AgCl) under simulated solar light. The $BiVO_4$/TiO_2-GO photoanode achieved a complete (100%) removal of diclofenac within 3 hours, while removal efficiencies of 54% for carbamazepine, 36% for benzotriazole, and 33% for caffeine were obtained. Compared to the pristine $BiVO_4$ photoanode, the heterojunction exhibited approximately 50% higher removal efficiencies for benzotriazole, carbamazepine, and caffeine, demonstrating the enhanced performance resulting from improved charge separation and extended light absorption introduced by the TiO_2-GO layer. First-order reaction kinetics analysis revealed that the rate coefficient for diclofenac degradation was approximately nine times higher than that of carbamazepine, and about fifteen times higher than those of benzotriazole and caffeine.

RQ 5: how can CFD modelling be used to upscale the reaction kinetics of a $BiVO_4$/TiO_2-GO heterojunction photoanode from lab-scale experiments?

In Chapter 5, a CFD model was developed for a conceptually up-scaled PEC reactor. The model incorporated the experimentally determined reaction rate constants and examined the influence of reactor geometry and hydrodynamic conditions on OMP removal. Simulations under turbulent flow conditions showed significantly improved removal efficiencies for all

four OMPs, due to enhanced eddy diffusion and convective mixing. The optimized reactor design achieved up to 80% removal efficiency for all four OMPs within 25 minutes under a light intensity of 400 W m^{-2}.

6.2 Comparison with other AOPs

An important benchmark for the PEC-based approach developed in this dissertation is the class of established AOPs used in practice, particularly the UV/H_2O_2-based treatment technology. In recent pilot work in the Netherlands [257], UV/ H_2O_2 has been evaluated in combination with direct nanofiltration for municipal WWTP effluent, where multiple membranes and UV/ H_2O_2 intensities have been tested and overall OMP removal targets assessed. The study has illustrated the strength of UV/H_2O_2 as a mature and effective oxidation concept but also has highlighted practical considerations that can influence full-scale feasibility, such as sensitivity to optical water quality and system-wide energy and material demands. The UV/H_2O_2 performance has explicitly been linked to (low) effluent UV-transmission, which reduces treatment efficiency and increases the required UV dose. In addition, hybrid trains that rely on membranes create a separate challenge, which is the management of concentrate streams that can substantially affect both costs and environmental footprint and has been identified as a key remaining uncertainty for nanofiltration - UV/H_2O_2 technology [258]. Long term reliance on conventional UV/H_2O_2 technology is also challenged by the ongoing phase-out of mercury-containing UV lamps in regulation [259]. Under the EU RoHS framework, mercury in lamps is restricted and only permitted via time-limited exemptions, the exemption for lamps emitting mainly in the ultraviolet spectrum is currently set to expire in 2027.

Against this background, the PEC-based process, presented in this dissertation, is competitive in two main ways. First, PEC uses a UV-visible-light-driven photoanode and generates reactive species at the electrode surface without the continuous addition, storage, and handling of H_2O_2, thereby offering a pathway to reduce chemical logistics and associated safety measures. Second, CFD modelling, as presented in this dissertation, has indicated that, with an optimized flow and light distribution, high simultaneous removal of multiple OMPs can be achieved within practical residence times, suggesting a credible route toward compact reactor designs, if validated. At the same time, UV/H_2O_2 currently benefits from higher technological maturity, well-established reactor designs, and extensive operational experience. Therefore, the most meaningful way to position PEC for future implementation is to integrate it into treatment trains where its specific advantages matter most. Promising directions could include (i) PEC as a polishing step after conventional tertiary treatment where chemical-free operation is valued, and (ii) PEC targeted treatment of specific streams (e.g., concentrates or side streams), where controllable electrochemical driving force may help overcome matrix effects that limit purely photolytic processes. To complement performance comparison, the environmental impact was also assessed at system level. A life cycle assessment (LCA) of the conceptual up-scaled PEC design and CFD-based results, as reported in Chapter 5, has been carried out and

compared with alternative treatment options [260]. The LCA has indicated that use-phase and end-of-life impacts can be lower than a full-scale ozonation reference in the Netherlands, even though construction impacts are higher. It also identifies solar energy use and material reuse/recycling as major levers to further improve the footprint.

6.3 Outlook and recommendations for further studies

This dissertation demonstrated the potential of $BiVO_4$ based heterojunction photoanodes for the PEC removal of OMPs at concentrations lower than 50 µg L^{-1}. While the developed materials and reactor-scale modelling approaches provide a solid foundation, the findings of this work are still at a low technology readiness level (TRL 3-4). Therefore, to move towards higher TRLs and real-world implementation, further research is essential.

One of the key recommendations is the need to move beyond model systems using demineralized water and test the photoanodes under more realistic conditions, such as actual secondary effluent from municipal WWTPs. These real matrices contain coexisting substances such as natural organic matter (NOM), inorganic ions (e.g., Cl^-, SO_4^{2-}), and microorganisms that may interfere with the PEC performance by competing for reactive species (e.g., •OH, $•O_2^-$), blocking active sites on the photoanode surface, or scattering and absorbing incident light, thereby reducing the effective generation of charge carriers and reducing removal efficiency. Future studies should assess how such components affect light absorption, photoanode surface interactions, and the stability of reactive species generated during the PEC process.

Moreover, the developed photoanodes were tested using a batch-type PEC cell. Although this setup was sufficient for proof-of-concept studies, it does not represent the hydrodynamics and light distribution challenges faced in flow-through or continuous systems. To bridge this gap, further studies should explore the performance of $BiVO_4$ based photoanodes in flow-through reactors. This is particularly relevant in the context of the CFD simulations developed in this thesis. While the CFD model included experimental kinetic data, light distribution, and flow parameters, it was based on a conceptual design. Future work should couple this modelling approach with experimental validation using lab-scale flow cells, allowing model refinement and greater accuracy in performance predictions.

The results of reusability studies in this thesis showed that while $BiVO_4$ and $BiVO_4$ based heterojunctions maintained reasonable activity over multiple cycles, performance degradation was still observed. Further research is needed to better understand the mechanisms behind this loss in activity. It is recommended that future studies focus on long-term operational stability under realistic light conditions and repeated use, with special attention to potential fouling, material degradation, and surface reconstruction. Post-experiment characterization using surface analysis techniques could help identify material changes and inform strategies for improved durability.

Finally, although this work demonstrated enhanced removal efficiency through heterojunction engineering, a better understanding is still needed of how these heterojunctions influence charge separation under working PEC conditions. More advanced spectroscopic and electrochemical techniques could be used in future work to gain deeper mechanistic insight into interfacial charge dynamics. Additionally, the influence of light intensity and wavelength on heterojunction behaviour could be explored to better match real solar conditions.

References:

[1] V. Matamoros, J.M. Bayona, Elimination of Pharmaceuticals and Personal Care Products in Subsurface Flow Constructed Wetlands, Environ. Sci. Technol. 40 (2006) 5811–5816. https://doi.org/10.1021/es0607741.

[2] A.R. Ribeiro, O.C. Nunes, M.F.R. Pereira, A.M.T. Silva, An overview on the advanced oxidation processes applied for the treatment of water pollutants defined in the recently launched Directive 2013/39/EU, Environment International 75 (2015) 33–51. https://doi.org/10.1016/j.envint.2014.10.027.

[3] J. Rogowska, M. Cieszynska-Semenowicz, W. Ratajczyk, L. Wolska, Micropollutants in treated wastewater, Ambio 49 (2020) 487–503. https://doi.org/10.1007/s13280-019-01219-5.

[4] A. Jurado, E. Pujades, M. Walther, M.S. Diaz-Cruz, Occurrence, fate, and risk of the organic pollutants of the surface water watch List in European groundwaters: a review, Environ Chem Lett 20 (2022) 3313–3333. https://doi.org/10.1007/s10311-022-01441-w.

[5] S. Guerra-Rodríguez, A.R.L. Ribeiro, R.S. Ribeiro, E. Rodríguez, A.M.T. Silva, J. Rodríguez-Chueca, UV-A activation of peroxymonosulfate for the removal of micropollutants from secondary treated wastewater, Science of The Total Environment 770 (2021) 145299. https://doi.org/10.1016/j.scitotenv.2021.145299.

[6] R. Yang, N. Li, M. Ma, Z. Wang, Combined effects of estrogenic chemicals with the same mode of action using an estrogen receptor binding bioassay, Environmental Toxicology and Pharmacology 38 (2014) 829–837. https://doi.org/10.1016/j.etap.2014.10.001.

[7] H.N. Phong Vo, G.K. Le, T.M. Hong Nguyen, X.-T. Bui, K.H. Nguyen, E.R. Rene, T.D.H. Vo, N.-D. Thanh Cao, R. Mohan, Acetaminophen micropollutant: Historical and current occurrences, toxicity, removal strategies and transformation pathways in different environments, Chemosphere 236 (2019) 124391. https://doi.org/10.1016/j.chemosphere.2019.124391.

[8] M. Włodarczyk-Makuła, Selected organic micropollutants in the aquatic environment, Desalination and Water Treatment 317 (2024) 100061. https://doi.org/10.1016/j.dwt.2024.100061.

[9] P.A. Neale, S. Ait-Aissa, W. Brack, N. Creusot, M.S. Denison, B. Deutschmann, K. Hilscherová, H. Hollert, M. Krauss, J. Novák, T. Schulze, T.-B. Seiler, H. Serra, Y. Shao, B.I. Escher, Linking in Vitro Effects and Detected Organic Micropollutants in Surface Water Using Mixture-Toxicity Modeling, Environ. Sci. Technol. 49 (2015) 14614–14624. https://doi.org/10.1021/acs.est.5b04083.

[10] T. Backhaus, M. Faust, Predictive Environmental Risk Assessment of Chemical Mixtures: A Conceptual Framework, Environ. Sci. Technol. 46 (2012) 2564–2573. https://doi.org/10.1021/es2034125.

[11] K.E.C. Smith, S.N. Schmidt, N. Dom, R. Blust, M. Holmstrup, P. Mayer, Baseline Toxic Mixtures of Non-Toxic Chemicals: “Solubility Addition” Increases Exposure for Solid Hydrophobic Chemicals, Environ. Sci. Technol. 47 (2013) 2026–2033. https://doi.org/10.1021/es3040472.

[12] R. Servien, C. Leenknecht, K. Bonnot, V. Rossard, E. Latrille, L. Mamy, P. Benoit, A. Hélias, D. Patureau, Improved impact assessment of micropollutants release from

WWTPs, Case Studies in Chemical and Environmental Engineering 5 (2022) 100172. https://doi.org/10.1016/j.cscee.2021.100172.
[13] J.O. Eniola, R. Kumar, M.A. Barakat, J. Rashid, A review on conventional and advanced hybrid technologies for pharmaceutical wastewater treatment, Journal of Cleaner Production 356 (2022) 131826. https://doi.org/10.1016/j.jclepro.2022.131826.
[14] M. Adeel, G. Maniakova, L. Rizzo, Tertiary/quaternary treatment of urban wastewater by UV/H2O2 or ozonation: Microplastics may affect removal of *E. coli* and contaminants of emerging concern, Science of The Total Environment 907 (2024) 167940. https://doi.org/10.1016/j.scitotenv.2023.167940.
[15] Procedure File: 2022/0345(COD) | Legislative Observatory | European Parliament, (n.d.). https://oeil.secure.europarl.europa.eu/oeil/popups/ficheprocedure.do?lang=en&reference=2022/0345(COD) (accessed August 19, 2024).
[16] G. Mezohegyi, F.P. van der Zee, J. Font, A. Fortuny, A. Fabregat, Towards advanced aqueous dye removal processes: A short review on the versatile role of activated carbon, Journal of Environmental Management 102 (2012) 148–164. https://doi.org/10.1016/j.jenvman.2012.02.021.
[17] C.L. Chen, X.K. Wang, M. Nagatsu, Europium Adsorption on Multiwall Carbon Nanotube/Iron Oxide Magnetic Composite in the Presence of Polyacrylic Acid, Environ. Sci. Technol. 43 (2009) 2362–2367. https://doi.org/10.1021/es803018a.
[18] S. Gupta, N.-H. Tai, Carbon materials as oil sorbents: a review on the synthesis and performance, J. Mater. Chem. A 4 (2016) 1550–1565. https://doi.org/10.1039/C5TA08321D.
[19] M. Miao, Q. Lu, X. Wang, Y. Zhang, N.H. Wong, J. Sunarso, C. Xiao, N. Li, Removal of micro-organic contaminants from wastewater: A critical review of treatment technology, Next Materials 1 (2023) 100016. https://doi.org/10.1016/j.nxmate.2023.100016.
[20] R. Barrios, M. Siebel, A. van der Helm, K. Bosklopper, H. Gijzen, Environmental and financial life cycle impact assessment of drinking water production at Waternet, Journal of Cleaner Production 16 (2008) 471–476. https://doi.org/10.1016/j.jclepro.2006.07.052.
[21] P. Loganathan, J. Kandasamy, S. Jamil, H. Ratnaweera, S. Vigneswaran, Ozonation/adsorption hybrid treatment system for improved removal of natural organic matter and organic micropollutants from water – A mini review and future perspectives, Chemosphere 296 (2022) 133961. https://doi.org/10.1016/j.chemosphere.2022.133961.
[22] T.E. Agustina, H.M. Ang, V.K. Vareek, A review of synergistic effect of photocatalysis and ozonation on wastewater treatment, Journal of Photochemistry and Photobiology C: Photochemistry Reviews 6 (2005) 264–273. https://doi.org/10.1016/j.jphotochemrev.2005.12.003.
[23] O. Rozas, C. Baeza, K. Núñez, A. Rossner, R. Urrutia, H.D. Mansilla, Organic micropollutants (OMPs) oxidation by ozone: Effect of activated carbon on toxicity abatement, Science of The Total Environment 590–591 (2017) 430–439. https://doi.org/10.1016/j.scitotenv.2016.12.120.

[24] J. Altmann, A.S. Ruhl, F. Zietzschmann, M. Jekel, Direct comparison of ozonation and adsorption onto powdered activated carbon for micropollutant removal in advanced wastewater treatment, Water Research 55 (2014) 185–193. https://doi.org/10.1016/j.watres.2014.02.025.
[25] J. Derco, A.Ž. Gotvajn, O. Čižmárová, J. Dudáš, L. Sumegová, K. Šimovičová, Removal of Micropollutants by Ozone-Based Processes, Processes 9 (2021) 1013. https://doi.org/10.3390/pr9061013.
[26] N.K. Khanzada, M.U. Farid, J.A. Kharraz, J. Choi, C.Y. Tang, L.D. Nghiem, A. Jang, A.K. An, Removal of organic micropollutants using advanced membrane-based water and wastewater treatment: A review, Journal of Membrane Science 598 (2020) 117672. https://doi.org/10.1016/j.memsci.2019.117672.
[27] S. Rodriguez-Mozaz, M. Ricart, M. Köck-Schulmeyer, H. Guasch, C. Bonnineau, L. Proia, M.L. de Alda, S. Sabater, D. Barceló, Pharmaceuticals and pesticides in reclaimed water: Efficiency assessment of a microfiltration–reverse osmosis (MF–RO) pilot plant, Journal of Hazardous Materials 282 (2015) 165–173. https://doi.org/10.1016/j.jhazmat.2014.09.015.
[28] D. Roy, A. Khosravanipour Mostafazadeh, P. Drogui, R.D. Tyagi, Chapter 12 - Removal of organic micro-pollutants by membrane filtration, in: S. Varjani, A. Pandey, R.D. Tyagi, H.H. Ngo, C. Larroche (Eds.), Current Developments in Biotechnology and Bioengineering, Elsevier, 2020: pp. 281–307. https://doi.org/10.1016/B978-0-12-819594-9.00012-7.
[29] S. Ebrahimzadeh, B. Wols, A. Azzellino, B.J. Martijn, J.P. van der Hoek, Quantification and modelling of organic micropollutant removal by reverse osmosis (RO) drinking water treatment, Journal of Water Process Engineering 42 (2021) 102164. https://doi.org/10.1016/j.jwpe.2021.102164.
[30] V. Albergamo, B. Blankert, E.R. Cornelissen, B. Hofs, W.-J. Knibbe, W. van der Meer, P. de Voogt, Removal of polar organic micropollutants by pilot-scale reverse osmosis drinking water treatment, Water Research 148 (2019) 535–545. https://doi.org/10.1016/j.watres.2018.09.029.
[31] J. Cevallos-Mendoza, C.G. Amorim, J.M. Rodríguez-Díaz, M. da C.B.S.M. Montenegro, Removal of Contaminants from Water by Membrane Filtration: A Review, Membranes 12 (2022). https://doi.org/10.3390/membranes12060570.
[32] D. Ma, H. Yi, C. Lai, X. Liu, X. Huo, Z. An, L. Li, Y. Fu, B. Li, M. Zhang, L. Qin, S. Liu, L. Yang, Critical review of advanced oxidation processes in organic wastewater treatment, Chemosphere 275 (2021) 130104. https://doi.org/10.1016/j.chemosphere.2021.130104.
[33] X.-H. Ma, L. Zhao, Y.-H. Dong, Oxidation degradation of 2,2′,5-trichlorodiphenyl in a chelating agent enhanced Fenton reaction: Influencing factors, products, and pathways, Chemosphere 246 (2020) 125849. https://doi.org/10.1016/j.chemosphere.2020.125849.
[34] L. Zhan, W. Li, L. Liu, T. Han, M. Li, Z. Qiang, Degradation of micropolluants in flow-through VUV/UV/H2O2 reactors: Effects of H2O2 dosage and reactor internal diameter, Journal of Environmental Sciences 110 (2021) 28–37. https://doi.org/10.1016/j.jes.2021.03.012.

[35] M. Włodarczyk-Makuła, S. Myszograj, M. Włodarczyk, Removal of Organic Micro-Pollutants from Wastewater in Electrochemical Processes—Review, Energies 16 (2023) 5591. https://doi.org/10.3390/en16155591.
[36] X. Huo, Y. Yang, Q. Niu, Y. Zhu, G. Zeng, C. Lai, H. Yi, M. Li, Z. An, D. Huang, Y. Fu, B. Li, L. Li, M. Zhang, A direct Z-scheme oxygen vacant BWO/oxygen-enriched graphitic carbon nitride polymer heterojunction with enhanced photocatalytic activity, Chemical Engineering Journal 403 (2021) 126363. https://doi.org/10.1016/j.cej.2020.126363.
[37] P. Zawadzki, Visible Light–Driven Advanced Oxidation Processes to Remove Emerging Contaminants from Water and Wastewater: a Review, Water Air Soil Pollut 233 (2022) 374. https://doi.org/10.1007/s11270-022-05831-2.
[38] A. Balapure, J.R. Dutta, R. Ganesan, Recent advances in semiconductor heterojunctions: a detailed review of the fundamentals of photocatalysis, charge transfer mechanism and materials, RSC Applied Interfaces 1 (2024) 43–69. https://doi.org/10.1039/D3LF00126A.
[39] B. G, F. Banat, M. Abu Haija, Photoelectrochemical advanced oxidation processes for simultaneous removal of antibiotics and heavy metal ions in wastewater using 2D-on-2D WS2@CoFe2O4 heteronanostructures, Environmental Pollution 339 (2023) 122753. https://doi.org/10.1016/j.envpol.2023.122753.
[40] A. Fernandes, M. Gągol, P. Makoś, J.A. Khan, G. Boczkaj, Integrated photocatalytic advanced oxidation system (TiO2/UV/O3/H2O2) for degradation of volatile organic compounds, Separation and Purification Technology 224 (2019) 1–14. https://doi.org/10.1016/j.seppur.2019.05.012.
[41] Y.N. Kanafin, A. Abduvalov, M. Kaikanov, S.G. Poulopoulos, T.Sh. Atabaev, A review on WO3 photocatalysis used for wastewater treatment and pesticide degradation, Heliyon 11 (2025) e40788. https://doi.org/10.1016/j.heliyon.2024.e40788.
[42] N. Roy, S. Chakraborty, ZnO as photocatalyst: An approach to waste water treatment, Materials Today: Proceedings 46 (2021) 6399–6403. https://doi.org/10.1016/j.matpr.2020.06.264.
[43] V. Rani, A. Sharma, A. Kumar, P. Singh, S. Thakur, A. Singh, Q.V. Le, V.H. Nguyen, P. Raizada, ZrO2-Based Photocatalysts for Wastewater Treatment: From Novel Modification Strategies to Mechanistic Insights, Catalysts 12 (2022) 1418. https://doi.org/10.3390/catal12111418.
[44] P. Mane, H. Bae, V. Burungale, S.-W. Lee, M. Misra, H. Parbat, A.N. Kadam, J.-S. Ha, Interface-engineered Z-scheme of BiVO4/g-C3N4 photoanode for boosted photoelectrochemical water splitting and organic contaminant elimination under solar light, Chemosphere 308 (2022) 136166. https://doi.org/10.1016/j.chemosphere.2022.136166.
[45] B.O. Orimolade, O.A. Arotiba, Bismuth vanadate in photoelectrocatalytic water treatment systems for the degradation of organics: A review on recent trends, Journal of Electroanalytical Chemistry 878 (2020) 114724. https://doi.org/10.1016/j.jelechem.2020.114724.
[46] Y. Wen, G. Schoups, N. van de Giesen, Organic pollution of rivers: Combined threats of urbanization, livestock farming and global climate change, Sci Rep 7 (2017) 43289. https://doi.org/10.1038/srep43289.

[47] R.K. Mishra, S.S. Mentha, Y. Misra, N. Dwivedi, Emerging pollutants of severe environmental concern in water and wastewater: A comprehensive review on current developments and future research, Water-Energy Nexus 6 (2023) 74–95. https://doi.org/10.1016/j.wen.2023.08.002.

[48] N.G. Menon, S. Mohapatra, L.P. Padhye, S.S.V. Tatiparti, S. Mukherji, Review on Occurrence and Toxicity of Pharmaceutical Contamination in Southeast Asia, in: M. Kumar, D.D. Snow, R. Honda (Eds.), Emerging Issues in the Water Environment during Anthropocene: A South East Asian Perspective, Springer, Singapore, 2020: pp. 63–91. https://doi.org/10.1007/978-981-32-9771-5_4.

[49] C. Sanchez-Huerta, F. Baasher, C. Wang, S. Zhang, P.-Y. Hong, Global occurrence of organic micropollutants in surface and ground water: Highlighting the importance of wastewater sanitation to tackle organic micropollutants, Journal of Environmental Chemical Engineering 12 (2024) 112861. https://doi.org/10.1016/j.jece.2024.112861.

[50] S. Mohapatra, S. Bhatia, K.Y.K. Senaratna, M.-C. Jong, C.M.B. Lim, G.R. Gangesh, J.X. Lee, G.S. Giek, C. Cheung, L. Yutao, Y. Luhua, N.H. Yong, L.C. Peng, J.C.C. Wong, N.L. Ching, K.Y.-H. Gin, Wastewater surveillance of SARS-CoV-2 and chemical markers in campus dormitories in an evolving COVID − 19 pandemic, Journal of Hazardous Materials 446 (2023) 130690. https://doi.org/10.1016/j.jhazmat.2022.130690.

[51] J. Aravind kumar, T. Krithiga, S. Sathish, A.A. Renita, D. Prabu, S. Lokesh, R. Geetha, S.K.R. Namasivayam, M. Sillanpaa, Persistent organic pollutants in water resources: Fate, occurrence, characterization and risk analysis, Science of The Total Environment 831 (2022) 154808. https://doi.org/10.1016/j.scitotenv.2022.154808.

[52] U. Hübner, S. Spahr, H. Lutze, A. Wieland, S. Rüting, W. Gernjak, J. Wenk, Advanced oxidation processes for water and wastewater treatment – Guidance for systematic future research, Heliyon 10 (2024) e30402. https://doi.org/10.1016/j.heliyon.2024.e30402.

[53] Y. Deng, R. Zhao, Advanced Oxidation Processes (AOPs) in Wastewater Treatment, Curr Pollution Rep 1 (2015) 167–176. https://doi.org/10.1007/s40726-015-0015-z.

[54] S. Mohapatra, J.L.L. Xian, A. Galvez-Rodriguez, O.S. Ekande, J.E. Drewes, K.Y.-H. Gin, Photochemical fate of quaternary ammonium compounds (QACs) and degradation pathways prediction through computational, Journal of Hazardous Materials 465 (2024) 133483. https://doi.org/10.1016/j.jhazmat.2024.133483.

[55] K.E. O'Shea, D.D. Dionysiou, Advanced Oxidation Processes for Water Treatment, J. Phys. Chem. Lett. 3 (2012) 2112–2113. https://doi.org/10.1021/jz300929x.

[56] S. Mohapatra, D. Snow, P. Shea, A. Gálvez-Rodríguez, M. Kumar, L.P. Padhye, S. Mukherji, Photodegradation of a mixture of five pharmaceuticals commonly found in wastewater: Experimental and computational analysis, Environmental Research 216 (2023) 114659. https://doi.org/10.1016/j.envres.2022.114659.

[57] P. Kaur, Y. Park, I. Minami, M.A. Imteaz, M.A. Khan, A.A.S. Al-Othman, Z.A. Alothman, M. Sillanpää, Y. Li, Photoelectrocatalytic treatment of municipal wastewater with emerging concern pollutants using modified multi-layer catalytic anode, Chemosphere 339 (2023) 139575. https://doi.org/10.1016/j.chemosphere.2023.139575.

[58] J. Rodríguez-Chueca, J. Carbajo, P. García-Muñoz, Intensification of Photo-Assisted Advanced Oxidation Processes for Water Treatment: A Critical Review, Catalysts 13 (2023) 401. https://doi.org/10.3390/catal13020401.
[59] V. Kaswan, H. Kaur, A comparative study of advanced oxidation processes for wastewater treatment, Water Practice and Technology 18 (2023) 1233–1254. https://doi.org/10.2166/wpt.2023.061.
[60] S.-Y. Lee, S.-J. Park, TiO2 photocatalyst for water treatment applications, Journal of Industrial and Engineering Chemistry 19 (2013) 1761–1769. https://doi.org/10.1016/j.jiec.2013.07.012.
[61] S. Rajeswari, R. Venckatesh, Chapter 24 - ZnO-based nanoparticles for wastewater treatment: A review, in: K.A. Abd-Elsalam (Ed.), Zinc-Based Nanostructures for Environmental and Agricultural Applications, Elsevier, 2021: pp. 485–507. https://doi.org/10.1016/B978-0-12-822836-4.00022-7.
[62] J. Georgieva, E. Valova, S. Armyanov, N. Philippidis, I. Poulios, S. Sotiropoulos, Bi-component semiconductor oxide photoanodes for the photoelectrocatalytic oxidation of organic solutes and vapours: A short review with emphasis to TiO2–WO3 photoanodes, Journal of Hazardous Materials 211–212 (2012) 30–46. https://doi.org/10.1016/j.jhazmat.2011.11.069.
[63] T. He, Y. Zhao, D. Benetti, B. Moss, L. Tian, S. Selim, R. Li, F. Fan, Q. Li, X. Wang, C. Li, J.R. Durrant, Facet-Engineered BiVO4 Photocatalysts for Water Oxidation: Lifetime Gain Versus Energetic Loss, J. Am. Chem. Soc. 146 (2024) 27080–27089. https://doi.org/10.1021/jacs.4c09219.
[64] M. Dimitropoulos, C.A. Aggelopoulos, L. Sygellou, S.T. Tsantis, P.G. Koutsoukos, S.N. Yannopoulos, Unveiling the photocorrosion mechanism of zinc oxide photocatalyst: Interplay between surface corrosion and regeneration, Journal of Environmental Chemical Engineering 12 (2024) 112102. https://doi.org/10.1016/j.jece.2024.112102.
[65] P. Mane, H. Bae, V. Burungale, S.-W. Lee, M. Misra, H. Parbat, A.N. Kadam, J.-S. Ha, Interface-engineered Z-scheme of BiVO4/g-C3N4 photoanode for boosted photoelectrochemical water splitting and organic contaminant elimination under solar light, Chemosphere 308 (2022) 136166. https://doi.org/10.1016/j.chemosphere.2022.136166.
[66] L. Fu, W. Lian, Y. Lin, W. Fang, R. Xv, X. Shang, Enhanced Charge Separation and Transfer by BiVO4 Heterojunction and N-Doped for TiO2 Nanotubes during Photoelectrochemical Water Splitting, ACS Appl. Energy Mater. 6 (2023) 10116–10127. https://doi.org/10.1021/acsaem.3c01747.
[67] S. Tokunaga, H. Kato, A. Kudo, Selective Preparation of Monoclinic and Tetragonal BiVO4 with Scheelite Structure and Their Photocatalytic Properties, Chem. Mater. 13 (2001) 4624–4628. https://doi.org/10.1021/cm0103390.
[68] K.R. Tolod, S. Hernández, N. Russo, Recent Advances in the BiVO4 Photocatalyst for Sun-Driven Water Oxidation: Top-Performing Photoanodes and Scale-Up Challenges, Catalysts 7 (2017) 13. https://doi.org/10.3390/catal7010013.
[69] J.K. Cooper, S. Gul, F.M. Toma, L. Chen, Y.-S. Liu, J. Guo, J.W. Ager, J. Yano, I.D. Sharp, Indirect Bandgap and Optical Properties of Monoclinic Bismuth Vanadate, J. Phys. Chem. C 119 (2015) 2969–2974. https://doi.org/10.1021/jp512169w.

[70] Y. Park, K.J. McDonald, K.-S. Choi, Progress in bismuth vanadate photoanodes for use in solar water oxidation, Chem. Soc. Rev. 42 (2013) 2321–2337. https://doi.org/10.1039/C2CS35260E.
[71] Z. Zhao, Z. Li, Z. Zou, Electronic structure and optical properties of monoclinic clinobisvanite BiVO4, Phys. Chem. Chem. Phys. 13 (2011) 4746–4753. https://doi.org/10.1039/C0CP01871F.
[72] Y. Bennani, P. Perez-Rodriguez, M.J. Alani, W.A. Smith, L.C. Rietveld, M. Zeman, A.H.M. Smets, Photoelectrocatalytic oxidation of phenol for water treatment using a BiVO4 thin-film photoanode, Journal of Materials Research 31 (2016) 2627–2639. https://doi.org/10.1557/jmr.2016.290.
[73] A.-U.-R. Bacha, H. Cheng, J. Han, I. Nabi, K. Li, T. Wang, Y. Yang, S. Ajmal, Y. Liu, L. Zhang, Significantly accelerated PEC degradation of organic pollutant with addition of sulfite and mechanism study, Applied Catalysis B: Environmental 248 (2019) 441–449. https://doi.org/10.1016/j.apcatb.2019.02.049.
[74] H. Shao, Y. Wang, H. Zeng, J. Zhang, Y. Wang, M. Sillanpää, X. Zhao, Enhanced photoelectrocatalytic degradation of bisphenol a by BiVO4 photoanode coupling with peroxymonosulfate, Journal of Hazardous Materials 394 (2020) 121105. https://doi.org/10.1016/j.jhazmat.2019.121105.
[75] K. Wang, G. Liang, M. Waqas, B. Yang, K. Xiao, C. Zhu, J. Zhang, Peroxymonosulfate enhanced photoelectrocatalytic degradation of ofloxacin using an easily coated cathode, Separation and Purification Technology 236 (2020) 116301. https://doi.org/10.1016/j.seppur.2019.116301.
[76] L. Cheng, T. Jiang, K. Yan, J. Gong, J. Zhang, A dual-cathode photoelectrocatalysis-electroenzymatic catalysis system by coupling BiVO4 photoanode with hemin/Cu and carbon cloth cathodes for degradation of tetracycline, Electrochimica Acta 298 (2019) 561–569. https://doi.org/10.1016/j.electacta.2018.12.086.
[77] D. Cao, Y. Wang, M. Qiao, X. Zhao, Enhanced photoelectrocatalytic degradation of norfloxacin by an Ag3PO4/BiVO4 electrode with low bias, Journal of Catalysis 360 (2018) 240–249. https://doi.org/10.1016/j.jcat.2018.01.017.
[78] B.O. Orimolade, B.N. Zwane, B.A. Koiki, L. Tshwenya, G.M. Peleyeju, N. Mabuba, M. Zhou, O.A. Arotiba, Solar photoelectrocatalytic degradation of ciprofloxacin at a FTO/BiVO4/MnO2 anode: Kinetics, intermediate products and degradation pathway studies, Journal of Environmental Chemical Engineering 8 (2020) 103607. https://doi.org/10.1016/j.jece.2019.103607.
[79] B.O. Orimolade, O.A. Arotiba, Towards visible light driven photoelectrocatalysis for water treatment: Application of a FTO/BiVO4/Ag2S heterojunction anode for the removal of emerging pharmaceutical pollutants, Sci Rep 10 (2020) 5348. https://doi.org/10.1038/s41598-020-62425-w.
[80] H. Du, W. Pu, Y. Wang, K. Yan, J. Feng, J. Zhang, C. Yang, J. Gong, Synthesis of BiVO4/WO3 composite film for highly efficient visible light induced photoelectrocatalytic oxidation of norfloxacin, Journal of Alloys and Compounds 787 (2019) 284–294. https://doi.org/10.1016/j.jallcom.2019.01.390.
[81] K.R. Davies, M.G. Allan, S. Nagarajan, R. Townsend, T. Dunlop, J.D. McGettrick, V.S. Asokan, S. Ananthraj, T. Watson, A.R. Godfrey, J.R. Durrant, M.M. Maroto-Valer, M.F. Kuehnel, S. Pitchaimuthu, Solar light-driven simultaneous pharmaceutical pollutant degradation and green hydrogen production using a mesoporous nanoscale

WO3/BiVO4 heterostructure photoanode, Journal of Environmental Chemical Engineering 11 (2023) 110256. https://doi.org/10.1016/j.jece.2023.110256.
[82] X. Sun, T. Su, X. Cui, H. Yu, Y. Lu, W. Qin, M. Huo, A TiO2 nanotube photoanode (blue TiO2 nanotube/RuO2/BiVO4) for efficient acetaminophen degradation and nitrogen removal, Journal of Water Process Engineering 60 (2024) 105230. https://doi.org/10.1016/j.jwpe.2024.105230.
[83] T. Mohlala, T.L. Yusuf, N. Mabuba, Photoelectrocatalytic degradation of emerging organic pollutants in water on an FTO/BiVO4/NiS photoanode, Journal of Electroanalytical Chemistry 947 (2023) 117806. https://doi.org/10.1016/j.jelechem.2023.117806.
[84] X. Chen, J. Cao, C. Chen, A. Chen, W. Zheng, Degradation of organic dyes with solar PEC cells based on Bi2S3/BiVO4/TiO2 photoanode, Inorganic Chemistry Communications 160 (2024) 111849. https://doi.org/10.1016/j.inoche.2023.111849.
[85] W. Wang, X. Liu, J. Jing, J. Mu, R. Wang, C. Du, Y. Su, Photoelectrocatalytic peroxymonosulfate activation over CoFe2O4-BiVO4 photoanode for environmental purification: Unveiling of multi-active sites, interfacial engineering and degradation pathways, Journal of Colloid and Interface Science 644 (2023) 519–532. https://doi.org/10.1016/j.jcis.2023.03.202.
[86] Y. Wang, N. Lu, M. Luo, L. Fan, K. Zhao, J. Qu, J. Guan, X. Yuan, Enhancement mechanism of fiddlehead-shaped TiO2-BiVO4 type II heterojunction in SPEC towards RhB degradation and detoxification, Applied Surface Science 463 (2019) 234–243. https://doi.org/10.1016/j.apsusc.2018.08.239.
[87] J. Feng, L. Cheng, J. Zhang, O.K. Okoth, F. Chen, Preparation of BiVO4/ZnO composite film with enhanced visible-light photoelectrocatalytic activity, Ceramics International 44 (2018) 3672–3677. https://doi.org/10.1016/j.ceramint.2017.11.124.
[88] Z. Zheng, Y.H. Ng, Y. Tang, Y. Li, W. Chen, J. Wang, X. Li, L. Li, Visible-light-driven photoelectrocatalytic activation of chloride by nanoporous MoS2@BiVO4 photoanode for enhanced degradation of bisphenol A, Chemosphere 263 (2021) 128279. https://doi.org/10.1016/j.chemosphere.2020.128279.
[89] H. Fan, G. Yi, Z. Zhang, X. Zhang, P. Li, C. Zhang, L. Chen, Y. Zhang, Q. Sun, Fabrication of Ag particles deposited BiVO4 photoanode for significantly efficient visible-light driven photoelectrocatalytic degradation of β-naphthol, Journal of Environmental Chemical Engineering 10 (2022) 107221. https://doi.org/10.1016/j.jece.2022.107221.
[90] Y. Li, X. Sun, Y. Tang, Y.H. Ng, L. Li, F. Jiang, J. Wang, W. Chen, L. Li, Understanding photoelectrocatalytic degradation of tetracycline over three-dimensional coral-like ZnO/BiVO4 nanocomposite, Materials Chemistry and Physics 271 (2021) 124871. https://doi.org/10.1016/j.matchemphys.2021.124871.
[91] Y. Chen, L. Liu, L. Zhang, S. Li, X. Zhang, W. Yu, F. Wang, W. Xue, H. Wang, Z. Bian, Construction of Z-type heterojunction BiVO4/Sm/α-Fe2O3 photoanode for selective degradation: Efficient removal of bisphenol A based on multifunctional Sm-doped modification, Applied Catalysis B: Environment and Energy 333 (2023) 122775. https://doi.org/10.1016/j.apcatb.2023.122775.
[92] J. Sun, Y. Guo, Y. Wang, D. Cao, S. Tian, K. Xiao, R. Mao, X. Zhao, H2O2 assisted photoelectrocatalytic degradation of diclofenac sodium at g-C3N4/BiVO4 photoanode

under visible light irradiation, Chemical Engineering Journal 332 (2018) 312–320. https://doi.org/10.1016/j.cej.2017.09.041.
[93] T.M. do Prado, F.L. Silva, G. Grosseli, P.S. Fadini, O. Fatibello-Filho, F.C. de Moraes, Using BiVO4/CuO-Based Photoelectrocatalyzer for 4-Nitrophenol Degradation, Materials 13 (2020). https://doi.org/10.3390/ma13061322.
[94] B.O. Orimolade, B.A. Koiki, B.N. Zwane, G.M. Peleyeju, N. Mabuba, O.A. Arotiba, Interrogating solar photoelectrocatalysis on an exfoliated graphite–BiVO4/ZnO composite electrode towards water treatment, RSC Adv. 9 (2019) 16586–16595. https://doi.org/10.1039/C9RA02366F.
[95] X. Li, J. Wan, Y. Ma, Y. Wang, X. Li, Study on cobalt-phosphate (Co-Pi) modified BiVO4/Cu2O photoanode to significantly inhibit photochemical corrosion and improve the photoelectrochemical performance, Chemical Engineering Journal 404 (2021) 127054. https://doi.org/10.1016/j.cej.2020.127054.
[96] K.R. Davies, M.G. Allan, S. Nagarajan, R. Townsend, V. Asokan, T. Watson, A.R. Godfrey, M.M. Maroto-Valer, M.F. Kuehnel, S. Pitchaimuthu, Photoelectrocatalytic Surfactant Pollutant Degradation and Simultaneous Green Hydrogen Generation, Ind. Eng. Chem. Res. 62 (2023) 19084–19094. https://doi.org/10.1021/acs.iecr.3c00840.
[97] Y. Cong, W. Zhang, W. Ding, T. Zhang, Y. Zhang, N. Chi, Q. Wang, Fabrication of electrochemically-modified BiVO4-MoS2-Co3O4composite film for bisphenol A degradation, Journal of Environmental Sciences 102 (2021) 341–351. https://doi.org/10.1016/j.jes.2020.09.027.
[98] Y. Yang, X. Zhang, J. Jiang, J. Han, W. Li, X. Li, K.M. Yee Leung, S.A. Snyder, P.J.J. Alvarez, Which Micropollutants in Water Environments Deserve More Attention Globally?, Environ. Sci. Technol. 56 (2022) 13–29. https://doi.org/10.1021/acs.est.1c04250.
[99] C.J. Houtman, J. Kroesbergen, K. Lekkerkerker-Teunissen, J.P. van der Hoek, Human health risk assessment of the mixture of pharmaceuticals in Dutch drinking water and its sources based on frequent monitoring data, Science of The Total Environment 496 (2014) 54–62. https://doi.org/10.1016/j.scitotenv.2014.07.022.
[100] M.V. Pablos, P. García-Hortigüela, C. Fernández, Acute and chronic toxicity of emerging contaminants, alone or in combination, in Chlorella vulgaris and Daphnia magna, Environ Sci Pollut Res 22 (2015) 5417–5424. https://doi.org/10.1007/s11356-015-4119-1.
[101] M.O. Barbosa, N.F.F. Moreira, A.R. Ribeiro, M.F.R. Pereira, A.M.T. Silva, Occurrence and removal of organic micropollutants: An overview of the watch list of EU Decision 2015/495, Water Research 94 (2016) 257–279. https://doi.org/10.1016/j.watres.2016.02.047.
[102] E.M.M. Wanda, H. Nyoni, B.B. Mamba, T.A.M. Msagati, Application of silica and germanium dioxide nanoparticles/ polyethersulfone blend membranes for removal of emerging micropollutants from water, Physics and Chemistry of the Earth, Parts A/B/C 108 (2018) 28–47. https://doi.org/10.1016/j.pce.2018.08.004.
[103] T. Rasheed, M. Bilal, F. Nabeel, M. Adeel, H.M.N. Iqbal, Environmentally-related contaminants of high concern: Potential sources and analytical modalities for detection, quantification, and treatment, Environment International 122 (2019) 52–66. https://doi.org/10.1016/j.envint.2018.11.038.

[104] M. Hecker, H. Hollert, Endocrine disruptor screening: regulatory perspectives and needs, Environmental Sciences Europe 23 (2011) 15. https://doi.org/10.1186/2190-4715-23-15.
[105] E. Neczaj, A. Grosser, Circular Economy in Wastewater Treatment Plant–Challenges and Barriers, Proceedings 2 (2018) 614. https://doi.org/10.3390/proceedings2110614.
[106] A. Chavoshani, M. Hashemi, M. Mehdi Amin, S.C. Ameta, Chapter 1 - Introduction, in: A. Chavoshani, M. Hashemi, M. Mehdi Amin, S.C. Ameta (Eds.), Micropollutants and Challenges, Elsevier, 2020: pp. 1–33. https://doi.org/10.1016/B978-0-12-818612-1.00001-5.
[107] Z.A. Yacouba, J. Mendret, G. Lesage, F. Zaviska, S. Brosillon, Removal of organic micropollutants from domestic wastewater: The effect of ozone-based advanced oxidation process on nanofiltration, Journal of Water Process Engineering 39 (2021) 101869. https://doi.org/10.1016/j.jwpe.2020.101869.
[108] Y. Dubowski, Y. Alfiya, Y. Gilboa, S. Sabach, E. Friedler, Removal of organic micropollutants from biologically treated greywater using continuous-flow vacuum-UV/UVC photo-reactor, Environ Sci Pollut Res 27 (2020) 7578–7587. https://doi.org/10.1007/s11356-019-07399-7.
[109] S. Garcia-Segura, E. Brillas, Applied photoelectrocatalysis on the degradation of organic pollutants in wastewaters, Journal of Photochemistry and Photobiology C: Photochemistry Reviews 31 (2017) 1–35. https://doi.org/10.1016/j.jphotochemrev.2017.01.005.
[110] T.A. Aragaw, F.M. Bogale, B.A. Aragaw, Iron-based nanoparticles in wastewater treatment: A review on synthesis methods, applications, and removal mechanisms, Journal of Saudi Chemical Society 25 (2021) 101280. https://doi.org/10.1016/j.jscs.2021.101280.
[111] M.C. Collivignarelli, A. Abbà, M. Carnevale Miino, G. Bertanza, S. Sorlini, S. Damiani, H. Arab, M. Bestetti, S. Franz, Photoelectrocatalysis on TiO2 meshes: different applications in the integrated urban water management, Environ Sci Pollut Res 28 (2021) 59452–59461. https://doi.org/10.1007/s11356-021-12606-5.
[112] M. Liao, L. Su, Y. Deng, S. Xiong, R. Tang, Z. Wu, C. Ding, L. Yang, D. Gong, Strategies to improve WO3-based photocatalysts for wastewater treatment: a review, J Mater Sci 56 (2021) 14416–14447. https://doi.org/10.1007/s10853-021-06202-8.
[113] D.T. Sponza, R. Oztekin, Treatment of olive mill wastewater by photooxidation with ZrO2-doped TiO2 nanocomposite and its reuse capability, Environ Technol 37 (2016) 865–879. https://doi.org/10.1080/09593330.2015.1088579.
[114] T. Ahmed, M. Ammar, A. Saleem, H. Zhang, H. Xu, Z-scheme 2D-m-BiVO4 networks decorated by a g-CN nanosheet heterostructured photocatalyst with an excellent response to visible light, RSC Adv. 10 (2020) 3192–3202. https://doi.org/10.1039/C9RA09473C.
[115] B. Samran, S. lunput, S. Tonnonchiang, S. Chaiwichian, BiFeO3/BiVO4 nanocomposite photocatalysts with highly enhanced photocatalytic activity for rhodamine B degradation under visible light irradiation, Physica B: Condensed Matter 561 (2019) 23–28. https://doi.org/10.1016/j.physb.2019.02.049.
[116] H. Jiang, H. Dai, X. Meng, L. Zhang, J. Deng, K. Ji, Morphology-Dependent Photocatalytic Performance of Monoclinic BiVO4 for Methyl Orange Degradation

under Visible-Light Irradiation, Chinese Journal of Catalysis 32 (2011) 939–949. https://doi.org/10.1016/S1872-2067(10)60215-X.
[117] L. Xia, J. Li, J. Bai, L. Li, Q. Zeng, Q. Xu, B. Zhou, Preparation of a BiVO4 nanoporous photoanode based on peroxovanadate reduction and conversion for efficient photoelectrochemical performance, Nanoscale 10 (2018) 2848–2855. https://doi.org/10.1039/C7NR07566A.
[118] C. Regmi, Y.K. Kshetri, T.-H. Kim, R.P. Pandey, S.K. Ray, S.W. Lee, Fabrication of Ni-doped BiVO4 semiconductors with enhanced visible-light photocatalytic performances for wastewater treatment, Applied Surface Science 413 (2017) 253–265. https://doi.org/10.1016/j.apsusc.2017.04.056.
[119] P. Perez-Rodriguez, Y. Bennani, M.J. Alani, W. Smith, L.C. Rietveld, M. Zeman, A.H.M. Smets, Treatment of Organic Pollutants Using a Solar Energy Driven Photo-Oxidation Device, Adv. Sustainable Syst. 1 (2017) 1700010. https://doi.org/10.1002/adsu.201700010.
[120] R. Loos, B.M. Gawlik, G. Locoro, E. Rimaviciute, S. Contini, G. Bidoglio, EU-wide survey of polar organic persistent pollutants in European river waters, Environmental Pollution 157 (2009) 561–568. https://doi.org/10.1016/j.envpol.2008.09.020.
[121] H.-G. Ni, F.-H. Lu, X.-L. Luo, H.-Y. Tian, E.Y. Zeng, Occurrence, Phase Distribution, and Mass Loadings of Benzothiazoles in Riverine Runoff of the Pearl River Delta, China, Environ. Sci. Technol. 42 (2008) 1892–1897. https://doi.org/10.1021/es071871c.
[122] H. Janna, M.D. Scrimshaw, R.J. Williams, J. Churchley, J.P. Sumpter, From Dishwasher to Tap? Xenobiotic Substances Benzotriazole and Tolyltriazole in the Environment, Environ. Sci. Technol. 45 (2011) 3858–3864. https://doi.org/10.1021/es103267g.
[123] N.K. Vel Leitner, B. Roshani, Kinetic of benzotriazole oxidation by ozone and hydroxyl radical, Water Research 44 (2010) 2058–2066. https://doi.org/10.1016/j.watres.2009.12.018.
[124] A.A. Mazioti, A.S. Stasinakis, G. Gatidou, N.S. Thomaidis, H.R. Andersen, Sorption and biodegradation of selected benzotriazoles and hydroxybenzothiazole in activated sludge and estimation of their fate during wastewater treatment, Chemosphere 131 (2015) 117–123. https://doi.org/10.1016/j.chemosphere.2015.03.029.
[125] E. Borowska, E. Felis, J. Kalka, Oxidation of benzotriazole and benzothiazole in photochemical processes: Kinetics and formation of transformation products, Chemical Engineering Journal 304 (2016) 852–863. https://doi.org/10.1016/j.cej.2016.06.123.
[126] N.H.S. Javadi, M. Baghdadi, N. Mehrdadi, M. Mortazavi, Removal of benzotriazole from secondary municipal wastewater effluent by catalytic ozonation in the presence of magnetic alumina nanocomposite, Journal of Environmental Chemical Engineering 6 (2018) 6421–6430. https://doi.org/10.1016/j.jece.2018.09.063.
[127] J. Xu, L. Li, C. Guo, Y. Zhang, S. Wang, Removal of benzotriazole from solution by BiOBr photocatalysis under simulated solar irradiation, Chemical Engineering Journal 221 (2013) 230–237. https://doi.org/10.1016/j.cej.2013.01.081.
[128] M.J. Elman, J. Sugar, R. Fiscella, T.A. Deutsch, J. Noth, M. Nyberg, K. Packo, R.J. Anderson, The effect of propranolol versus placebo on resident surgical performance., Trans Am Ophthalmol Soc 96 (1998) 283–294.

[129] M. Petrović, B. Škrbić, J. Živančev, L. Ferrando-Climent, D. Barcelo, Determination of 81 pharmaceutical drugs by high performance liquid chromatography coupled to mass spectrometry with hybrid triple quadrupole–linear ion trap in different types of water in Serbia, Science of The Total Environment 468–469 (2014) 415–428. https://doi.org/10.1016/j.scitotenv.2013.08.079.
[130] Q. Zheng, D.K. Unruh, K.M. Hutchins, Removal of the Micropollutants Propranolol Hydrochloride and 2-Naphthol From Water by Pyridine-Functionalized Polymers, Frontiers in Chemistry 9 (2022). https://www.frontiersin.org/articles/10.3389/fchem.2021.793870 (accessed March 20, 2023).
[131] Y. Somasundar, L.Q. Shen, A.G. Hoane, L.L. Tang, M.R. Mills, A.E. Burton, A.D. Ryabov, T.J. Collins, Structural, Mechanistic, and Ultradilute Catalysis Portrayal of Substrate Inhibition in the TAML–Hydrogen Peroxide Catalytic Oxidation of the Persistent Drug and Micropollutant, Propranolol, J. Am. Chem. Soc. 140 (2018) 12280–12289. https://doi.org/10.1021/jacs.8b08108.
[132] T. Giordani, J. Dose, Y. Kuskoski, J. Schultz, A.S. Mangrich, J.M.M. de Mello, L.L. Silva, R.C.F. Zeferino, M. Zanetti, M.A. Fiori, G.L. Colpani, Photocatalytic degradation of propranolol hydrochloride using Nd–TiO2 nanoparticles under UV and visible light, Journal of Materials Research 36 (2021) 1584–1599. https://doi.org/10.1557/s43578-021-00207-4.
[133] H. Nsubuga, C. Basheer, A. Jalilov, M.B. Haider, A.A. Al-Saadi, Droplet flow-assisted heterogeneous electro-Fenton reactor for degradation of beta-blockers: response surface optimization, and mechanism elucidation, Environ Sci Pollut Res 26 (2019) 14313–14327. https://doi.org/10.1007/s11356-019-04551-1.
[134] M. Sajid, S. Bari, M. Saif Ur Rehman, M. Ashfaq, Y. Guoliang, G. Mustafa, Adsorption characteristics of paracetamol removal onto activated carbon prepared from Cannabis sativum Hemp, Alexandria Engineering Journal 61 (2022) 7203–7212. https://doi.org/10.1016/j.aej.2021.12.060.
[135] W.J. Lee, P.S. Goh, W.J. Lau, A.F. Ismail, Removal of Pharmaceutical Contaminants from Aqueous Medium: A State-of-the-Art Review Based on Paracetamol, Arab J Sci Eng 45 (2020) 7109–7135. https://doi.org/10.1007/s13369-020-04446-1.
[136] Y. Ouarda, Electro-oxidation of secondary effluents from various wastewater plants for the removal of acetaminophen and dissolved organic matter, Science of the Total Environment (2020) 8.
[137] B.O. Orimolade, B.A. Koiki, G.M. Peleyeju, O.A. Arotiba, Visible light driven photoelectrocatalysis on a FTO/BiVO4/BiOI anode for water treatment involving emerging pharmaceutical pollutants, Electrochimica Acta 307 (2019) 285–292. https://doi.org/10.1016/j.electacta.2019.03.217.
[138] B. Quinn, F. Gagné, C. Blaise, Evaluation of the acute, chronic and teratogenic effects of a mixture of eleven pharmaceuticals on the cnidarian, Hydra attenuata, Science of The Total Environment 407 (2009) 1072–1079. https://doi.org/10.1016/j.scitotenv.2008.10.022.
[139] M. Ijaz, T. Ahmed, A. Iftikhar Ahmad, Toxic Organic Micropollutants and Associated Health Impacts, in: T. Ahmed, M.Z. Hashmi (Eds.), Hazardous Environmental Micro-Pollutants, Health Impacts and Allied Treatment Technologies, Springer International Publishing, Cham, 2022: pp. 205–217. https://doi.org/10.1007/978-3-030-96523-5_9.

[140] A.Z. Ali, Y. Wu, Y.-D. Bennani, H. Spanjers, J.P. van der Hoek, Photo-electrocatalytic based removal of acetaminophen: Application of visible light driven heterojunction based BiVO4/BiOI photoanode, Chemosphere 324 (2023) 138322. https://doi.org/10.1016/j.chemosphere.2023.138322.
[141] S. Meng, T. Ogawa, H. Okumura, K.N. Ishihara, Enhanced Photocatalytic Activity of BiVO4/Bi2S3/SnS2 Heterojunction under Visible Light, Catalysts 10 (2020) 1294. https://doi.org/10.3390/catal10111294.
[142] Y. Zhang, L. Shi, Z. Geng, T. Ren, Z. Yang, The improvement of photocatalysis O2 production over BiVO4 with amorphous FeOOH shell modification, Sci Rep 9 (2019) 19090. https://doi.org/10.1038/s41598-019-54940-2.
[143] T. Xia, M. Chen, L. Xiao, W. Fan, B. Mao, D. Xu, P. Guan, J. Zhu, W. Shi, Dip-coating synthesis of P-doped BiVO4 photoanodes with enhanced photoelectrochemical performance, Journal of the Taiwan Institute of Chemical Engineers 93 (2018) 582–589. https://doi.org/10.1016/j.jtice.2018.09.003.
[144] H. Huang, C. Ma, Z. Zhu, X. Yao, Y. Liu, Z. Liu, C. Li, Y. Yan, Insights into enhanced visible light photocatalytic activity of t-Se nanorods/BiOCl ultrathin nanosheets 1D/2D heterojunctions, Chemical Engineering Journal 338 (2018) 218–229. https://doi.org/10.1016/j.cej.2017.12.012.
[145] R.G. Pearson, Absolute electronegativity and hardness: application to inorganic chemistry, Inorg. Chem. 27 (1988) 734–740. https://doi.org/10.1021/ic00277a030.
[146] D.K. Zhong, S. Choi, D.R. Gamelin, Near-Complete Suppression of Surface Recombination in Solar Photoelectrolysis by "Co-Pi" Catalyst-Modified W:BiVO4, J. Am. Chem. Soc. 133 (2011) 18370–18377. https://doi.org/10.1021/ja207348x.
[147] H.L. Tan, R. Amal, Y.H. Ng, Alternative strategies in improving the photocatalytic and photoelectrochemical activities of visible light-driven BiVO4: a review, J. Mater. Chem. A 5 (2017) 16498–16521. https://doi.org/10.1039/C7TA04441K.
[148] S. Bai, J. Liu, M. Cui, R. Luo, J. He, A. Chen, Two-step electrodeposition to fabricate the p–n heterojunction of a Cu2O/BiVO4 photoanode for the enhancement of photoelectrochemical water splitting, Dalton Trans. 47 (2018) 6763–6771. https://doi.org/10.1039/C7DT04258B.
[149] Y. Li, X. Sun, Y. Tang, Y.H. Ng, L. Li, F. Jiang, J. Wang, W. Chen, L. Li, Understanding photoelectrocatalytic degradation of tetracycline over three-dimensional coral-like ZnO/BiVO4 nanocomposite, Materials Chemistry and Physics 271 (2021) 124871. https://doi.org/10.1016/j.matchemphys.2021.124871.
[150] S.W. Hwang, J.U. Kim, J.H. Baek, S.S. Kalanur, H.S. Jung, H. Seo, I.S. Cho, Solution-processed TiO2/BiVO4/SnO2 triple-layer photoanode with enhanced photoelectrochemical performance, Journal of Alloys and Compounds 785 (2019) 1245–1252. https://doi.org/10.1016/j.jallcom.2019.01.251.
[151] M. Serdechnova, V.L. Ivanov, M.R.M. Domingues, D.V. Evtuguin, M.G.S. Ferreira, M.L. Zheludkevich, Photodegradation of 2-mercaptobenzothiazole and 1,2,3-benzotriazole corrosion inhibitors in aqueous solutions and organic solvents, Phys. Chem. Chem. Phys. 16 (2014) 25152–25160. https://doi.org/10.1039/C4CP03867C.
[152] R. Xiong, Z. Lu, Q. Tang, X. Huang, H. Ruan, W. Jiang, Y. Chen, Z. Liu, J. Kang, D. Liu, UV-LED/chlorine degradation of propranolol in water: Degradation pathway and product toxicity, Chemosphere 248 (2020) 125957. https://doi.org/10.1016/j.chemosphere.2020.125957.

[153] P. Attri, Y.H. Kim, D.H. Park, J.H. Park, Y.J. Hong, H.S. Uhm, K.-N. Kim, A. Fridman, E.H. Choi, Generation mechanism of hydroxyl radical species and its lifetime prediction during the plasma-initiated ultraviolet (UV) photolysis, Sci Rep 5 (2015) 9332. https://doi.org/10.1038/srep09332.

[154] H.A. Nájera-Aguilar, R. Mayorga-Santis, R.F. Gutiérrez-Hernández, A. Santiesteban-Hernández, F.J. Rodríguez-Valadez, D.A. Ulloa-Gutiérrez, J.A. Araiza-Aguilar, A. Cruz-Salomón, Propranolol degradation through processes based on the generation of hydroxyl free radical, Journal of Water and Health 20 (2021) 216–226. https://doi.org/10.2166/wh.2021.156.

[155] M. Qutob, M.A. Hussein, K.A. Alamry, M. Rafatullah, A review on the degradation of acetaminophen by advanced oxidation process: pathway, by-products, biotoxicity, and density functional theory calculation, RSC Adv. 12 (2022) 18373–18396. https://doi.org/10.1039/D2RA02469A.

[156] N. Singhal, O. Perez-Garcia, Degrading Organic Micropollutants: The Next Challenge in the Evolution of Biological Wastewater Treatment Processes, Frontiers in Environmental Science 4 (2016). https://www.frontiersin.org/articles/10.3389/fenvs.2016.00036 (accessed April 4, 2023).

[157] E. Kudlek, A. Lempart-Rapacewicz, M. Dudziak, Identification of Potential Harmful Transformation Products of Selected Micropollutants in Outdoor and Indoor Swimming Pool Water, Int J Environ Res Public Health 19 (2022) 5660. https://doi.org/10.3390/ijerph19095660.

[158] F. Audino, J.M. Toro Santamaria, L.J. del Valle Mendoza, M. Graells, M. Pérez-Moya, Removal of Paracetamol Using Effective Advanced Oxidation Processes, International Journal of Environmental Research and Public Health 16 (2019) 505. https://doi.org/10.3390/ijerph16030505.

[159] F. Ghanbari, A. Yaghoot-Nezhad, S. Wacławek, K.-Y.A. Lin, J. Rodríguez-Chueca, F. Mehdipour, Comparative investigation of acetaminophen degradation in aqueous solution by UV/Chlorine and UV/H2O2 processes: Kinetics and toxicity assessment, process feasibility and products identification, Chemosphere 285 (2021) 131455. https://doi.org/10.1016/j.chemosphere.2021.131455.

[160] F. Ghanbari, M. Khatebasreh, M. Mahdavianpour, K.-Y.A. Lin, Oxidative removal of benzotriazole using peroxymonosulfate/ozone/ultrasound: Synergy, optimization, degradation intermediates and utilizing for real wastewater, Chemosphere 244 (2020) 125326. https://doi.org/10.1016/j.chemosphere.2019.125326.

[161] R. Wang, J. Bai, Y. Li, Q. Zeng, J. Li, B. Zhou, BiVO4/TiO2(N2) Nanotubes Heterojunction Photoanode for Highly Efficient Photoelectrocatalytic Applications, Nano-Micro Lett. 9 (2016) 14. https://doi.org/10.1007/s40820-016-0115-3.

[162] Z. Chi, J. Zhao, Y. Zhang, H. Yu, H. Yu, Coral-like WO3/BiVO4 photoanode constructed via morphology and facet engineering for antibiotic wastewater detoxification and hydrogen recovery, Chemical Engineering Journal 428 (2022) 131817. https://doi.org/10.1016/j.cej.2021.131817.

[163] Y. Bennani, P. Perez-Rodriguez, M.J. Alani, W.A. Smith, L.C. Rietveld, M. Zeman, A.H.M. Smets, Photoelectrocatalytic oxidation of phenol for water treatment using a BiVO4 thin-film photoanode, Journal of Materials Research 31 (2016) 2627–2639. https://doi.org/10.1557/jmr.2016.290.

[164] Y. Lu, Y. Chu, W. Zheng, M. Huo, H. Huo, J. Qu, H. Yu, Y. Zhao, Significant tetracycline hydrochloride degradation and electricity generation in a visible-light-driven dual photoelectrode photocatalytic fuel cell using BiVO4/TiO2 NT photoanode and Cu2O/TiO2 NT photocathode, Electrochimica Acta 320 (2019) 134617. https://doi.org/10.1016/j.electacta.2019.134617.
[165] M.A. Behnajady, B. Vahid, N. Modirshahla, M. Shokri, Evaluation of electrical energy per order (EEO) with kinetic modeling on the removal of Malachite Green by US/UV/H2O2 process, Desalination 249 (2009) 99–103. https://doi.org/10.1016/j.desal.2008.07.025.
[166] J.R. Bolton, K.G. Bircher, W. Tumas, C.A. Tolman, Figures-of-merit for the technical development and application of advanced oxidation technologies for both electric- and solar-driven systems (IUPAC Technical Report):, Pure and Applied Chemistry 73 (2001) 627–637. https://doi.org/10.1351/pac200173040627.
[167] THE 17 GOALS | Sustainable Development, (n.d.). https://sdgs.un.org/goals (accessed July 21, 2022).
[168] J.P. van der Hoek, C. Bertelkamp, A.R.D. Verliefde, N. Singhal, Drinking water treatment technologies in Europe: state of the art – challenges – research needs, Journal of Water Supply: Research and Technology-Aqua 63 (2014) 124–130. https://doi.org/10.2166/aqua.2013.007.
[169] L. Corominas, V. Acuña, A. Ginebreda, M. Poch, Integration of freshwater environmental policies and wastewater treatment plant management, Science of The Total Environment 445–446 (2013) 185–191. https://doi.org/10.1016/j.scitotenv.2012.12.055.
[170] D. Puyol, D.J. Batstone, T. Hülsen, S. Astals, M. Peces, J.O. Krömer, Resource Recovery from Wastewater by Biological Technologies: Opportunities, Challenges, and Prospects, Frontiers in Microbiology 7 (2017). https://www.frontiersin.org/articles/10.3389/fmicb.2016.02106 (accessed July 21, 2022).
[171] M. Smol, C. Adam, M. Preisner, Circular economy model framework in the European water and wastewater sector, J Mater Cycles Waste Manag 22 (2020) 682–697. https://doi.org/10.1007/s10163-019-00960-z.
[172] B. Petrie, R. Barden, B. Kasprzyk-Hordern, A review on emerging contaminants in wastewaters and the environment: Current knowledge, understudied areas and recommendations for future monitoring, Water Research 72 (2015) 3–27. https://doi.org/10.1016/j.watres.2014.08.053.
[173] N. Ratola, A. Cincinelli, A. Alves, A. Katsoyiannis, Occurrence of organic microcontaminants in the wastewater treatment process. A mini review, J Hazard Mater 239–240 (2012) 1–18. https://doi.org/10.1016/j.jhazmat.2012.05.040.
[174] O. Golovko, A.-L. Rehrl, S. Köhler, L. Ahrens, Organic micropollutants in water and sediment from Lake Mälaren, Sweden, Chemosphere 258 (2020) 127293. https://doi.org/10.1016/j.chemosphere.2020.127293.
[175] S. Garcia-Segura, E. Brillas, Applied photoelectrocatalysis on the degradation of organic pollutants in wastewaters, Journal of Photochemistry and Photobiology C: Photochemistry Reviews 31 (2017) 1–35. https://doi.org/10.1016/j.jphotochemrev.2017.01.005.

[176] N.G. Deshpande, C.H. Ahn, R.R. Koli, A.S. Jamadar, D.S. Kim, Y.B. Kim, S.H. Jung, H.K. Cho, Controlled nanostructured morphology of BiVO4 photoanodes for efficient on-demand catalysis in solar water-splitting and sustainable water-treatment, Applied Surface Science 514 (2020) 146075. https://doi.org/10.1016/j.apsusc.2020.146075.
[177] H. Shao, Y. Wang, H. Zeng, J. Zhang, Y. Wang, M. Sillanpää, X. Zhao, Enhanced photoelectrocatalytic degradation of bisphenol a by BiVO4 photoanode coupling with peroxymonosulfate, Journal of Hazardous Materials 394 (2020) 121105. https://doi.org/10.1016/j.jhazmat.2019.121105.
[178] B.O. Orimolade, O.A. Arotiba, Bismuth vanadate in photoelectrocatalytic water treatment systems for the degradation of organics: A review on recent trends, Journal of Electroanalytical Chemistry 878 (2020) 114724. https://doi.org/10.1016/j.jelechem.2020.114724.
[179] L.-P. Li, M. Liu, W.-D. Zhang, Electrodeposition of CdS onto BiVO4 films with high photoelectrochemical performance, J Solid State Electrochem 22 (2018) 2569–2577. https://doi.org/10.1007/s10008-018-3973-4.
[180] D. Cao, Y. Wang, M. Qiao, X. Zhao, Enhanced photoelectrocatalytic degradation of norfloxacin by an Ag3PO4/BiVO4 electrode with low bias, Journal of Catalysis 360 (2018) 240–249. https://doi.org/10.1016/j.jcat.2018.01.017.
[181] S. Ni, T. Zhou, H. Zhang, Y. Cao, P. Yang, BiOI/BiVO4 Two-Dimensional Heteronanostructures for Visible-Light Photocatalytic Degradation of Rhodamine B, ACS Appl. Nano Mater. 1 (2018) 5128–5141. https://doi.org/10.1021/acsanm.8b01161.
[182] T. He, D. Wu, Y. Tan, Fabrication of BiOI/BiVO4 heterojunction with efficient visible-light-induced photocatalytic activity, Materials Letters 165 (2016) 227–230. https://doi.org/10.1016/j.matlet.2015.12.002.
[183] A. Chowdhury, M. Sajid, N. Jahan, T.I. Adelusi, P. Maitra, G. Yin, X. Wu, Y. Gao, S. Wang, A secondary approach with conventional medicines and supplements to recuperate current COVID-19 status, Biomedicine & Pharmacotherapy 142 (2021) 111956. https://doi.org/10.1016/j.biopha.2021.111956.
[184] M.Á. López Zavala, D.A. Vega, J.M. Álvarez Vega, O.F. Castillo Jerez, R.A. Cantú Hernández, Electrochemical oxidation of acetaminophen and its transformation products in surface water: effect of pH and current density, Heliyon 6 (2020) e03394. https://doi.org/10.1016/j.heliyon.2020.e03394.
[185] T.W. Kim, K.-S. Choi, Nanoporous BiVO4 Photoanodes with Dual-Layer Oxygen Evolution Catalysts for Solar Water Splitting, Science 343 (2014) 990–994. https://doi.org/10.1126/science.1246913.
[186] C. Liang, H.-W. Su, Identification of Sulfate and Hydroxyl Radicals in Thermally Activated Persulfate, Ind. Eng. Chem. Res. 48 (2009) 5558–5562. https://doi.org/10.1021/ie9002848.
[187] Y. Liu, H. Li, X. Zhang, S. Liu, Y. Zhang, Q. Li, J. Liu, PEG-assisted hydrothermal synthesis of novel flower-like hierarchical BiVO4 with enhanced visible light photocatalytic activity, IOP Conf. Ser.: Mater. Sci. Eng. 452 (2018) 042105. https://doi.org/10.1088/1757-899X/452/4/042105.
[188] X. Xiao, Y. Lin, B. Pan, W. Fan, Y. Huang, Photocatalytic degradation of methyl orange by BiOI/Bi4O5I2 microspheres under visible light irradiation, Inorganic Chemistry Communications 93 (2018) 65–68. https://doi.org/10.1016/j.inoche.2018.05.009.

[189] W. Tang, Y. Zhang, H. Guo, Y. Liu, Heterogeneous activation of peroxymonosulfate for bisphenol AF degradation with BiOI0.5Cl0.5, RSC Adv. 9 (2019) 14060–14071. https://doi.org/10.1039/C9RA01687B.
[190] K.J. McDonald, K.-S. Choi, A new electrochemical synthesis route for a BiOI electrode and its conversion to a highly efficient porous BiVO4 photoanode for solar water oxidation, Energy Environ. Sci. 5 (2012) 8553–8557. https://doi.org/10.1039/C2EE22608A.
[191] J. Hou, K. Jiang, M. Shen, R. Wei, X. Wu, F. Idrees, C. Cao, Micro and nano hierachical structures of BiOI/activated carbon for efficient visible-light-photocatalytic reactions, Sci Rep 7 (2017) 11665. https://doi.org/10.1038/s41598-017-12266-x.
[192] P. Ju, Y. Wang, Y. Sun, D. Zhang, Controllable one-pot synthesis of a nest-like Bi2WO6/BiVO4 composite with enhanced photocatalytic antifouling performance under visible light irradiation, Dalton Trans. 45 (2016) 4588–4602. https://doi.org/10.1039/C6DT00118A.
[193] Z. Xiang, Y. Wang, D. Zhang, P. Ju, BiOI/BiVO4 p□n heterojunction with enhanced photocatalytic activity under visible-light irradiation, Journal of Industrial and Engineering Chemistry 40 (2016) 83–92. https://doi.org/10.1016/j.jiec.2016.06.009.
[194] S. Li, W. Xu, L. Meng, W. Tian, L. Li, Recent Progress on Semiconductor Heterojunction-Based Photoanodes for Photoelectrochemical Water Splitting, Small Science 2 (2022) 2100112. https://doi.org/10.1002/smsc.202100112.
[195] H. Gong, N. Freudenberg, M. Nie, R. van de Krol, K. Ellmer, BiVO4 photoanodes for water splitting with high injection efficiency, deposited by reactive magnetron co-sputtering, AIP Advances 6 (2016) 045108. https://doi.org/10.1063/1.4947121.
[196] E. Moctezuma, E. Leyva, C.A. Aguilar, R.A. Luna, C. Montalvo, Photocatalytic degradation of paracetamol: Intermediates and total reaction mechanism, Journal of Hazardous Materials 243 (2012) 130–138. https://doi.org/10.1016/j.jhazmat.2012.10.010.
[197] D. Vogna, R. Marotta, A. Napolitano, M. d'Ischia, Advanced Oxidation Chemistry of Paracetamol. UV/H2O2-Induced Hydroxylation/Degradation Pathways and 15N-Aided Inventory of Nitrogenous Breakdown Products., J. Org. Chem. 67 (2002) 6143–6151. https://doi.org/10.1021/jo025604v.
[198] G. Byzynski, D.P. Volanti, C. Ribeiro, V.R. Mastelaro, E. Longo, Direct photo-oxidation and superoxide radical as major responsible for dye photodegradation mechanism promoted by TiO2–rGO heterostructure, J Mater Sci: Mater Electron 29 (2018) 17022–17037. https://doi.org/10.1007/s10854-018-9799-0.
[199] N.A. Abbasi, S.U. Shahid, M. Majid, A. Tahir, Chapter 1 - Introduction to environmental micropollutants, in: M.Z. Hashmi, S. Wang, Z. Ahmed (Eds.), Environmental Micropollutants, Elsevier, 2022: pp. 1–12. https://doi.org/10.1016/B978-0-323-90555-8.00010-6.
[200] Y. Luo, W. Guo, H.H. Ngo, L.D. Nghiem, F.I. Hai, J. Zhang, S. Liang, X.C. Wang, A review on the occurrence of micropollutants in the aquatic environment and their fate and removal during wastewater treatment, Science of The Total Environment 473–474 (2014) 619–641. https://doi.org/10.1016/j.scitotenv.2013.12.065.
[201] D. Bunke, S. Moritz, W. Brack, D.L. Herráez, L. Posthuma, M. Nuss, Developments in society and implications for emerging pollutants in the aquatic environment,

Environmental Sciences Europe 31 (2019) 32. https://doi.org/10.1186/s12302-019-0213-1.
[202] A.T. Besha, A.Y. Gebreyohannes, R.A. Tufa, D.N. Bekele, E. Curcio, L. Giorno, Removal of emerging micropollutants by activated sludge process and membrane bioreactors and the effects of micropollutants on membrane fouling: A review, Journal of Environmental Chemical Engineering 5 (2017) 2395–2414. https://doi.org/10.1016/j.jece.2017.04.027.
[203] M.A. Abbas, M. Iqbal, H.M. Tauqeer, V. Turan, M. Farhad, Chapter 16 - Microcontaminants in wastewater, in: M.Z. Hashmi, S. Wang, Z. Ahmed (Eds.), Environmental Micropollutants, Elsevier, 2022: pp. 315–329. https://doi.org/10.1016/B978-0-323-90555-8.00018-0.
[204] V. Vinayagam, K.N. Palani, S. Ganesh, S. Rajesh, V.V. Akula, R. Avoodaiappan, O.S. Kushwaha, A. Pugazhendhi, Recent developments on advanced oxidation processes for degradation of pollutants from wastewater with focus on antibiotics and organic dyes, Environmental Research 240 (2024) 117500. https://doi.org/10.1016/j.envres.2023.117500.
[205] P. Koundle, N. Nirmalkar, M. Momotko, S. Makowiec, G. Boczkaj, Tetracycline degradation for wastewater treatment based on ozone nanobubbles advanced oxidation processes (AOPs) – Focus on nanobubbles formation, degradation kinetics, mechanism and effects of water composition, Chemical Engineering Journal 501 (2024) 156236. https://doi.org/10.1016/j.cej.2024.156236.
[206] Y. Yan, B. Lin, L. Zhang, Y. Wang, H. Zhang, H. Zheng, T. Zhou, Y. Zhan, Z. Yu, Y. Kuang, J. Tang, Electrochemical oxidation processes based on renewable energy towards carbon neutrality: Oxidation fundamentals, catalysts, challenges and prospects, Chemical Engineering Journal 487 (2024) 150447. https://doi.org/10.1016/j.cej.2024.150447.
[207] T. Zhou, J. Du, Z. Wang, G. Xiao, L. Luo, M. Faheem, H. Ling, J. Bao, Degradation of sulfamethoxazole by MnO2/heat-activated persulfate: Kinetics, synergistic effect and reaction mechanism, Chemical Engineering Journal Advances 9 (2022) 100200. https://doi.org/10.1016/j.ceja.2021.100200.
[208] J.E. Kumar, T. Mulai, W. Kharmawphlang, R.N. Sharan, M.K. Sahoo, The efficiency of Fenton, Fenton/MW and UV/oxidant processes in the treatment of a mixture of higher concentrations of azo dyes, Chemical Engineering Journal Advances 15 (2023) 100515. https://doi.org/10.1016/j.ceja.2023.100515.
[209] Q. Zhang, D. Zheng, B. Bai, Z. Ma, S. Zong, Insight into antibiotic removal by advanced oxidation processes (AOPs): Performance, mechanism, degradation pathways, and ecotoxicity assessment, Chemical Engineering Journal 500 (2024) 157134. https://doi.org/10.1016/j.cej.2024.157134.
[210] R. Suresh, S. Rajendran, P.S. Kumar, T.K.A. Hoang, M. Soto-Moscoso, Halides and oxyhalides-based photocatalysts for abatement of organic water contaminants – An overview, Environmental Research 212 (2022) 113149. https://doi.org/10.1016/j.envres.2022.113149.
[211] O.J. Ajala, J.O. Tijani, M.T. Bankole, A.S. Abdulkareem, A critical review on graphene oxide nanostructured material: Properties, Synthesis, characterization and application in water and wastewater treatment, Environmental Nanotechnology, Monitoring & Management 18 (2022) 100673. https://doi.org/10.1016/j.enmm.2022.100673.

[212] E.D.H. Kong, J.H.F. Chau, C.W. Lai, C.S. Khe, G. Sharma, A. Kumar, S. Siengchin, M.R. Sanjay, GO/TiO2-Related Nanocomposites as Photocatalysts for Pollutant Removal in Wastewater Treatment, Nanomaterials 12 (2022) 3536. https://doi.org/10.3390/nano12193536.
[213] Â. Almeida, A.M.V.M. Soares, V.I. Esteves, R. Freitas, Occurrence of the antiepileptic carbamazepine in water and bivalves from marine environments: A review, Environmental Toxicology and Pharmacology 86 (2021) 103661. https://doi.org/10.1016/j.etap.2021.103661.
[214] D.P. Mohapatra, S.K. Brar, R.D. Tyagi, P. Picard, R.Y. Surampalli, Analysis and advanced oxidation treatment of a persistent pharmaceutical compound in wastewater and wastewater sludge-carbamazepine, Science of The Total Environment 470–471 (2014) 58–75. https://doi.org/10.1016/j.scitotenv.2013.09.034.
[215] N.A. Mansor, K.S. Tay, Potential toxic effects of chlorination and UV/chlorination in the treatment of hydrochlorothiazide in the water, Science of The Total Environment 714 (2020) 136745. https://doi.org/10.1016/j.scitotenv.2020.136745.
[216] C. Liu, Z.T. How, Y. Ju, L. Feng, X. Ren, M. Gamal El-Din, Experimental and theoretical insight into carbamazepine degradation by chlorine-based advanced oxidation processes: Efficiency, energy consumption, mechanism and DBPs formation, Journal of Environmental Sciences 139 (2024) 72–83. https://doi.org/10.1016/j.jes.2023.05.012.
[217] R. Shaddel, S. Rajabi-Moghaddam, Encapsulation of caffeine in chitosan-coated nanoliposomes and its application in drink formulation, Food Hydrocolloids 149 (2024) 109598. https://doi.org/10.1016/j.foodhyd.2023.109598.
[218] M.T. Pham, T.T.H. Chu, D.C. Vu, Mitigation of caffeine micropollutants in wastewater through Ag-doped ZnO photocatalyst: mechanism and environmental impacts, Environ Geochem Health 46 (2024) 168. https://doi.org/10.1007/s10653-024-01952-1.
[219] M.R. Karim, A. Mohammad, C.B. Mukta, J. Lee, T. Yoon, Biofilm-engineered fabrication of Ag nanoparticles with modified ZIF-8-derived ZnO for a high-performance supercapacitor, Journal of Energy Storage 75 (2024) 109646. https://doi.org/10.1016/j.est.2023.109646.
[220] P. Sathishkumar, R.A.A. Meena, T. Palanisami, V. Ashokkumar, T. Palvannan, F.L. Gu, Occurrence, interactive effects and ecological risk of diclofenac in environmental compartments and biota - a review, Science of The Total Environment 698 (2020) 134057. https://doi.org/10.1016/j.scitotenv.2019.134057.
[221] Z. Wang, S. Guo, B. Zhang, J. Fang, L. Zhu, Interfacially crosslinked β-cyclodextrin polymer composite porous membranes for fast removal of organic micropollutants from water by flow-through adsorption, Journal of Hazardous Materials 384 (2020) 121187. https://doi.org/10.1016/j.jhazmat.2019.121187.
[222] K. Fischer, S. Sydow, J. Griebel, S. Naumov, C. Elsner, I. Thomas, A. Abdul Latif, A. Schulze, Enhanced Removal and Toxicity Decline of Diclofenac by Combining UVA Treatment and Adsorption of Photoproducts to Polyvinylidene Difluoride, Polymers 12 (2020) 2340. https://doi.org/10.3390/polym12102340.
[223] Verwijdering van organische microverontreinigingen. Handvatten voor de keuze van behandelingstechniek in combinatie met de benodigde hydraulische capaciteit |

STOWA, (2020). https://www.stowa.nl/publicaties/verwijdering-van-organische-microverontreinigingen-handvatten-voor-de-keuze-van (accessed February 7, 2025).
[224] S.E. Jujjavarapu, T. Kumar, S. Gupta, CFD Modelling for Optimization of Wastewater Treatment Processes: Towards a Low-Cost Cleaner Future Tool, in: S.E. Jujjavarapu, T. Kumar, S. Gupta (Eds.), Computational Fluid Dynamics Applications in Bio and Biomedical Processes: Biotechnology Applications, Springer Nature, Singapore, 2024: pp. 35–70. https://doi.org/10.1007/978-981-99-7129-9_2.
[225] B. Devipriya, S. Mohanan, A. Surenjan, CFD modelling of an immobilised photocatalytic reactor for phenol degradation, Water Science and Technology 88 (2023) 2121–2135. https://doi.org/10.2166/wst.2023.306.
[226] R. Peralta Muniz Moreira, G. Li Puma, Multiphysics Computational Fluid-Dynamics (CFD) Modeling of Annular Photocatalytic Reactors by the Discrete Ordinates Method (DOM) and the Six-Flux Model (SFM) and Evaluation of the Contaminant Intrinsic Kinetics Constants, Catalysis Today 361 (2021) 77–84. https://doi.org/10.1016/j.cattod.2020.01.012.
[227] H. Seyyedbagheri, R. Alizadeh, B. Mirzayi, M. Valibeknejad, Modeling and CFD simulation of photocatalytic removal of tetracycline by ZnO/PbBiO2Cl nanocomposite catalyst, Journal of Molecular Liquids 399 (2024) 124398. https://doi.org/10.1016/j.molliq.2024.124398.
[228] A.Z. Ali, Y. Wu, Y.-D. Bennani, H. Spanjers, J.P. van der Hoek, Photo-electrocatalytic based removal of acetaminophen: Application of visible light driven heterojunction based BiVO4/BiOI photoanode, Chemosphere 324 (2023) 138322. https://doi.org/10.1016/j.chemosphere.2023.138322.
[229] G. Sagawe, R.J. Brandi, D. Bahnemann, A.E. Cassano, Photocatalytic reactors for treating water pollution with solar illumination: A simplified analysis for *n*-steps flow reactors with recirculation, Solar Energy 79 (2005) 262–269. https://doi.org/10.1016/j.solener.2004.11.010.
[230] A. Sraw, T. Kaur, Y. Pandey, A. Sobti, R.K. Wanchoo, A.P. Toor, Fixed bed recirculation type photocatalytic reactor with TiO2 immobilized clay beads for the degradation of pesticide polluted water, Journal of Environmental Chemical Engineering 6 (2018) 7035–7043. https://doi.org/10.1016/j.jece.2018.10.062.
[231] L. Suhadolnik, A. Pohar, U. Novak, B. Likozar, A. Mihelič, M. Čeh, Continuous photocatalytic, electrocatalytic and photo-electrocatalytic degradation of a reactive textile dye for wastewater-treatment processes: Batch, microreactor and scaled-up operation, Journal of Industrial and Engineering Chemistry 72 (2019) 178–188. https://doi.org/10.1016/j.jiec.2018.12.017.
[232] K. Zhang, Y. Liu, J. Deng, S. Xie, X. Zhao, J. Yang, Z. Han, H. Dai, Co–Pd/BiVO4: High-performance photocatalysts for the degradation of phenol under visible light irradiation, Applied Catalysis B: Environmental 224 (2018) 350–359. https://doi.org/10.1016/j.apcatb.2017.10.044.
[233] E. Han, K. Vijayarangamuthu, J. Youn, Y.-K. Park, S.-C. Jung, K.-J. Jeon, Degussa P25 TiO2 modified with H2O2 under microwave treatment to enhance photocatalytic properties, Catalysis Today 303 (2018) 305–312. https://doi.org/10.1016/j.cattod.2017.08.057.

[234] A.R. Nanakkal, L.K. Alexander, Graphene/BiVO4/TiO2 nanocomposite: tuning band gap energies for superior photocatalytic activity under visible light, J Mater Sci 52 (2017) 7997–8006. https://doi.org/10.1007/s10853-017-1002-0.
[235] P. Gangwar, S. Singh, N. Khare, Study of optical properties of graphene oxide and its derivatives using spectroscopic ellipsometry, Appl. Phys. A 124 (2018) 620. https://doi.org/10.1007/s00339-018-1999-1.
[236] K.R. Reyes-Gil, D.B. Robinson, WO3-Enhanced TiO2 Nanotube Photoanodes for Solar Water Splitting with Simultaneous Wastewater Treatment, ACS Appl. Mater. Interfaces 5 (2013) 12400–12410. https://doi.org/10.1021/am403369p.
[237] J. Resasco, H. Zhang, N. Kornienko, N. Becknell, H. Lee, J. Guo, A.L. Briseno, P. Yang, TiO2/BiVO4 Nanowire Heterostructure Photoanodes Based on Type II Band Alignment, ACS Cent. Sci. 2 (2016) 80–88. https://doi.org/10.1021/acscentsci.5b00402.
[238] H. Liu, Y. Meng, J. Li, X. Wang, T. Zhang, Mechanistic insights into UV photolysis of carbamazepine and caffeine: Active species, reaction sites, and toxicity evolution, Chemosphere 308 (2022) 136418. https://doi.org/10.1016/j.chemosphere.2022.136418.
[239] C. Weidauer, C. Davis, J. Raeke, B. Seiwert, T. Reemtsma, Sunlight photolysis of benzotriazoles – Identification of transformation products and pathways, Chemosphere 154 (2016) 416–424. https://doi.org/10.1016/j.chemosphere.2016.03.090.
[240] Y. Jia, Z. Wang, Y. Ma, J. Liu, W. Shi, Y. Lin, X. Hu, K. Zhang, Boosting interfacial charge migration of TiO2/BiVO4 photoanode by W doping for photoelectrochemical water splitting, Electrochimica Acta 300 (2019) 138–144. https://doi.org/10.1016/j.electacta.2019.01.106.
[241] P. Iovino, M. Lavorgna, E. Orlo, C. Russo, B. De Felice, N. Campolattano, L. Muscariello, A. Fenti, S. Chianese, M. Isidori, D. Musmarra, An integrated approach for the assessment of the electrochemical oxidation of diclofenac: By-product identification, microbiological and eco-genotoxicological evaluation, Science of The Total Environment 909 (2024) 168511. https://doi.org/10.1016/j.scitotenv.2023.168511.
[242] S. Wang, S. Pei, J. Zhang, J. Huang, S. You, Flow-through electrochemical removal of benzotriazole by electroactive ceramic membrane, Water Research 218 (2022) 118454. https://doi.org/10.1016/j.watres.2022.118454.
[243] Y. Yao, Y. Xie, B. Zhao, L. Zhou, Y. Shi, Y. Wang, Y. Sheng, H. Zhao, J. Sun, H. Cao, N-dependent ozonation efficiency over nitrogen-containing heterocyclic contaminants: A combined density functional theory study on reaction kinetics and degradation pathways, Chemical Engineering Journal 382 (2020) 122708. https://doi.org/10.1016/j.cej.2019.122708.
[244] C. Zhao, Z. Liao, W. Liu, F. Liu, J. Ye, J. Liang, Y. Li, Carbon quantum dots modified tubular g-C3N4 with enhanced photocatalytic activity for carbamazepine elimination: Mechanisms, degradation pathway and DFT calculation, Journal of Hazardous Materials 381 (2020) 120957. https://doi.org/10.1016/j.jhazmat.2019.120957.
[245] Y. Li, Y. Yang, J. Lei, W. Liu, M. Tong, J. Liang, The degradation pathways of carbamazepine in advanced oxidation process: A mini review coupled with DFT calculation, Science of The Total Environment 779 (2021) 146498. https://doi.org/10.1016/j.scitotenv.2021.146498.

[246] M. Gholami Shirkoohi, R.D. Tyagi, P.A. Vanrolleghem, P. Drogui, Modelling and optimization of psychoactive pharmaceutical caffeine removal by electrochemical oxidation process: A comparative study between response surface methodology (RSM) and adaptive neuro fuzzy inference system (ANFIS), Separation and Purification Technology 290 (2022) 120902. https://doi.org/10.1016/j.seppur.2022.120902.
[247] I. Dalmázio, L.S. Santos, R.P. Lopes, M.N. Eberlin, R. Augusti, Advanced Oxidation of Caffeine in Water: On-Line and Real-Time Monitoring by Electrospray Ionization Mass Spectrometry, Environ. Sci. Technol. 39 (2005) 5982–5988. https://doi.org/10.1021/es047985v.
[248] D.B. Naik, P.N. Moorthy, Studies on the transient species formed in the pulse radiolysis of benzotriazole, Radiation Physics and Chemistry 46 (1995) 353–357. https://doi.org/10.1016/0969-806X(94)00129-8.
[249] B.A. Wols, C.H.M. Hofman-Caris, Review of photochemical reaction constants of organic micropollutants required for UV advanced oxidation processes in water, Water Research 46 (2012) 2815–2827. https://doi.org/10.1016/j.watres.2012.03.036.
[250] T. Mohlala, T.L. Yusuf, N. Mabuba, Photoelectrocatalytic degradation of emerging organic pollutants in water on an FTO/BiVO4/NiS photoanode, Journal of Electroanalytical Chemistry 947 (2023) 117806. https://doi.org/10.1016/j.jelechem.2023.117806.
[251] T. Jiang, L. Cheng, Y. Han, J. Feng, J. Zhang, One-pot hydrothermal synthesis of Bi2O3-WO3 p-n heterojunction film for photoelectrocatalytic degradation of norfloxacin, Separation and Purification Technology 238 (2020) 116428. https://doi.org/10.1016/j.seppur.2019.116428.
[252] B.A. Koiki, B.O. Orimolade, B.N. Zwane, D. Nkosi, N. Mabuba, O.A. Arotiba, Cu2O on anodised TiO2 nanotube arrays: A heterojunction photoanode for visible light assisted electrochemical degradation of pharmaceuticals in water, Electrochimica Acta 340 (2020) 135944. https://doi.org/10.1016/j.electacta.2020.135944.
[253] G.M. Peleyeju, E.H. Umukoro, J.O. Babalola, O.A. Arotiba, Solar-Light-Responsive Titanium-Sheet-Based Carbon Nanoparticles/B-BiVO4/WO3 Photoanode for the Photoelectrocatalytic Degradation of Orange II Dye Water Pollutant, ACS Omega 5 (2020) 4743–4750. https://doi.org/10.1021/acsomega.9b02148.
[254] T. Hanamorn, P. Vas-Umnuay, CFD modeling and simulation of benzyl alcohol oxidation coupled with hydrogen production in a continuous-flow photoelectrochemical reactor, Sci Rep 13 (2023) 22568. https://doi.org/10.1038/s41598-023-50102-7.
[255] G.C. Tedesco, P.B. Moraes, Innovative design of a continuous flow photoelectrochemical reactor: Hydraulic design, CFD simulation and prototyping, Journal of Environmental Chemical Engineering 9 (2021) 105917. https://doi.org/10.1016/j.jece.2021.105917.
[256] D. Borrás-Jiménez, W. Silva-López, C. Nieto-Londoño, Towards the Configuration of a Photoelectrocatalytic Reactor: Part 2—Selecting Photoreactor Flow Configuration and Operating Variables by a Numerical Approach, Nanomaterials 12 (2022) 3030. https://doi.org/10.3390/nano12173030.
[257] Pilot direct nanofiltration and UV/peroxide at Asten WWTP (IPMV) | STOWA, (2023). https://www.stowa.nl/publicaties/pilot-directe-nanofiltratie-en-uvperoxide-op-rwzi-asten-ipmv (accessed February 16, 2026).

[258] C.T.K. Finnerty, A.E. Childress, K.M. Hardy, E.M.V. Hoek, M.S. Mauter, M.H. Plumlee, J.B. Rose, M.D. Sobsey, P. Westerhoff, P.J.J. Alvarez, M. Elimelech, The Future of Municipal Wastewater Reuse Concentrate Management: Drivers, Challenges, and Opportunities, Environ. Sci. Technol. 58 (2024) 3–16. https://doi.org/10.1021/acs.est.3c06774.

[259] Directive 2011/65/EU of the European Parliament and of the Council of 8 June 2011 on the restriction of the use of certain hazardous substances in electrical and electronic equipment (recast) (Text with EEA relevance), 2025. http://data.europa.eu/eli/dir/2011/65/2025-01-01 (accessed February 16, 2026).

[260] G. Amaya Santos, A.Z. Ali, P. Lettieri, Sustainable advanced wastewater treatment via photoelectrocatalytic oxidation: insights from life cycle assessment, Npj Clean Water 8 (2025) 94. https://doi.org/10.1038/s41545-025-00522-x.

Acknowledgements

Reaching the end of this PhD gives me an opportunity to look back on a journey that began in May 2020, during the COVID-19 pandemic. Starting a doctoral project under such unusual circumstances was not easy. University life, laboratory work, and everyday interactions were all affected, and there were many moments of uncertainty. I could not have completed this journey without the people who supported me, guided me, and helped me to keep moving forward.

First, I would like to express my sincere gratitude to my promotors, Henri Spanjers and Jan Peter van der Hoek. Their unconditional support, patience, and guidance were invaluable throughout my PhD, particularly during its challenging beginning. At a time when the usual ways of working and communicating were not always possible, they continued to make time for me, listen to my concerns, and help me find a way forward. Their trust gave me the confidence to develop as an independent researcher, while their constructive feedback continually improved both my research and this thesis. I am deeply grateful not only for their scientific guidance, but also for the understanding and encouragement they showed me throughout these years.

I am also very grateful to my promotor, Luuk Rietveld, for his involvement during the final stage of my PhD. At a point when the remaining work sometimes felt overwhelming, his encouragement and confidence gave me renewed motivation. His thoughtful advice and support helped me bring the different parts of the thesis together and continue towards its completion. I sincerely appreciate the energy and reassurance he gave me during this important phase.

My sincere thanks also go to Yasmina, who was my daily supervisor during the early stage of the project. Her practical support was especially important while I was finding my way in the laboratory. She helped me establish my experimental setups, solve practical problems, and make the connections within TU Delft that enabled me to conduct different experiments. Her guidance gave me a strong foundation at the beginning of the project, and I remain very thankful for the time and effort she invested in helping me.

I was fortunate to share this journey with many wonderful colleagues. I would especially like to thank David, Nessia, Anik, Apporva, and Sanjeeb, as well as all my other colleagues. The conversations, shared experiences, encouragement, and moments of laughter made my time at TU Delft much more enjoyable. A PhD can sometimes feel like a lonely journey, but your friendship and support reminded me that I was not doing it alone. You made the difficult days lighter and the good days more memorable.

I would also like to thank the members of my doctoral committee for taking the time to read and evaluate this thesis and for their positive assessment of my work. I greatly appreciate the attention, expertise, and consideration they have given to it.

My deepest and most personal thanks go to my wife, Zoha. We married during my PhD, and our life together became closely connected with this journey. She experienced both its rewarding moments and its difficulties and supported me through all of them. On the days when my motivation was low or progress seemed slow, she encouraged me, listened to me, and reminded me to keep going. Most importantly, she created a peaceful and supportive environment at home that allowed me to concentrate on and complete this work. Her patience, understanding, and belief in me meant more than I can express in words. Zoha, this achievement would not have been possible without you.

I remember my parents with love and gratitude. Although my mother and father are no longer with us, their influence remained with me throughout this journey. From my childhood, they encouraged me to learn, to ask questions, and to remain curious about the world. They gave me the confidence to pursue my education and the freedom to think independently. I wish they could have been here to see this moment, and I hope that completing this PhD honours the values they gave me.

I am deeply thankful to my brothers, Agha Shaheryar and Agha Hyder Ali, for their constant encouragement and for supporting me throughout my education and my PhD. Their confidence in me has always been a source of strength. I would also like to thank my sister, Afsheen, for her love and support throughout this journey. Knowing that my family stood behind me gave me the motivation to continue, even during the most demanding periods.

Finally, to everyone who supported me in ways large or small during these years: thank you. This thesis may carry my name, but its completion reflects the encouragement, kindness, and support of many people. I will always remain grateful to all of you.

Curriculum Vitae

Agha Zeeshan Ali

Agha Zeeshan Ali has an interdisciplinary background in materials engineering, physical chemistry, environmental engineering, and electrochemical technologies. He obtained his Bachelor of Science in Metallurgy and Materials Engineering from the University of the Punjab in Lahore, Pakistan, in 2016. His bachelor's research focused on the fabrication and characterization of superhydrophobic coatings on aluminium alloy Al-606. After graduating, he received a Chinese Government Scholarship for Chinese language study.

In 2017, he received an Erasmus+ scholarship to join the international SERP+ master's programme, studying at the University of Paris-Saclay in France and the University of Porto in Portugal. He completed his Master of Science in Chemistry in 2019. His master's research was carried out at the Laboratory of Physical Chemistry at the University of Paris-Saclay within the CNRS-funded MOMENTOM project and focused on sustainable dye-sensitized solar cells.

In May 2020, he joined the Department of Water Management at Delft University of Technology as a Marie Curie PhD researcher within the European InnovEOX project. His doctoral research investigated visible-light-driven $BiVO_4$-based photoanodes for the removal of organic micropollutants from water. The work combined materials development and characterization, photoelectrochemical experiments, water-treatment studies, reactor design, and computational fluid dynamics for scale-up analysis. Alongside his research, he coordinated Work Package 2, collaborated with KWR Water Research Institute and Nijhuis Saur Industries, and supervised three master's thesis projects. During an industrial secondment at Nijhuis Water Technology in 2023, he designed a pilot-scale solar-driven reactor for treating industrial and municipal wastewater and evaluated its scale-up and process-integration requirements. He received the Best Paper Award at the CoEEE 2022 conference in Stockholm.

Since September 2024, he has worked as a researcher in Renewable Energy Carriers at Avans University of Applied Sciences and MNEXT in Breda. His current work focuses on green hydrogen, electrolysis, power-to-X technologies, e-fuels, and industrial decarbonization. He develops applied research projects and coordinates public-private consortia involving companies, knowledge institutions, and applied research organizations. His work connects electrochemistry, materials science, process modelling, and reactor scale-up with practical energy-transition challenges and pilot-scale implementation.

List of Publications

Agha Zeeshan Ali, Sanjeeb Mohapatra, Jan Peter van der Hoek, Henri Spanjers, BiVO4-based photoanodes for the photoelectrocatalytic removal of trace organic pollutants from water: A mini review on recent developments, Current Opinion in Environmental Science & Health, Volume 45, 2025, 100615, https://doi.org/10.1016/j.coesh.2025.100615

Agha Zeeshan Ali, Yuhao Wu, Bas Wols, Mohamad Zeidan, Henri Spanjers, Jan Peter van der Hoek, Simultaneous removal of multiple organic micropollutants via UV-visible light driven BiVO4/TiO2-GO photoanode: Experimental and CFD study, Chemical Engineering Journal Advances, Volume 22, 2025, 100721, https://doi.org/10.1016/j.ceja.2025.100721

Agha Zeeshan Ali, Sadhna Jagannathan, Yasmina-Doekhi Bennani, Jan Peter van der Hoek, Henri Spanjers, Photoelectrocatalytic based simultaneous removal of multiple organic micro-pollutants by using a visible light driven $BiVO_4$ photoanode, Journal of Water Process Engineering, Volume 56, 2023, 104471, https://doi.org/10.1016/j.jwpe.2023.104471.

Agha Zeeshan Ali, Yiqian Wu, Yasmina-Doekhi Bennani, Henri Spanjers, Jan Peter van der Hoek, Photo-electrocatalytic based removal of acetaminophen: Application of visible light driven Heterojunction based $BiVO_4$/BiOI photoanode, Chemosphere, Volume 324, 2023, 138322, https://doi.org/10.1016/j.chemosphere.2023.138322.

Amaya Santos, G., Ali, A.Z. & Lettieri, P. Sustainable advanced wastewater treatment via photoelectrocatalytic oxidation: insights from life cycle assessment. npj Clean Water 8, 94 (2025). https://doi.org/10.1038/s41545-025-00522-x

